A COMBINED SIZE REDUCTION AND LIBERATION MODEL OF GRINDING

by

Woo-Zin Choi

Dissertation submitted to the Faculty of the
Virginia Polytechnic Institute and State University
in partial fulfillment of the requirements for the degree of

DOCTOR OF PHILOSOPHY

in

Mining and Minerals Engineering

APPROVED:

R. H. Yoon, Chairman

G. T. Adel, Co-Chairman

J. R. Craig

R. L. Wiegel

J. R. Lucas

December, 1986

Blacksburg, Virginia

A COMBINED SIZE REDUCTION AND LIBERATION MODEL OF GRINDING

by

Woo-Zin Choi

Committee Chairmen: Drs. R.H. Yoon and G.T. Adel
Mining and Minerals Engineering

(ABSTRACT)

The grinding models developed previously are concerned with size reduction only. Although they have proven to be useful in the simulation and design of grinding mills, they do not provide information on liberation which is the main objective of most comminution operations. In the present investigation, a population balance model describing the combined processes of size reduction and mineral liberation has been developed for batch grinding operation. The model parameters include conventional breakage rate and breakage distribution functions, along with a new parameter i.e., liberation function that is used to describe changes in particle composition. These parameters have been determined experimentally by examining mill products under optical microscope using a SEM-IPS image analyzer. The areal assays, obtained from the image analysis of monosized particle mounts, have been found to correspond quite closely to the actual chemical assays. It has been found that the method used to prepare particle mounts is critical in achieving accuracy.

In the present work, it has been shown that the breakage

characteristics of component minerals can be determined by examining the mill feeds and products using an image analyzer. The model parameter analysis has shown that while the breakage rate functions are sensitive to the grinding environment, breakage distribution functions are independent of it. Furthermore, the breakage distribution functions have been found to be normalizable with feed size, thus reducing the number of parameters that must be estimated. The study has also shown that both the breakage rate and the liberation function suggest a preferential breakage of sphalerite over dolomite gangue.

The model has been validated by simulating the batch grinding of a sphalerite ore from ASARCO's Young Mine in eastern Tennessee. The model can predict the product size distributions for the total ore and its components, including gangue, sphalerite, and composite particles. An excellent agreement between the model predictions and the experimental results has been observed for both monosized and multisized feed materials. The model is capable of handling multiple classes of composite particles for a binary ore; however, the model has been verified against experimental results by considering only two composite classes. The method of determining liberation functions has also been discussed. The liberation function has been found to be useful for analyzing the liberation mechanisms of composite particles.

ACKNOWLEDGMENT

The author wishes to express his sincere gratitude to Dr. R. H. Yoon and Dr. G. T. Adel for their guidance, support, and helpful suggestions throughout the course of this study. Special thanks are also due to Dr. J. R. Craig for his interest and gracious support throughout this work and for his permission to use the facilities at the Geology Laboratory, and to Dr. R. L. Wiegel, International Minerals and Chemical Corporation, for his continued interest in liberation studies and image analysis work. Thanks are also due to ASARCO for permission to take ore samples from the Young Mine, Jefferson City, Tennessee.

The author also acknowledges the financial support received from the National Science Foundation (Grant No.), which made this work possible. He also expresses his gratitude to Dr. J. R. Lucas and the Department of Mining and Minerals Engineering for the tuition scholarships provided to the author.

Acknowledgments are also extended to for reading the thesis and for her work in conducting the chemical assays, and to for his technical support. The friendship of the many fellow graduate students the author came to know at Virginia Tech, particularly that of

, is also appreciated.

Finally, the author wishes to express his deep appreciation to his mother, his wife, , and his twins, and for their understanding and encouragement.

TABLE OF CONTENTS

LIST OF FIGURES

LIST OF TABLES

CHAPTER 1.

INTRODUCTION

1.1 General Statement of the Problem

One of the primary objectives of comminution in mineral beneficiation is the liberation of valuable minerals. The extent of liberation achieved during comminution can play an important role in determining the final concentrate grades and recoveries obtainable in a mineral processing plant. In froth flotation, for example, a low concentrate grade can be attributed to the recovery of composite particles or to the non-selective recovery of liberated gangue material. In either case, the corrective action needed to improve the grade is highly dependent upon knowing the manner in which free and composite particles are distributed in the feed and froth product. Furthermore, if this type of information can be obtained as material leaves the grinding circuit, it may be possible to optimize the flotation feed on the basis of both size and mineral content distribution.

Over the past 20 years, mathematical models of the grinding process have been thoroughly developed and studied by numerous researchers to the point where estimation of model parameters and prediction of size distributions from

grinding mills have become commonplace. These models have proven to be useful in the simulation and design of grinding circuits when product size is the only consideration; however, they provide no information on one of the main objectives of grinding, i.e., mineral liberation.

To evaluate the effect of liberation on various mineral separation processes, it is desirable to obtain information regarding the particle size distributions for both free and composite particles. Size analysis alone is not sufficient, and chemical analysis can only tell how much of a particular mineral occurs within a given size range.

The field of mineralogy has provided, over the years, a number of techniques for determining the amount of a given mineral contained in a composite particle. These include linear intercept methods (Rosiwol, 1898), area tracing methods (Delesse, 1848), and point counting methods (Thompson, 1930). With recent advances in computerized image analysis technology, it is now possible to gather detailed information on the distribution of free and composite particles quite rapidly. A software package called GIPSY (General Image Processing System), for example, has been used extensively at Virginia Tech for making area-based liberation measurements (Craig et al., 1982, 1984; Pong et al., 1983). Instruments involving a moving microprobe or scanning electron microscope have also been

demonstrated (Jones and Shaw, 1973; Miller et al., 1982). Indeed, image analysis has been gaining ground in recent years as a useful tool for studying various aspects of mineral processing operations.

In the study of liberation during comminution, however, very little use has been made of image analysis. This is largely because much of the work in liberation modeling (Gaudin, 1939; Wiegel and Li, 1967) was done prior to the development of sophisticated image analysis system. Only recent studies have been able to take advantage of such equipment (King, 1979). In addition, few of the existing liberation models are capable of representing the joint behavior of size reduction and liberation during comminution.

The purpose of this investigation is, therefore, to develop a combined size reduction and liberation model for the breakage of binary ores during batch grinding. In the present work, a computerized optical image processing system (Kontron SEM-IPS) has been used to quantify mineral liberation as a function of the extent of size reduction. Heavy emphasis has been placed on experimental determination of the model parameters, as opposed to mathematically fitting the parameters, in order to gain a better mechanistic understanding of the liberation process. As a result of this work, it is hoped that the successful

application of a liberation model will ultimately be useful in the design, control and simulation of grinding circuits on the basis of liberation rather than on size reduction alone.

1.2 Literature Review

1.2.1 Grinding Theories and Models

a. Grinding theories: For almost a century, the process of size reduction was studied in terms of the energy consumed during the operation of a grinding mill. This was a logical starting point because size reduction is responsible for a large proportion of the cost of ore treatment due to the high consumption of energy. In these early investigations, two approaches were taken. In the first approach, the energy consumption was represented as a function of surface area increase during comminution by recognizing that breaking a particle caused the production of a new surface (Rittinger, 1867). In the other approach, the energy consumption was directly related to reduction in average particle size during comminution (Kick, 1885). For many years there was vigorous controversy in the technical literature about the merits of these hypotheses, Kick's hypothesis being favored by those working with coarse particles and Rittinger's hypothesis by those working with fine particles.

In 1952, Bond criticized both Rittinger's and Kick's theories and postulated that energy input is proportional to the new crack length produced. He also drew attention to the continual accumulation, over successive stages, of energy available for further reduction in the form of incompletely exploited cracks and flaws. Bond's law is sometimes called, "The Third Theory".

These empirical laws have been used for many years to estimate mill capacity and power requirements. Since there is little theoretical basis, they fit experimental data only for a limited range of variables and only in certain cases (Hukki, 1961). For the last three decades, most of the mill design work has been based on the empirical Bond equation. Although the empirical methods have proven to be fairly reliable in mill design with regard to capacity, power requirements, etc., they are able to provide little information regarding the product size distribution except the 80% passing size. Thus, the Bond method is unsuitable for meaningful process simulation and control system design. Over the last few years, many attempts have been made to describe grinding as a rate process. A brief review of some of the investigations in comminution kinetics is given below.

A more realistic approach to ball mill modeling and scale-up appears to be through the use of population

balance models capable of predicting complete product size distributions. An early practical application of this approach was described by Epstein (1947), who expressed the breakage process as a number of steps and defined two basic functions in his model. He defined the selection function, $[S_n(y)]$, as the probability of breakage of a particle, size y, in the nth step of the breakage process, and the distribution function, $[B_{(x,y)}]$, as the cumulative weight distribution of particles appearing in or below size class x as a result of breakage from a unit mass of size y. He assumed that each time a particle was broken, two equal-sized pieces were produced. Although his assumption is too simple to account for the complex breakage phenomena, his concept of the two breakage parameters has become well-established in comminution research and is currently being employed by many workers in this field.

Using Epstein's basic concept of selection and breakage functions, Broadbent and Callcott (1956) developed a matrix approach to the breakage process. In general, they represented the size distribution of an assembly of particles by a vector, the elements of which are derived from the sieve analysis of the assembly. They assumed the distribution function to be the same for all grinding systems, materials, and sizes considered. The matrix method, although an excellent approach to understanding the

comminution process, had a major difficulty in that the distribution function had to be assumed to be the same for all cases.

Gardner and Austin (1962) modified the ideas of the selection and distribution functions of the previous researchers and derived a size-mass balance equation in differential terms to construct a breakage model for batch grinding. They hypothesized that if the basic parameters of selection and distribution could be measured experimentally, then the appropriate size-mass balance equation could be solved for any set of feed size conditions. In order to measure the breakage functions, they used a radioactive tracer technique.

In recent years, much experimental evidence has been produced to show that grinding equations based on the above concepts can be used to accurately predict the variation of the product size distribution with time in batch grinding (Herbst and Fuerstenau, 1968; Klimpel and Austin, 1970). The equations can also be adapted to predict sizes from continuous operations through either a predominantly empirical approach (Lynch et al., 1967) or a more theoretical treatment incorporating the dynamics of the system (Kelsall and Reid, 1965). In the next section, the mathematical bases for the discrete batch grinding model are briefly reviewed.

b. Population balance models: As mentioned in the previous section, significant progress has been made in recent years in developing phenomenological grinding models derived from population balance considerations. This approach has led to the development of many simulators that can be used for controlling industrial grinding circuits. Herbst and Fuerstenau (1980) have reviewed the advantages of this approach, and others (Austin, Shoji and Luckie, 1976; Siddique, 1977; Kinneberg and Herbst, 1984) have discussed various scale-up models.

In this approach, the breakage process is described by two sets of physically interpretable parameters, i.e., breakage rate (S) and breakage distribution (B) functions. These parameters, which are size-discretized for mathematical convenience, allow the behavior of each size fraction in the mill to be represented mathematically. The formulation of the mass balance models and subsequent discussions of their characteristics have been presented by several workers (Reid, 1965; Grandy and Fuerstenau, 1970; Luckie and Austin, 1970).

The basic batch grinding equation in the time-continuous and size-discretized form for expressing the rate at which material from size class i changes due to comminution is given below;

$$\frac{dm_i(t)}{dt} = \sum_{\substack{j=1 \\ i>j}}^{i-1} b_{ij} S_j m_j(t) - S_i m_i(t), \qquad [1.1]$$

where $m_i(t)$ is the fraction of total mass present in size i at time t, S_i is the breakage rate function for material in the i-th size class (i.e., the fractional rate at which material is broken from the i-th size class ($time^{-1}$)), and b_{ij} is the breakage distribution function which gives the fraction of material that becomes particles in the i-th size class when material in the j-th size class is comminuted. Conventionally, the ascending size classes are taken to be the sieve opening in the Tyler $\sqrt{2}$ series of sieves, in descending order. For dry ball milling, the breakage rates have been found to be time-independent by many investigators (Herbst and Fuerstenau, 1968; Luckie and Austin, 1970).

The zero-order production relationship (i.e., fines being produced at a constant rate initially) is given below in the size-discretized form (Herbst and Fuerstenau, 1968):

$$\frac{dY_i}{dt} = F_i, \qquad [1.2]$$

where Y_i is the cumulative mass fraction smaller than size class i and F_i is the zero-order rate constant for the production of fines smaller than the stated size ($time^{-1}$).

In systems in which the breakage rate function is

environment-independent (i.e., the systems for which S_i remains substantially constant with time), the zero-order rate constant, the feed-size breakage rate function and the cumulative feed-size breakage distribution function (B_{i1}), are inter-related as follows:

$$B_{i1}S_1 = F_i. \qquad [1.3]$$

Therefore, from a knowledge of F_i and S_1, we can estimate the cumulative feed-size breakage distribution function, B_{i1}. B_{i1} is the total fraction of material produced finer than size i when material in feed size class 1 is comminuted. If we start with mono-sized feed, S_1 for the top size can be easily obtained from a semi-log plot of the fraction of original feed remaining vs. time, since Equation [1.1] reduces to the following form:

$$\frac{dm_1(t)}{dt} = -S_1 m_1(t). \qquad [1.4]$$

Integration between the limits when t = 0 and t = t yields

$$\ln \frac{m_1(t)}{m_1(0)} = S_1 t. \qquad [1.5]$$

Equation [1.5] shows that the slope of such a semi-log plot yields the value of S_1.

Another experimental technique used for the measurement

of breakage functions is known as the radioactive tracer technique. This method, introduced by Gardner and Austin (1962), consists of irradiating a selected size fraction of the material, remixing it with the original complete charge, and studying the distribution of the irradiated material at various grinding times.

Unfortunately, both of the above-mentioned techniques require a large number of experiments. In order to reduce this number, efforts have recently been made to determine both sets of parameters simultaneously from the size distribution data obtained by batch-grinding a known feed for several grinding times (Berube et al., 1979; Shoji and Austin, 1974; Herbst and Mika, 1973).

Several investigators have developed a back-calculation technique which is based on empirical functional forms for parameters (Austin and Klimpel, 1977; Gupta and Kapur, 1981). Here, the breakage parameters are adjusted until a model prediction best fits experimentally determined size distributions at different grinding times. Although the back-calculation method has the advantage of reducing the amount of experimental work, it is not always practical since several assumptions must be made (e.g., first-order breakage) and much computation time is required.

1.2.2 Liberation Theory and Models

a. Degree of liberation: One of the major objectives of comminution is the liberation of the valuable minerals from the associated gangue minerals. The ore should therefore be ground just long enough to liberate the valuable minerals from the gangue minerals, but no further. Overgrinding is wasteful since it needlessly consumes electric power and grinding media, reduces the through-put rate, and makes the subsequent recovery steps, such as flotation, less efficient. Therefore, achieving an optimum degree of liberation is the key to success in mineral processing. Since the degree of liberation cannot easily be measured, the usual practice in the mineral industry involves controlling the product size in crushing and grinding circuits.

Measurement of the degree of liberation is a useful guide in establishing an optimum grind for a given ore. The degree of liberation is defined as the percentage of a certain mineral occurring as free particles in the ore in relation to the total amount of that mineral occurring as free and locked forms. The degree of liberation (L_i) of mineral component, i, can be expressed by the following formula:

$$L_i = 100 \times \frac{W_i^f}{W_i^f + f_i W_i^l} , \qquad [1.6]$$

where W_i^f and W_i^l are the weight fractions of mineralogical component, i, occurring as free and locked particles, respectively, and f_i is the locking factor of the mineral. The locking factor, which is greater than one, is designed to give more weight to locked particles since a locked particle can be counted as a free particle depending upon its orientation, whereas a free particle always appears free during two-dimensional microscopic examination.

The degree of liberation, thus determined, can be plotted as a function of particle size for each mineral present in an ore sample. Such information will be useful in determining the optimum mesh of grind to be employed in the subsequent beneficiation processes for maximum recovery.

Direct measurement of the degree of liberation can be achieved by counting mineral particles under a microscope (Gaudin, 1939). This manual method is slow, tedious, and often inaccurate, however. In practice, the mineral industry often employs an indirect method based on the actual performance of the separation process. The decrease in recovery when a mineral is ground finer than the optimum grind size is mostly due to the deleterious effect of fine particles, say, less than 5 microns, on the separation process. In recent years, attempts have been made to speed up these methods using semi-automatic, or even fully automatic, image analysis techniques. Their actual

application to liberation studies will be discussed in a later section.

b. Liberation models: The importance of liberation in determining final concentrate grade and recovery has been recognized for some time; however, relatively little work has been done in the area of liberation modeling. The first attempt at developing a liberation model was made by Gaudin (1939). He proposed a model for the fracture of an ideal binary mineral system which related the fraction of each mineral liberated to the ratio of mineral grain size to particle size. His model was based, however, on unrealistic assumptions involving a cubical mineral grain structure in the ore and cubical fracture pattern resulting in cubical particles. Therefore, this model found very little practical application.

Nearly 30 years later, Wiegel and Li (1967) attempted to extend Gaudin's model by allowing a completely random arrangement of mineral grains as opposed to placing the grains of the least abundant mineral as far apart as possible. They also modified Gaudin's model to describe the distribution of mineral content among composite particles. While Wiegel and Li's modifications clearly improved Gaudin's original work, their model still suffered from the unrealistic assumptions of the original model.

It was not until the advent of computerized image

processing systems in the late 1970's that further progress was made in the modeling of mineral liberation. King (1979) developed a model based on the distribution of linear intercept lengths through minerals in an ore. From the stereological considerations needed to derive three-dimensional information from one-dimensional measurements, it was necessary to assume an isotropic, binary ore with no propensity to preferentially fracture along grain boundaries. The resulting model, expressed in terms of experimentally obtainable parameters and no empirical constants, predicts the fractional liberation, L(D), of the mineral at mesh size, D, and is given by:

$$L(D) = 1 - \frac{1}{\mu} \int_0^{D_u} [1 - N(l/D)][1 - F(l)]\, dl \qquad [1.6]$$

where F(l) is the distribution of linear intercept lengths (l) for the mineral, μ is the mean linear intercept length, N(l/D) is the linear intercept distribution function for particles of mesh size, D, and D_u is the largest intercept length across any particle of mesh size D. While experimental results demonstrated this model to be a substantial improvement over those of Gaudin and Wiegel (see Figure 1.1), some deviations in the predicted fractional liberation values were observed throughout the particle size

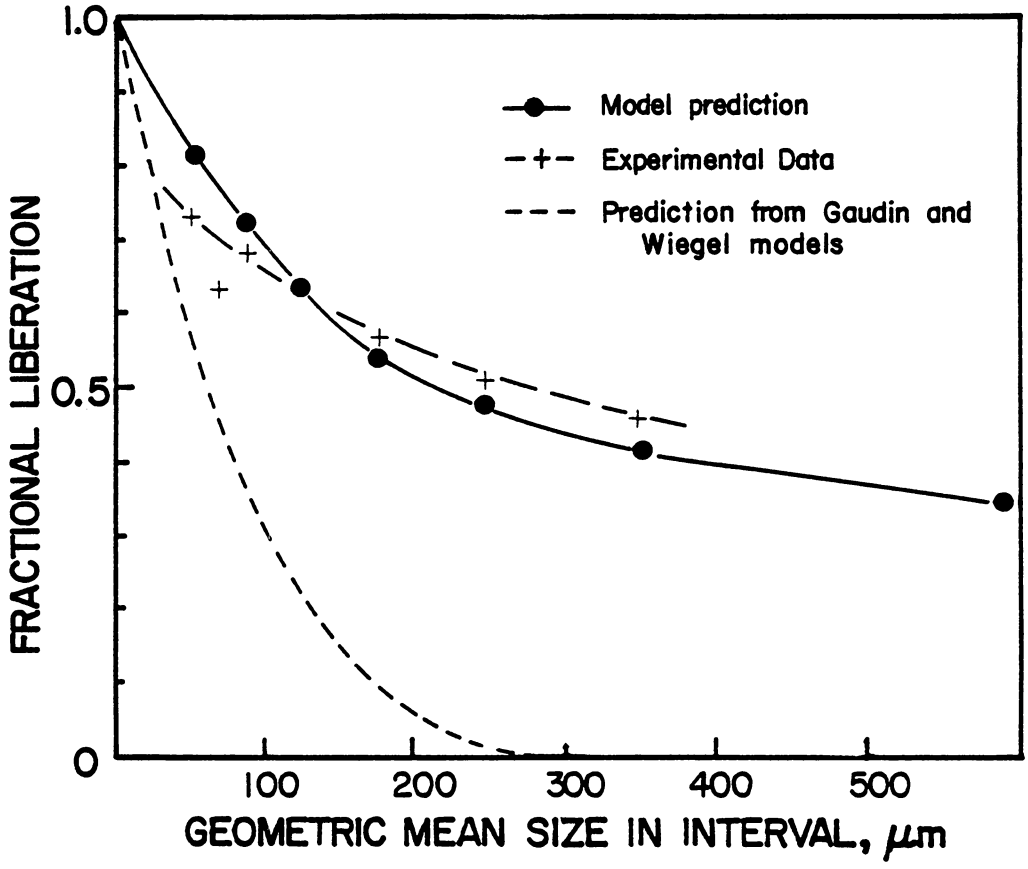

Figure 1.1 Comparison between theoretical prediction and experimental determination of fractional liberation at various particle sizes (King, 1979).

range, with the deviations becoming significant for large sizes (> 400 microns). These deviations from experimental data may possibly be related to the assumption of equivalence between one-dimensional measurements and three-dimensional properties, since any discrepancy in this area would tend to be more pronounced at larger particle sizes. In addition, the simplifying assumptions of isotropy and random breakage may not always be appropriate (Choi, 1982). This model has also been recently discussed and evaluated by Finch and Petruk (1984).

A more recent model developed for the liberation of pyrite and ash from coal (Klimpel and Austin 1983; Bagga and Luckie, 1983) used a Monte Carlo simulation procedure to create a computer-generated ore consisting of randomly selected mineral grains. By forcing the computer-generated ore to meet a specified size distribution, the extent of liberation for a particular grind was determined. Experimental comparisons with a synthetic ore of polystyrene, pyrite and quartz showed excellent agreement. The advantage of this model is that it can be used for systems containing more than two minerals. However, because of the Monte Carlo approach, completely random fracture must be assumed. This did not appear to be a limitation for the experimental results presented using the synthetic ore.

In another approach, specific attention has also been

given to the determination and use of specific area of mineral intergrowth for assessing the degree of liberation (Steiner, 1975). Recently, Davy (1984) presented an index between 0 and 1 to describe the degree of liberation. In this work, it has been shown that the index of liberation is related to the distribution of shape and size of particles and to the interaction between the fracture surfaces and the structure of the material. Further, the variation of the index with the extent of crushing is investigated together with the stereological estimation. Based on Davy's theory, Barbery(1985) developed a liberation model using a random Poisson polyhedra for fracture and fragment distribution from monosize particles.

Clearly, liberation models have improved in recent years to the point where one can get reasonably accurate predictions of the extent of liberation versus the fineness of grind. However, the existing models are only capable of describing open-circuit grinding operations. When a classification device is used to close the circuit, its operation is largely governed by the distribution of particles in both size and mineral content. Likewise, the operation of a concentration process, such as flotation, is influenced by this same joint distribution. Therefore, in order to simulate a complete mineral processing flowsheet, including size reduction, classification and concentration processes, it

must be possible to simulate individual mineral behavior at every point in the flowsheet. In the next section, previous studies on the grinding kinetics of fully-liberated mineral mixtures are reviewed and existing combined grinding-liberation models are briefly discussed.

1.2.3 Combined Grinding/Liberation Models

a. Earlier work on mixture grinding: As mentioned in the previous section, one of the principal purposes of grinding is to liberate the valuable minerals from the gangue material. However, the fully liberated constituents in a typical tumbling mill also undergo further size reduction to a considerable extent. An understanding of how the liberated constituents interact with each other and thereby affect the effectiveness of grinding would be a useful precursor to the study of grinding for liberation. However, the influence of mill parameters on the size distribution of the product of two or more materials when comminuted simultaneously in a mill has hitherto not been adequately investigated.

The earliest work in mixture grinding kinetics reported in the literature is by Holms and Patching in 1957. They simulated the continuous ball milling of limestone-quartz mixtures by carrying out locked-cycle experiments using the Maxon-Cadena-Bond method (Maxon et al., 1934). Their work

did not attempt to explain the breakage subprocesses, such as how a mineral particle distributes itself into daughter fragments upon breakage or how the presence of another mineral affects this distribution. Working on the wet rod milling of limestone-quartz mixtures, Fuerstenau and Sullivan (1962) observed that the distribution modulus of the ground product of the mineral in the Gaudin-Schumann size distribution was independent of whether the mineral was ground alone or as a component in a mixture, confirming Holmes and Patching's observation. They found that for mixture grinding, an energy-size reduction relationship similar in form to that of the Charles equation for a single mineral could be obtained. Fuerstenau and Sullivan (1962) in a subsequent paper on the ball milling of mixtures, postulated that the fraction of energy utilized to grind each component in ball mill grinding is proportional to its volume fraction in the feed. Their hypothesis, however, does not take into account the effects of such other important and relevant factors as hardness, fineness of grind grindability, etc. Halasyamani et al. (1966), who studied the grinding kinetics of quartz/limestone mixture in a ball mill, generally confirmed the results and observations made by Fuerstenau and Sullivan.

Somasundaran and Fuerstenau (1963) analyzed the dry batch ball mill grinding of limestone-quartz mixtures and

found that fines are produced at a constant rate during the initial period of grinding (up to 4 minutes of batch grinding), but as comminution is continued for a longer period, the rate of production of the softer mineral decreases while that of the harder mineral increases. The reason for this was that, as grinding is prolonged over long time periods, the softer mineral is ground to fine particles, leaving the harder, coarser component to be subjected to the comminution action in the ball mill. Tanaka and Selby (1976) also carried out experiments with a limestone-quartz mixture in a rod mill. They found the interaction of the components to be complex and attempted to offer a method for calculating the size distribution of components from the size distribution of the mixture and certain parameters for the components obtained from homogeneous grinding. However, they did not take into account the specific energy consumption (kwh/ton).

Upon review of the information available in the literature, it appears that the information regarding the effects of one of the constituents of the grinding kinetic parameters (like breakage rate and breakage distribution functions) on the other have never been experimentally verified, although certain assumptions have been made as to how the parameters of one component should respond to the presence of other mineral species. Recently, Venkataraman

and Fuerstenau (1984) studied the grinding kinetics of calcite, hematite and quartz, individually and as binary mixtures. Their experiments were designed to investigate in a quantitative way, how the values of the parameters of the population balance model - namely breakage rate function and breakage distribution function - differ when a mineral is ground alone and when it is ground as a component in a binary mixture. They concluded that the breakage distribution function is independent of the grinding conditions. The breakage rate function, however, is found to be environment-dependent; that is, the value of S depends on whether the mineral is ground alone or as a component in a mixture. They further concluded that reduced breakage rate functions are normalizable with respect to specific energy input to the grinding mill.

More recently, Choi et al. (1985), who have studied the breakage characteristics of complex sulfide ores in a batch ball mill, showed that the ore composition and textures have marked effects on the breakage rates. They also showed that, unlike the cases for grinding homogeneous materials, the experimental S values do not follow the power law and the B values are not generally normalizable with respect to feed size. They further concluded that the degree of non-normalizability depends on the complexity of the ore.

b. Combined size reduction-liberation models: A few investigators attempted to simultaneously account for liberation and size reduction during comminution. Steiner (1975) developed transformation matrices for liberation and size reduction to describe the changes in mineral composition and size which take place when a material is comminuted. The model appears to be rather complex to apply, however, and is somewhat limited by the assumption that interfacial area is conserved during comminution. Andrews and Mika (1975), on the other hand, modified the population balance model for grinding to accomodate a two-dimensional description of the particle population based on size and mineral content. The major limitation of this approach has been in estimating the necessary breakage and liberation parameters.

Wiegel (1976) also combined his liberation model with a batch grinding model to describe the liberation of a magnetite ore. By assuming i) a binary mineral system, AB, ii) breakage to the next lower size class only, and iii) the same selection function for all ore components, Wiegel's model for each component was as follows:

$$dWA_i/dt = WA_{i-1}SA_{i-1} + WAB_{i-1}SAB_{i-1}QA_{i,i-1} - WA_iSA_i \quad [1.7]$$

$$dWB_i/dt = WB_{i-1}SB_{i-1} + WAB_{i-1}SAB_{i-1}QB_{i,i-1} - WB_iSB_i \quad [1.8]$$

$$dWAB_i/dt = WAB_{i-1}SAB_{i-1}QAB_{i-1} - WAB_iSAB_i \quad [1.9]$$

where WA, WB and WAB are the quantities of species A, B and AB, respectively; SA, SB and SAB are selection functions for each component; and QA, QB and QAB are "directional coefficients" describing the quantity of AB from size class i-1 which appears as component A, B or AB in size i. The simplifying assumptions pertaining to the grinding parameters were not realistic, however, and some disagreement was found in experiment and model predictions comparisons. For example, previous work has shown that soft minerals tend to grind preferentially at a faster rate than hard minerals (Venkataraman 1981; Choi, 1982), implying that the selection functions should be different for different components.

As mentioned in the previous section, King (1979) developed a liberation model which based the liberation on the mineralogical structure of the ore. In this model, he decoupled the liberation and size reduction processes in relating linear intercept lengths through minerals in an ore to the fractional liberation of those minerals at a given product size. Finlayson and Hulbert (1980) combined King's liberation model with a population balance model for grinding to develop a dynamic simulator. This simulator predicted behavior of individual minerals and locked particles in a closed grinding circuit. Limited testing on a pilot-plant scale verified the capabilities of the

simulator.

Recent work at the University of Utah (Ruebush et al., 1980; Ruebush, 1982; Peterson, 1983) has focused on the development of a grinding model which combines mineral liberation and size reduction. The model has been incorporated into a total plant simulator and has been used as a stand-alone model for simulating single-component grinding, two-component grinding, or the grinding of two components plus a locked intermediate. Because of the complexity of the model, however, no attempt has been made to experimentally determine the breakage parameters and, therefore, "assumed" values were used for the simulation. More recently, Peterson and Herbst (1985) have demonstrated the utility of computerized parameter estimation techniques in determining the large number of parameters needed for the simultaneous representation of breakage and liberation. Because of the enormity of the task of experimentally determining these parameters, however, they were unable to verify many of the assumptions used in the estimation procedure.

1.2.4 Liberation Analysis Using Image Analysis Techniques

Liberation data are typically be obtained from microscopic evaluation of polished particle mounts. A number of techniques are available for determining the amount of a given mineral contained in a composite particle, including linear intercept methods (Rosiwol, 1898), area tracing methods (Delesse, 1848), and point counting methods (Thompson, 1930). With recent advances in computerized image analysis technology, it is now possible to gather detailed information on the distribution of free and composite particles. The basic premise of image analysis is that three-dimensional information can be generated from one- or two-dimensional data. The data of interest is typically the volumetric proportions of various minerals in a rock. A brief review of previous liberation analysis techniques is given below.

In the case of one-dimensional measurements, a line is superimposed over the surface of an ore specimen and the lengths of the intercepts across various mineral grains are determined. The volume proportion of mineral A in a particle is then determined by:

$$\frac{\text{length of intercepts on mineral A}}{\text{total particle intercept length}} = \text{volume proportion of A} \qquad [1.10]$$

This technique, originally practiced by Rosiwol (1898), has been more recently extended for use with modern image analysis equipment (Barbery, 1974; King, 1978) in transforming intercept distributions to grain-size distributions. A limitation of this linear scanning technique is that it assumes that the specimen is isotropic and the fracture occures randomly. At present, the assumption has been neither proven nor disproven.

Two-dimensional techniques involve the use of the entire mineral area as an estimate of the mineral volume. This can be represented mathematically as:

$$\frac{\text{area of mineral A}}{\text{total particle area}} = \text{volume proportion of mineral A} \quad [1.11]$$

Originally, the areas were determined by tracing the outlines of the mineral grains onto paper or tin foil and weighing each grain separately. The weights were then used directly to obtain the volume proportion (Delesse, 1848).

A later method, known as "point counting" (Thompson, 1930), used a superimposed grid of dots on the specimen surface to estimate mineral areas. The area was assumed to be proportional to the number of dots on the mineral surface. A modification of this method was described by Gaudin (1939) for determining the volume proportion of minerals contained in particles which are mounted in

briquettes. Since these particles may orient themselves in many directions, a single size fraction will appear to contain particles of widely varying sizes. Regardless of the two-dimensional appearance, Gaudin treated each particle equally. For the case of composite particles, the volume fraction of each grain was estimated by estimating the areal fraction of each grain and equating that to the volume fraction. This compensated for the orientation effect which created an apparent size distribution in a monosized sample.

Gaudin also defined a "locking factor" to correlate the area measurement to the three-dimensional reality of the composite particles. His locking factor was used to cancel out the overestimation of the apparent liberation as obtained from the two-dimensional measurement.

In recent years, efforts have been made to develop an experimental methodology aimed at providing reliable estimates of the volumetric grade distribution function as a measure of the extent of mineral liberation in any given population of particles. Stewart and Jones (1977) proposed correction factors for linear analysis, based on the stereological analysis of simple geometrical bodies, to estimate the relative abundance of liberated and composite particles in any specific mineral sample. Barbery et al. (1979) used computer simulation to access particle

composition distribution. Further, by use of a Monte Carlo simulation technique, Jones and Horton (1978) obtained fairly detailed information regarding the distribution of random chord lengths through composite particles of regular shape (sphere, cube, etc.). King (1982) proposed a mathematical relationship between linear intercept analysis of polished ore samples and three-dimensional grade distributions. At ICAM '84, Barbery presented a review of these methods. Most recently, Bloise et al. (1984) examined the bias for both linear and areal analysis and possible mathematical methods to obtain the volumetric abundance. Current work at the University of Utah (Lin et al., 1985, 1986) is involved with the development of a methodology for the prediction of volumetric grade distribution from one- or two-dimensional information regarding the composition of mineral particles of specific size. They show that linear or areal grade distribution can be transformed to an estimate of the volumetric grade distribution via a transformation function, or a conditional probability function. In its most abbreviated form, liberation analysis is simply a measure of the fraction of a particular phase that is free from all other phases, i.e., liberated, without regard to distribution of grade or particle size. In this regard, Petruk (1978) determined the bias of the abbreviated form of liberation analysis from areal grade measurements by

image analysis.

With the advent of modern image processing equipment, area-based techniques of textural analysis are becoming more common. Hard-wired instruments, such as the Quantimet 720, have been available since 1969, but the more recently developed computer-interfaced analyzers are much more flexible. These include Geoscan (Jones and Shaw, 1973) and QEM*SEM (Miller, Reid and Zuiderwyk, 1982), which are both based on linear techniques, the former using a moving microprobe and the latter using a scanning electron microscope. An area-measurement instrument makes the necessary measurement very rapidly and can provide the first size moments of the volumetric particle size distribution. The line-measuring devices, however, operate more slowly than the area-measuring devices, but provide a greatly improved phase discriminating capability. Because of the loss of one "order" of information, it is only possible to justify the calculation of the first three moments of the particle size distribution from linear data. A computer-interfaced system at Virginia Tech, GIPSY (General Image Processing System), has the capability of performing both area-based and linear-based measurements. GIPSY has been extensively tested on sulfide mineral liberation (Craig et al., 1982; Pong et al., 1983). More recently, the IBAS system manufactured by Zeiss has proven to be a useful tool

for identifying and classifying composite particles (Lin et al., 1984, 1985).

1.3 Scope of the Present Investigation

The general objective of the present investigation is to develop a model for representing the combined processes of size reduction and mineral liberation. The model being proposed is based on an extension of the population balance model for grinding to include the liberation behavior of a binary ore. Along with the breakage rate and breakage distribution functions required for all component minerals and composite particles, a liberation function has been introduced to describe the fraction of a composite particle breaking into free particles. In the present work, a detailed parameter estimation scheme has also been developed to determine the model parameters from image analysis data obtained from the batch grinding of monosized feed materials. An emphasis of this work is to learn the properties of the various model parameters through experiments. The validity of the size reduction/liberation model has been demonstrated for the batch grinding of a sphalerite ore from Tennessee. The specific objectives of this investigation have been as follows:

(1) To characterize the liberation of component minerals from a binary ore using an image analysis system.

(2) To develop a model capable of describing the size distribution of both free and composite particles during comminution, which will provide detailed information on mineral liberation.

(3) To develop methods which estimate breakage and liberation parameters for a two-component grinding system from experimental data.

(4) To extend the capability of the model to accomodate multiple classes of composite particle.

(5) To validate the model for the cases of dry batch grinding of monosized and multisized feed distribution.

CHAPTER II.

MODEL DEVELOPMENT

2.1 Model Description

2.1.1 Introduction

As a logical extension of the grinding models developed over the past twenty years, it is now appropriate and possible to include liberation as a direct part of a size reduction model. Computer techniques have been available for some time to estimate the numerous parameters contained in these models; however, it has been possible only recently that the process of liberation can be characterized by the recent advancements in image analysis systems. The breakage parameters of both free and composite particles can now be determined experimentally and models can be validated.

The model being presented here is based on an extension of the population balance model developed for grinding to include the liberation behavior of a binary ore. While more complex systems could be modeled, a binary ore was used for mathematical simplicity. To facilitate the handling of computations, the mass balance equation (Eq. [1.1]) given

in Section 1.2.1 can be expressed in matrix form as

$$\frac{d\hat{M}}{dt} = (\underline{BS} - \underline{S})\hat{M}, \qquad [2.1]$$

where $\hat{M}$ is the mass size distribution of the material in the mill at any time, t, $\underline{B}$ is the breakage function matrix, and $\underline{S}$ is the selection function matrix. Thus, $d\hat{M}/dt$ represents the mass change in each size fraction as grinding proceeds. Extension of the above model is presented in greater detail in the next section.

2.1.2 A Combined Size Reduction/Liberation Model

Figure 2.1 illustrates the process of breakage for a binary mineral system with respect to both size and mineral content. The binary system is represented by free A particles (perhaps a valuable mineral), free B particles (perhaps gangue), and composite AB particles (middling). The breakage of free A and B particles is represented by a simple size reduction process since no change in mineral composition can occur. Composite AB particles, on the other hand, can produce free A particles, free B particles, and several classes of AB combinations. Therefore, a mass balance of material having a given mineral content and reporting to a given size class is composed of two components: material which remains in the same mineral

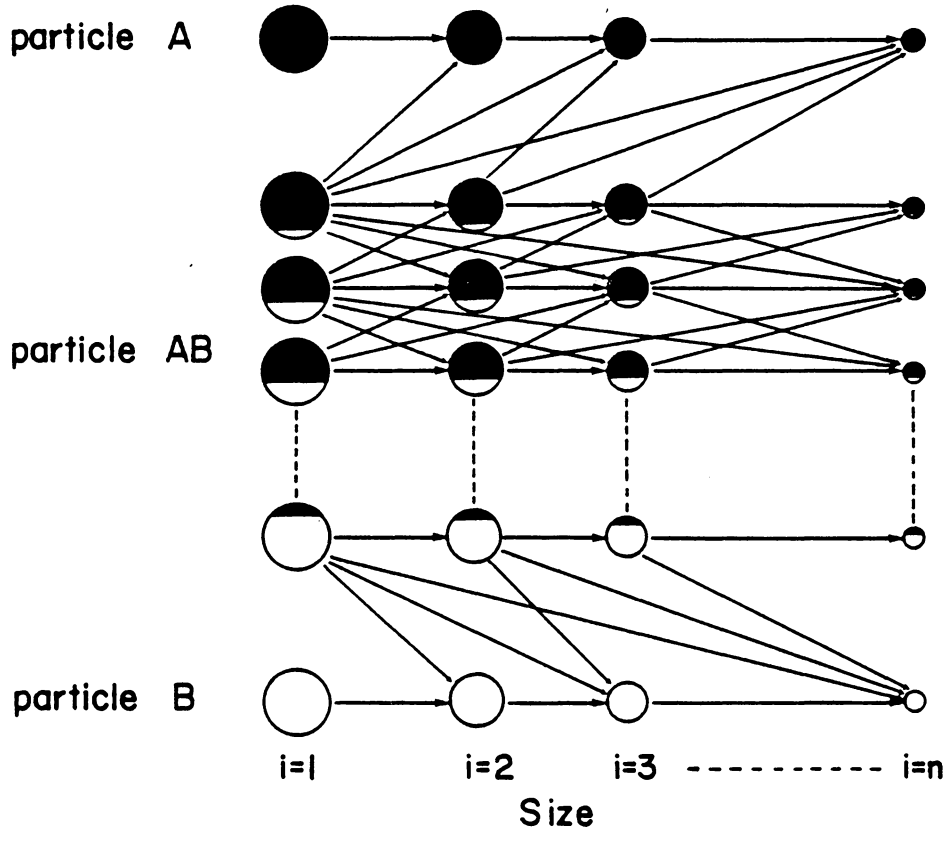

Figure 2.1. Schematic representation of the breakage of a binary ore.

content class and is simply reduced in size, and material which is liberated into and out of the mineral content class being considered. The first component is described by the classical population balance model for grinding. The second component, however, requires introduction of a term to describe the liberation of material from various size and mineral classes. This term is being referred to here as L, the liberation distribution function.

For the case of batch grinding and one class of AB composite material, the matrix form of the mass balance model describing the size reduction/liberation process is given by:

$$\frac{d\hat{M}_a}{dt} = (\underline{B}_a - \underline{I})\underline{S}_a\hat{M}_a + \underline{L}_a\underline{S}_{ab}\hat{M}_{ab} \qquad [2.2]$$

$$\frac{d\hat{M}_b}{dt} = (\underline{B}_b - \underline{I})\underline{S}_b\hat{M}_b + \underline{L}_b\underline{S}_{ab}\hat{M}_{ab} \qquad [2.3]$$

$$\frac{d\hat{M}_{ab}}{dt} = (\underline{B}_{ab} - \underline{I})\underline{S}_{ab}\hat{M}_{ab}, \qquad [2.4]$$

where the variables are defined as:

$\hat{M}_a$, $\hat{M}_b$, $\hat{M}_{ab}$ = mass fraction of particle type A, B, or AB contained in each size class.

$\underline{B}_a$, $\underline{B}_b$, $\underline{B}_{ab}$ = breakage distribution matrix for A, B, or

AB type particles (i.e., the fraction of primary breakage product of type A, B, or AB reporting to each size class).

$\underline{S}_a$, $\underline{S}_b$, $\underline{S}_{ab}$ = selection function (breakage rate) matrix for A, B, or AB type particles (i.e., the rate at which material breaks out of each composition class).

$\underline{L}_a$, $\underline{L}_b$ = liberation distribution matrix for A or B type particles (i.e., the fraction of primary breakage product of type AB which reports to another size class as free A or free B).

It should be noted in Equations [2.2] and [2.3], describing the free particles, that the first term in each equation represents appearance and disappearance in each size class due to breakage, and the second term represents appearance in each size class due to liberation from composite particles. The same term can also be found in Equation [2.4], describing the fate of the composite particles, which represents appearance and disappearance due to breakage. Thus, for the case of one composite particle class, all possible changes in size and mineral content are accounted for by these equations. By definition, the sum of all mass fractions at any time t, must equal one:

$$\sum_{i=i}^{N} [m^{a}{}_{i}(t) + m^{b}{}_{i}(t) + m^{ab}{}_{i}(t)] = 1. \qquad [2.5]$$

Here, $m^{a}{}_{i}$, $m^{b}{}_{i}$ and $m^{ab}{}_{i}$ are the mass fraction of material A, B, and AB, respectively, in the i-th size interval and N refers to the number of size intervals.

In order to satisfy the mass conservation of AB material, the total sum of cumulative breakage function of composite AB material and cumulative liberation functions of A and B material must be unity, or:

$$\sum_{i=j+1}^{N} (b^{ab}{}_{ij} + l^{a}{}_{ij} + l^{b}{}_{ij}) = 1.$$

$$\text{For each } j,\ 1 \leq j \leq N-1 \qquad [2.6]$$

In the above notation, $b^{ab}{}_{ij}$, $l^{a}{}_{ij}$ and $l^{b}{}_{ij}$ represent the size-discretized breakage function and liberation functions for AB, A, and B material, respectively.

When the breakage rate and breakage distribution functions are independent of both the size consist in the batch mill and time, the kinetic model is linear with respect to the coefficients. This will be the case developed here. Under such conditions, Equations [2.2], [2.3], and [2.4] represent a set of 3N simultaneous linear differential equations. These 3N equations have been solved simultaneously using the Runge-Kutta numerical method.

2.1.3 Model Extension with Multiple Classes of Composite Particles

In order to better understand the liberation mechanisms of composite particles, the model has been extended to include multiple classes of composite particles. For the case of batch grinding and multiple AB composite classes, the matrix form of the mass balance model becomes;

$$\frac{d\hat{M}_a}{dt} = (\underline{B}_a - \underline{I})\underline{S}_a\hat{M}_a + \underline{L}_a \sum_{i=1}^{J} \underline{S}_{ab,i}\hat{M}_{ab,i} \qquad [2.7]$$

$$\frac{d\hat{M}_b}{dt} = (\underline{B}_b - \underline{I})\underline{S}_b\hat{M}_b + \underline{L}_b \sum_{i=1}^{J} \underline{S}_{ab,i}\hat{M}_{ab,i} \qquad [2.8]$$

$$\frac{d\hat{M}_{ab,j}}{dt} = (\underline{B}_{ab,j} - \underline{I})\underline{S}_{ab,j}\hat{M}_{ab,j} + \sum_{\substack{i=1 \\ i\neq j}}^{J} \underline{L}_{ab,j\leftarrow i}\underline{S}_{ab,i}\hat{M}_{ab,i}, \qquad [2.9]$$

Where the new terms are defined as follows:

$\hat{M}_{ab,j}$ = mass fraction of particle type AB_j contained in each size class.

$\underline{B}_{ab,j}$ = breakage distribution matrix for AB_j type particles.

$\underline{S}_{ab,j}$ = selection function (breakage rate) matrix for AB_j type particles.

$\underline{L}_{ab,j\leftarrow i}$ = liberation distribution matrix for AB_i type particles (i.e., the fraction of primary breakage product of type AB_i which liberates into the jth composition class).

i, j = a specific composite particle class.

J = total number of composite particle classes.

As in the previous section, in Equations [2.7] and [2.8], the first term in each equation represents appearance and disappearance in each size class due to breakage, and the second term represents appearance in each size class due to liberation from various composite particles. The same terms can also be found in Equation [2.9] representing the fate of the composite particles; the first term describes appearance and disappearance due to breakage and the second term describes appearance due to liberation. The final term of this equation accounts for the appearance of AB particles in this class due to liberation from other composite classes. Thus, all possible changes in size and mineral content for multiple classes are accounted for by these equations. Furthermore, it should be noted that when only one class of composite particles is considered, the $\underline{L}_{ab,j\leftarrow i}$ terms drop out and the above three equations reduce to the form described in the previous section.

It can be noted from Equations [2.7] and [2.8] that

the amount of material which liberates into particle type A or type B from composite particle type AB is the same whether the AB particles are represented with one class or J classes. Since $\underline{L}_a$ and $\underline{L}_b$ represent the fraction of primary breakage product of type AB which liberates into type A or type B, however, $\underline{L}_a$ and $\underline{L}_b$ in Equations [2.7] and [2.8] actually represent "mean" values for all AB classes.

Equation [2.9] can be considered as the basis for a general form of the entire model. For example, by considering free A and B particles as extreme cases of the AB composite class, Equation [2.9] can be modified to give:

$$\frac{d\hat{M}_k}{dt} = (\underline{B}_k - \underline{I})\underline{S}_k\hat{M}_k + \sum_{\substack{i=2 \\ i\neq k}}^{K-1} (\underline{L}_{k\leftarrow i}\underline{S}_i\hat{M}_i), \qquad [2.10]$$

which encompasses all possible cases described by Figure 2.1 in one matrix equation. In this representation, k is the specific mineral content class out of a total of K classes. All other terms are as defined previously. Therefore, Equation [2.10] is the general expression for the combined size reduction and liberation model in which the composite particles are subdivided into K-2 classes.

2.2 Parameter Estimation

2.2.1 Introduction

The determination of the breakage and liberation parameters is a necessary prerequisite for the application of the combined size reduction-liberation model to a real grinding system. A number of methods have been described in the literature for the determination of breakage rate (S_i) and breakage distribution (b_{ij}) parameters, although some of the methods are based on various restrictive and simplifying assumptions. Several graphical methods (Austin and Bhatia, 1972; Herbst et al., 1974) are available to estimate both sets of breakage parameters for single component grinding. They are generally based on the measurement of initial slopes from plots of mass fraction versus time for a single size fraction being milled. Alternate methods of estimating parameters for a linear, lumped-parameter grinding model have been developed. Several of these are based on non-linear regression methods. A Goldfarb and Lapidus optimization method was used by Austin and Klimpel (1977) to estimate selection functions. The procedure used at the University of Utah (Herbst et al., 1972, 1977) is a modified Gauss-Newton technique. Clearly, it would be possible to represent many of the model parameters with functional forms and greatly simplify the experimental aspects of this work. However, it is important to have a clear understanding of

all model parameters before too many simplifying assumptions are made for developing functional forms. In the present work, therefore, emphasis has been placed on the experimental determination of model parameters as much as possible. The majority of the model parameters have been directly determined using computerized image processing equipment to analyze the products from batch grinding tests. The parameter estimation scheme developed here is an extension of those methods used in the customary single-component case that are based on the batch grinding of single size fractions for short times.

2.2.2 Direct Determination of Breakage Parameters Using Image Analysis

As described in the introductory section, the basic approach used in this investigation has been to directly measure as many of the parameters as possible using the technique employed for batch grinding monosized feeds (Herbst and Fuerstenau, 1968). For example, breakage rate functions for all components can be determined by following the disappearance of each component from a monosized feed. Assuming all material breaks to finer size classes, the slope of the disappearance plot gives the breakage rate function value for a given feed size. Since the fractions of A, B, and AB particles in the feed can be measured by

image analysis, all three breakage rate functions can be determined from the same series of grinding tests.

In order to estimate the breakage distribution and liberation distribution functions, it is necessary to apply the concept of zero-order fines production to the breakage-liberation model. Equations [2.2]-[2.4] are first written in cumulative form to give:

$$\frac{d\hat{Y}_a}{dt} = \overline{\underline{B}}_a \underline{S}_a \hat{M}_a + \overline{\underline{L}}_a \underline{S}_{ab} M_{ab} \qquad [2.11]$$

$$\frac{d\hat{Y}_b}{dt} = \overline{\underline{B}}_b \underline{S}_b \hat{M}_b + \overline{\underline{L}}_b \underline{S}_{ab} M_{ab} \qquad [2.12]$$

$$\frac{d\hat{Y}_{ab}}{dt} = \overline{\underline{B}}_{ab} \underline{S}_{ab} \hat{M}_{ab}, \qquad [2.13]$$

where the new terms are defined as:

$\hat{Y}_a$, $\hat{Y}_b$, $\hat{Y}_{ab}$ = the cumulative mass fraction of A, B, or AB finer than a given size.

$\overline{\underline{B}}_a$, $\overline{\underline{B}}_b$, $\overline{\underline{B}}_{ab}$ = the cumulative breakage function matrix.

$\overline{\underline{L}}_a$, $\overline{\underline{L}}_b$ = the cumulative liberation function matrix.

In Equations [2.11]-[2.13], all terms are constant except $\hat{Y}$ and $\hat{M}$ which are functions of time. In the limit as

time goes to zero (i.e., for short grinding times), however, little breakage takes place. Thus, $\hat{M}_a$, $\hat{M}_b$, and $\hat{M}_{ab}$ become the mass fractions of A, B, and AB material in the feed. Furthermore, the derivatives on the left-hand side of Equations [2.11]-[2.13] can be determined from the initial slopes of the standard zero-order production plots for each mineral component. This leaves three equations with five unknowns (i.e., the cumulative breakage distribution functions and the cumulative liberation distribution functions). Equations [2.11] and [2.12], however, can be used to solve directly for $\underline{B}_a$ and $\underline{B}_b$, provided that the amount of AB material in the monosized feed sample is small compared to the free A or free B material. This condition can be satisfied by using a monosized feed which is small enough to be sufficiently liberated, and by assuming that the breakage functions so determined are normalizable with respect to feed size. This is the only assumption needed other than those inherent in the model derivation. The assumption of breakage function normalizability will be verified in Chapter IV.

Therefore, in Equations [2.11]-[2.13], all parameters can be determined directly from experimental data except $\underline{L}_a$, $\underline{L}_b$ and $\underline{B}_{ab}$. These three matrices can be calculated from Equations [2.11]-[2.13], however, if feed size normalizability is assumed for the unknown parameters, and

if zero-order slopes are now measured using a coarser monosized feed having a substantial amount of composite material.

For the case of multiple AB composite classes, Equations [2.7]-[2.9] can be written in cumulative form to give:

$$\frac{d\hat{Y}_a}{dt} = \bar{B}_a \underline{S}_a \hat{M}_a + \bar{\underline{L}}_a \sum_{i=1}^{J} \underline{S}_{ab,i} \hat{M}_{ab,i} \qquad [2.14]$$

$$\frac{d\hat{Y}_b}{dt} = \bar{B}_b \underline{S}_b \hat{M}_b + \bar{\underline{L}}_b \sum_{i=1}^{J} \underline{S}_{ab,i} \hat{M}_{ab,i} \qquad [2.15]$$

$$\frac{d\hat{Y}_{ab,j}}{dt} = \bar{B}_{ab,j} \underline{S}_{ab,j} \hat{M}_{ab,j} + \sum_{\substack{i=1 \\ i \neq j}}^{J} \bar{\underline{L}}_{ab,j \leftarrow i} \underline{S}_{ab,i} \hat{M}_{ab,i} \,. \qquad [2.16]$$

When considering multiple classes of composite particles, the estimation of some of the model parameters, such as the liberation function, becomes much more difficult. For the case of two composite classes, the values determined previously for $\underline{L}_a$ and $\underline{L}_b$ are still valid. Therefore, the two equations arising out of Equation [2.16] must be used to determine the remaining four parameters, i.e., $\underline{L}_{ab,1\leftarrow 2}$, $\underline{L}_{ab,2\leftarrow 1}$, $\underline{B}_{ab,1}$, and $\underline{B}_{ab,2}$. In this preliminary application of the model for multiple composite classes, it has been assumed that the cumulative breakage

functions and liberation functions for composite particles can be estimated from their component parts in proportion to the volume fraction of each part present in the composite particle.

CHAPTER III.

EXPERIMENTAL PROCEDURES

3.1 Ore Sample

The ore sample used in the present work was a coarse-grained sphalerite ore obtained from ASARCO's Young Mine in Eastern Tennessee. This mine treats approximately 7,700 tons/day of 3% zinc. At the Young mill, ore goes through four basic processing stages, including two-stage crushing, dense media separation (DMS), ball mill grinding and flotation. The DMS process is designed to operate at a rate of 250 tons/hr. By utilizing the specific gravity differential of sphalerite (S.G.=4.0) and dolomite (S.G.=2.8), the DMS sinks the heavier zinc-bearing particles and floats 77% of the feed as coarse tailings. The separation takes place at 2.84 specific gravity obtained by using a mixture of 100- to 200-mesh ferrosilicon medium (Li, 1976).

A 400-pound sample of ore, containing approximately 12% zinc, was taken from the coarse concentrate stream from the dense media separator. Because of its large liberation size (35x48 mesh) and the fact that it very nearly approximated a binary mixture of sphalerite and dolomite (see Figure 3.1), the sample was ideally suited for the present work. Approximately 100 pounds of the dolomite gangue was also

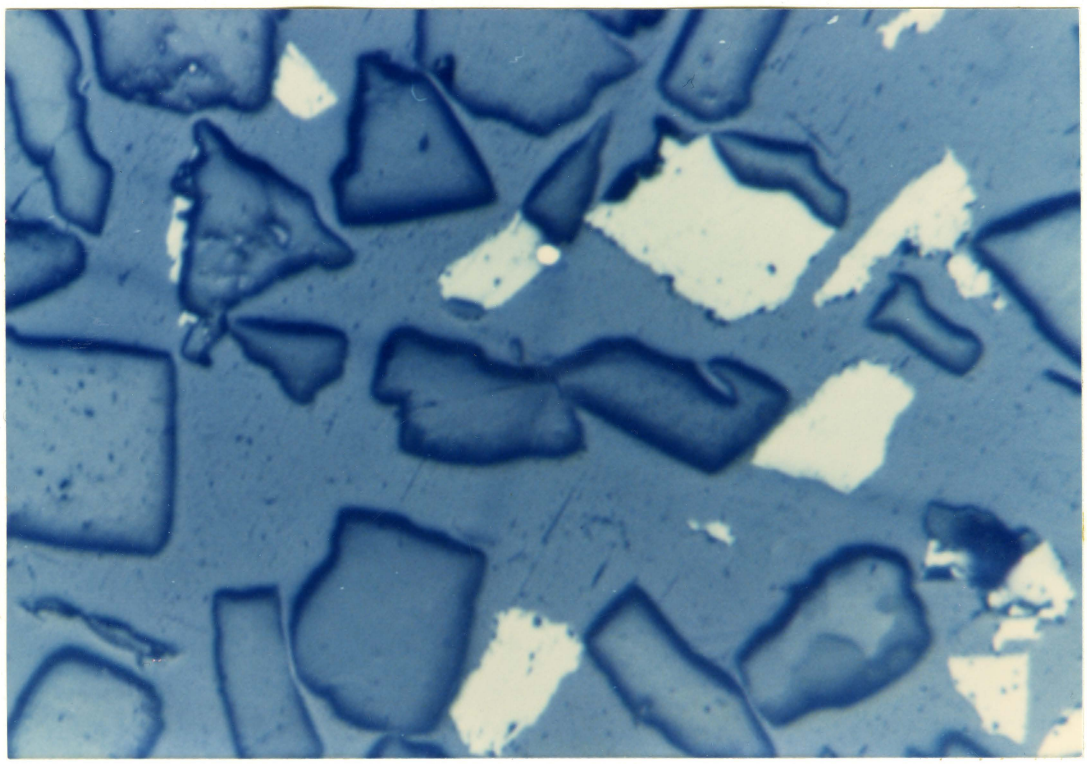

Figure 3.1. Photomicrograph of a coarse-grained sphalerite ore (20x28mesh) obtained from Asarco's Young Mine, Tennessee, showing near approximation to a binary mixture of sphalerite (bright) and dolomite (dark).

taken from the tailing stockpile site (DMS rejected materials). This sample contained approximately 0.3% zinc. This relatively pure gangue sample was used for batch grinding experiments in order to compare the grinding parameters determined using both pure and composite materials.

3.2 Grinding and Sizing Equipment

3.2.1 Grinding Equipment

Batch grinding experiments were conducted in a stainless steel mill, 25.4 cm in diameter and 29.2 cm in length. The mill was mounted on roller bearings, and a torque transducer was incorporated into the drive shaft to measure the torque. Yang et al. (1968) have described the details of the mill and its performance characteristics. The mill was charged with 30 kg of 2.5-cm steel balls, providing a volume filling of approximately 50%.

3.2.2 Sizing Equipment

Eight-inch diameter Tyler series sieves (from 10 mesh down to 400 mesh) were used in conjunction with a Ro-Tap shaker to determine the particle size of the mill products. The weights of the screen products were determined using on a Mettler balance that has an accuracy of $\pm$0.01 grams.

3.3 SEM-IPS Image Analyzer

A Scanning Electron Microscope-Image Processing System (SEM-IPS), manufactured by Kontron, was used for this study (see Figure 3.2). It is designed to accept image data and energy dispersive data directly from an SEM. The image can also be acquired from standard video input or from microscope photometer sources as well. The primary goal of this instrument is to provide quantitative evaluation of images on either a field- or object-specific basis. The main features of the SEM-IPS image analysis system are shown schematically in Figure 3.3. The main components are briefly described below;

(1) The host processor is a Z80A-based microcomputer with a 64K memory that allows fast calculation of image-extracted data, and free programmability. For storage of programs and data, the computer is provided with a 20 MByte Winchester hard disk drive and a 600 KByte floppy disk drive. No user access to the hard disk unit is necessary for operation of the IPS system.

(2) A 1-MByte image array processor, expandable to 16 MByte, is used for real-time image storage and manipulation, fast calculations and on-line storage of grey level pictures.

(3) A black and white monitor is used for communication and to display data, graphics, and instructions.

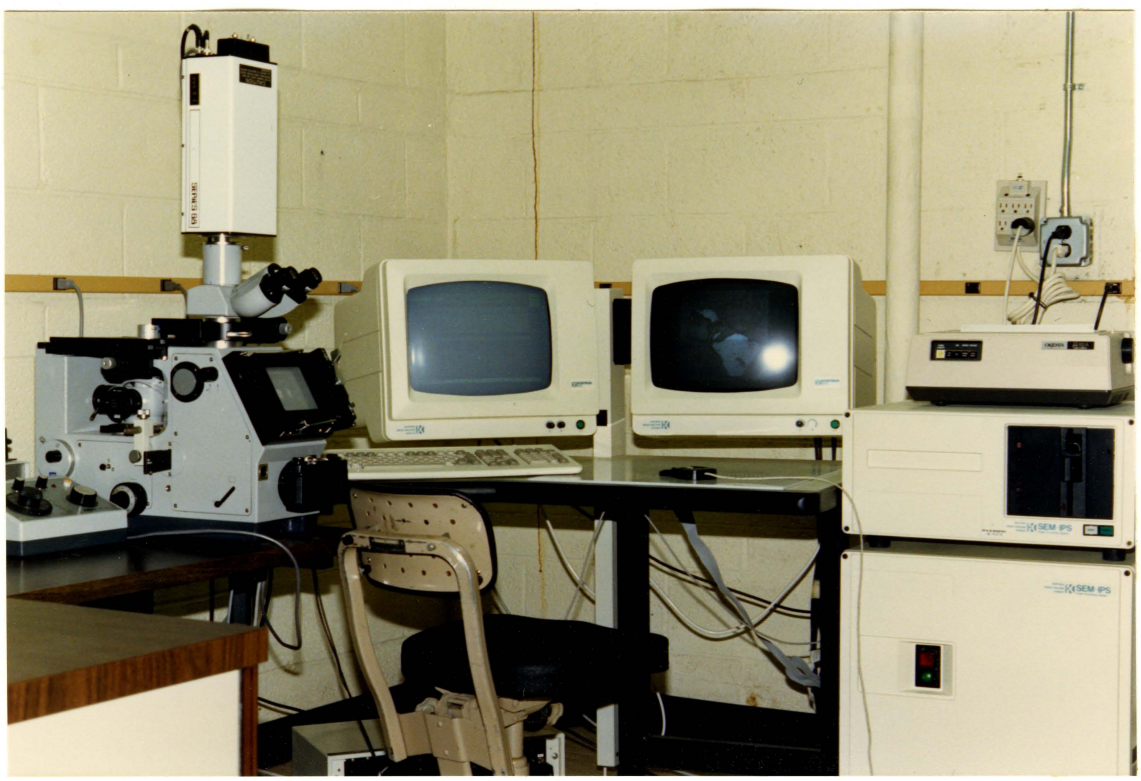

Figure 3.2 SEM-IPS image analyzer.

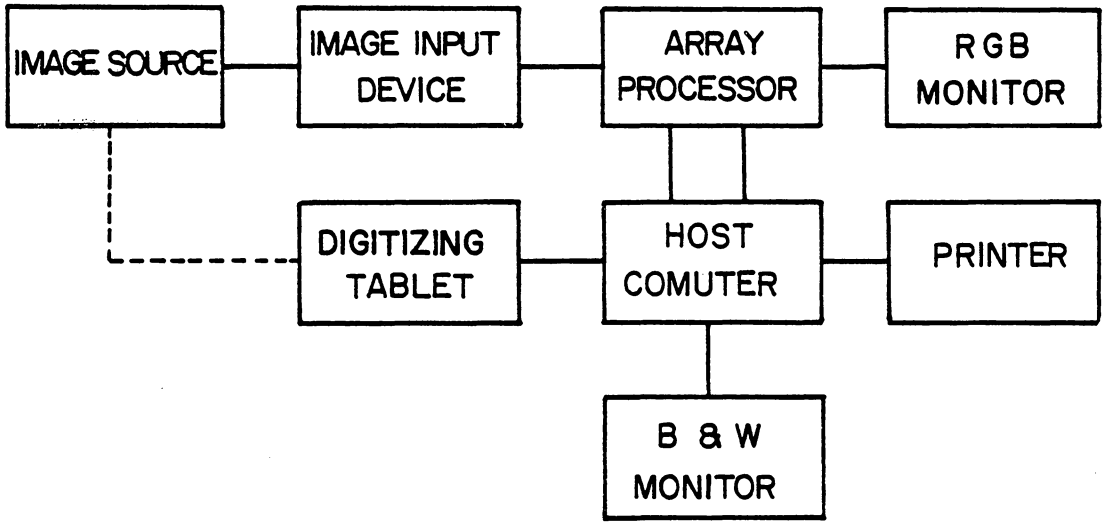

Figure 3.3 SEM-IPS (hardware) system.

(4) A color RGB monitor, 800x600 pixel, 0.3 mm resolution, is employed for image display.

(5) A fast analog-to-digital convertor provides the user with several options in image input devices: video, microscope, SEM, photometric. In the present work, the microscope (Zeiss Inverted Camera Microscope, Type 405) with a mounted television camera (MTI 68 Series) is used as an image input device.

(6) A digitizer tablet with crosshair cursor is used for interactive measurement and image manipulation.

(7) An ASCII keyboard is available for user commands and inputs, feature selection, and programming.

(8) A printer (OKIDATA, Microline 82A Type) provides a hard copy of the results and programs.

(9) Software (IPS) is used for the enhancement and processing of stored grey images. It is also used for extraction of the feature of interest from the grey-level image and for measurements of geometrical properties.

Regardless of how the digital image is obtained, the rest of the steps in the process are the same. The basic goal is to separate the objects of interest (those to be measured or counted) from the background of the image. This step is called segmentation or discrimination. The objects are usually segmented by a grey level thresholding step in which pixels with grey values within a range determined by

the operator have their grey values converted to a binary 1. All other pixels in the image are converted to binary 0. This binary image is a simple black-and-white picture of the objects of interest. This binary image can then be used to make measurements of either the field- or object-specific type. The result of such measurements would generate a size distribution histogram for the particles.

Segmentation or discrimination can be aided by a number of image processing procedures such as spatial filtering, grey level stretching, edge enhancement, etc. Once the image has been segmented, the binary image can be further manipulated to remove or ignore any object not of interest, but which may segment from the background in the same grey level range as the objects of interest. This can be accomplished by imposing size or shape limits on further measurements. The operator can also interactively edit either the grey level or the binary image.

Results of the image processing steps are displayed on a high resolution RGB monitor. Command prompts, the system menu and data lists are displayed on the host processor monitor. User interaction with the system is via a combination of keyboard inputs and choices selected from a menu on the host monitor. The menu choices are selected through the digitizing pad using a small cursor (now commonly called a "mouse"). This combination of menu-driven

and keyboard-selected interaction is very efficient given the large number of available functions the operator has to remember. There are more than 100 image processing functions available on the IPS.

The functions of the system are organized into groups, ranging from image input, enhancement, segmentation, identification, and measurement to utilities which handle image storage on floppy disk, memory clearing etc. The string of commands chosen by the operator is storable, editable and executable. So, once one has defined the necessary steps for processing certain images, those steps can be executed by a single keystroke without further operator intervention, or with intervention only at certain necessary steps along the way.

3.4 Experimental Procedure

3.4.1 Sample Preparation

Each ore sample was crushed to -10 mesh by passing it through laboratory crushers. The large pieces of ore were crushed by passing through a 5 x 6 -inch laboratory jaw crusher. The jaw crusher discharge was then passed through a hammer mill (8 x 6.5 -inch) until all the material passed through a 10-mesh screen. The samples of single size fractions were obtained by sieving the -10 mesh sample.

3.4.2 Grinding Experiments

All of the grinding tests were carried out using the laboratory ball mill described in Section 3.2.1. In each grinding experiment, a 3000-gram sample was ground. To determine the breakage rates, the monosized samples were dry-ground for varying time intervals of 1, 2, 4, and 6 minutes. At the end of each grinding time, the mill was kept stationary for approximately 5 minutes to allow the fines to settle to the bottom of the mill. The mill was then inverted into a collection pack to remove the sample and grinding media. To ensure complete removal of the sample, particles adhering to the grinding media and to the interior of the mill were brushed off. The ground product was then split into eight samples and the samples were dry-screened on a Ro-Tap sifter for 15 minutes to produce size

fractions ranging from 10 mesh to 400 mesh. Following dry screening, each size fraction was manually wet-screened to remove excess fines. As a means of independently validating the model, batch grinding tests were also carried out on multisized feed materials.

The product size distributions obtained for each series of grinding experiments are given in Appendix IV.

3.4.3 Size Analysis

The screening was done using 8-inch diameter Tyler series sieves ranging from 10- to 400-mesh. A mechanical shaker (Ro-Tap) was used for dry-screening. Most of the samples were usually screened for 15 to 20 minutes, depending on the fineness of the material. The amount of sample used for sieve analysis varied from approximately 150 to 300 grams. Following dry-screening, each size fraction was manually wet-screened to remove excess fines. At the end of each sieve analysis, each size fraction was weighed to check the loss of material. The loss was always less than 0.1% of the total charge.

3.4.4 Briquetting and Polishing

Representative portions of each size fraction were first treated with ethanol to help disperse the particles, and then mounted in a cold setting resin (EPOFIX Epoxy).

The particle mounts were prepared in two different ways. In method A, the particles were mixed with a small amount of resin and set aside to harden for about 30 minutes before filling the remaining volume of the mold with resin and allowing it to harden for approximately 24 hours. In method B, the briquette, prepared as such, was cut vertically and the slices were remounted in the epoxy resin. The particle mounts prepared as such were polished using a 600-grit metal-bonded diamond lap followed by polishing on a canvas using a 600-mesh silicon carbide. The final polishing was accomplished over a period of 24-72 hours using 0.05-micron alumina in a Syntron polishing machine.

3.4.5 Liberation Analysis

The image processing steps were usually performed as shown in Figure 3.4. The analog image from the optical microscope is first digitized through the TV camera and this digitized grey image is then displayed on the monitor. The features of interest are enhanced and/or processed, followed by extraction. The extraction process usually results in a binary image in which the features are represented as white areas on a black background. Finally, the geometrical properties of this binary image are measured. For the measurement, two different modes (object- or field-specific) can be selected for obtaining the required information.

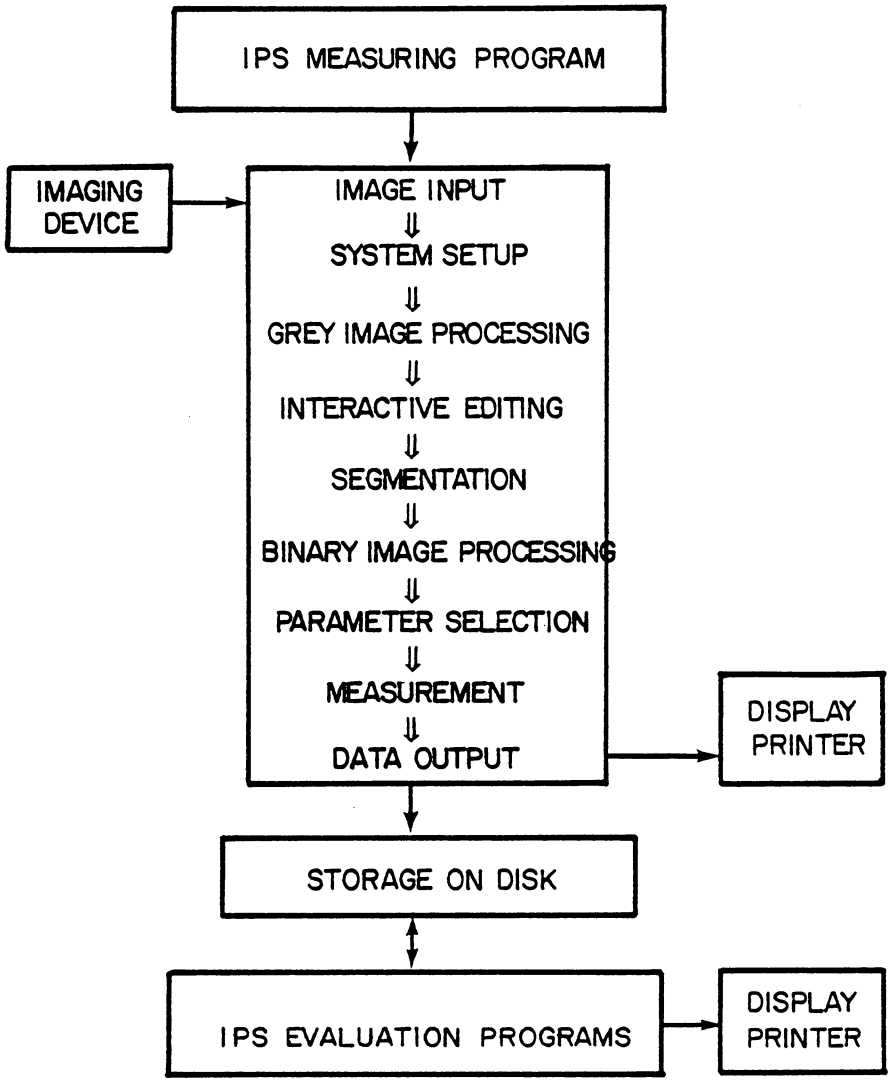

Figure 3.4 Structure of an SEM-IPS measuring program.

In order to obtain liberation data, polished particle mounts were examined using the SEM-IPS image analysis system. This system provided an areal assay of each particle which was assumed to directly correspond to the volumetric assay. All particles were assumed to have the same size in the measurement regardless of the apparent differences seen in the two-dimensional image. This approach was taken since each briquette contained closely-sized, monosized particles. All free particles identified by image analysis were assumed to be totally free and were not adjusted through the use of locking factors. Locked (or composite) particles, on the other hand, were subdivided into ten discrete classes of different compositions to obtain more detailed information. The volume fraction data, determined as such, were converted into weight fractions by multiplying the specific gravity of each component. The assumptions used in this analysis were later verified using chemical assay.

In order to determine the volume fractions for the various classes of composite particles, the IPS program for area fraction measurement has been developed. The basic sequence of this program is shown in Table 3.1. These are the most basic IPS functions. It can be noticed from Table 3.1, however, that the program contained a UPN routine. This routine adds even more flexibility to the IPS measuring

Table 3.1 SEM-IPS program list for area fraction measurement.

AREA FRACTION MEASUREMENT					PRGM # 111
Function	Integer		Variables: Logical	Real	
1. SCALE					
	SCNO	1			
2. UPN					
	NUPN	10			
3. USER					
	NUSE	2		LOW	0.000
	NCLS	10	OBJ	HIGH	1.0000
	MODX	1			
	MODY	1	SINGLE CLASS		
4. LAB:					
	LBL#	2			
5. ID. NO					
6. LAB:					
	LBL#	1			
7. TVON					
			ONLINE		
8. PASUE					
9. TVINP					
	INP	1			
10. NORMGR					
	INP	1			
	OUT	2			
	THRS	1			
11. LOWPAS					
	INP	2		FAC1	1.0000
	OUT	3		FAC2	1.0000
	AUX	7			

Table 3.1 Continued

	SIZX	100	
	SIZY	100	
	CNT	5	
12. SHDEF			
	INP	3	
	SHRF	3	
13. SHADE			
	INP	2	
	OUT	4	
	SHRF	3	
	RG+-	0	
14. PAUSE			
15. MESINT			
	INP	4	
	AUX	7	CLOSE
	CHAN	0	CONTI
			OBJ
16. CLROVL			
	INP	4	
17. OUTCLS			
			HISTO
			HALT
18. GOTO			
	LBL#	1	
19. OUTSGL			
			STORE
			HALT
20. RESET			
			TREAT
			SINGLE
			CLASS
21. GOTO			
	LBL#	2	
22. PAUSE			

TOTAL PROGRAM LENGH 270 BYTES

program by introducing new measurement parameters, defined as a combination of basic parameters like area, perimeter, etc. In the above program, the UPN routine actually calculates the area fraction of the various mineral components contained in the composite particles. All UPN programs are defined by an identification number in the range of 1-999. Therefore, the variable NUPN selects the associated program. All further images of the same series can then be evaluated using this program, with the individual functions being executed automatically or step by step. After completing the measurements, the output data can be displayed using the OUTCLS routine. Figures 3.5a-c illustrate how IPS displays the histogram of the measured data. As shown, data can be obtained either by frequency, or relative frequencies, or cumulative frequencies.

In addition, some liberation data were obtained using the simple planimeter-based image analysis technique. In this case, photographs were taken of the microscope images. An electronic planimeter was then used to measure the areas of the various mineral components contained in a given composite particle.

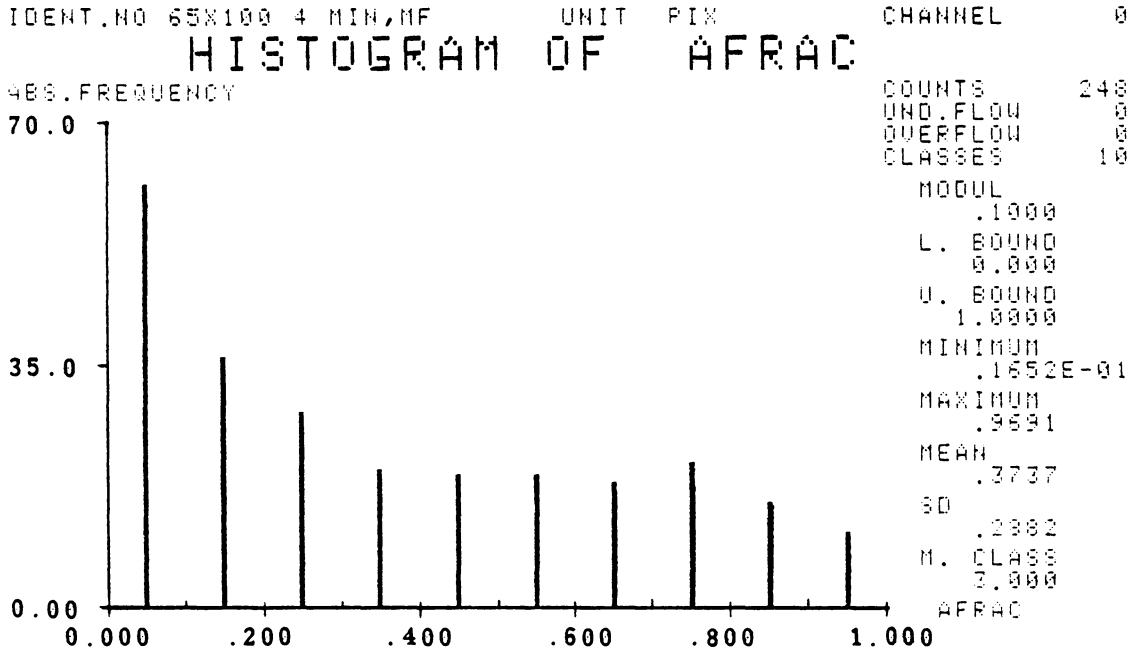

Figure 3.5a. Frequency histogram of area fraction measurements.

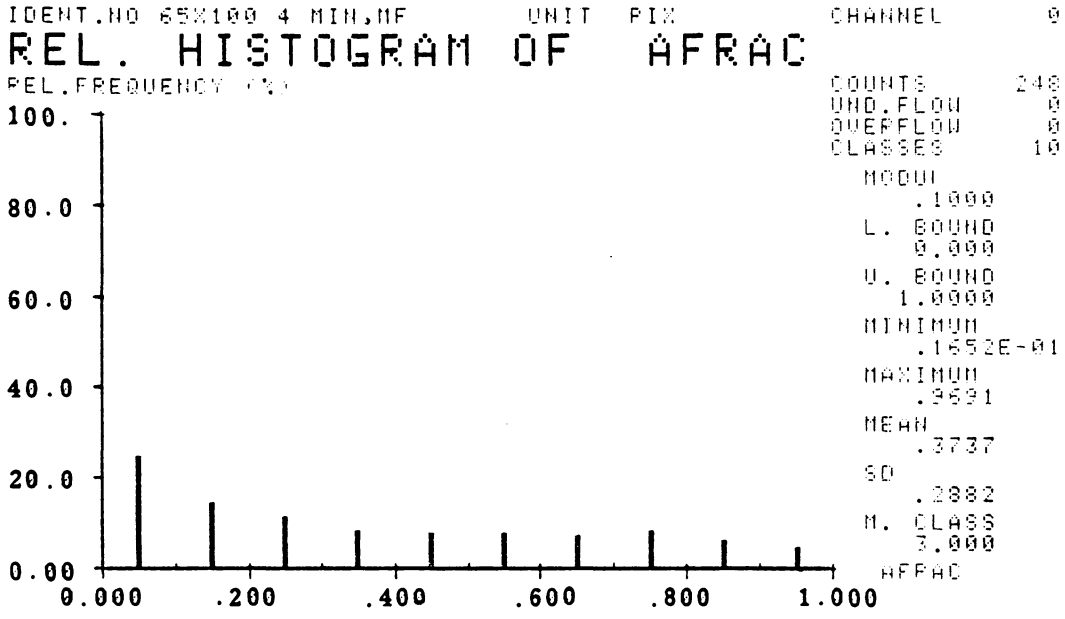

Figure 3.5b. Relative histogram of area fraction measurements.

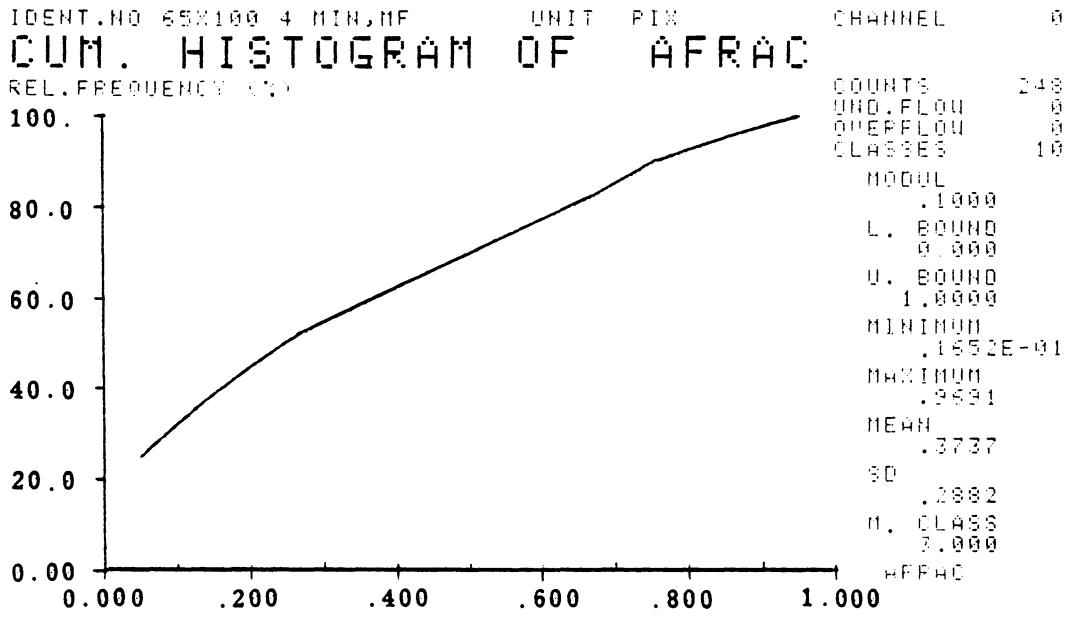

Figure 3.5c. Cumulative histogram of area fraction measurements.

CHAPTER IV.

EXPERIMENTAL RESULTS (MODEL VALIDATION)

In order to verify the proposed model and parameter estimation scheme, a series of batch grinding tests was performed on a coarse-grained sphalerite ore. Some of the important model parameters, such as breakage rate functions, breakage distribution functions and liberation functions, have been determined experimentally by examining samples produced from a batch grimding experiment using the SEM-IPS image analyzer. On the basis of the experimentally determined model parameters, computer simulations of dry batch ball milling were carried out to predict the product size distribution for each component in the ore.

4.1 Sample Characterization

4.1.1 Comparison of Image Analysis Results against Chemical Assays.

Figure 4.1 compares the zinc assays from image analysis with the chemical assays. The particle mounts have been prepared according to method A as described in the previous chapter. With this sample preparation technique, the image analysis gave significantly higher zinc values than did

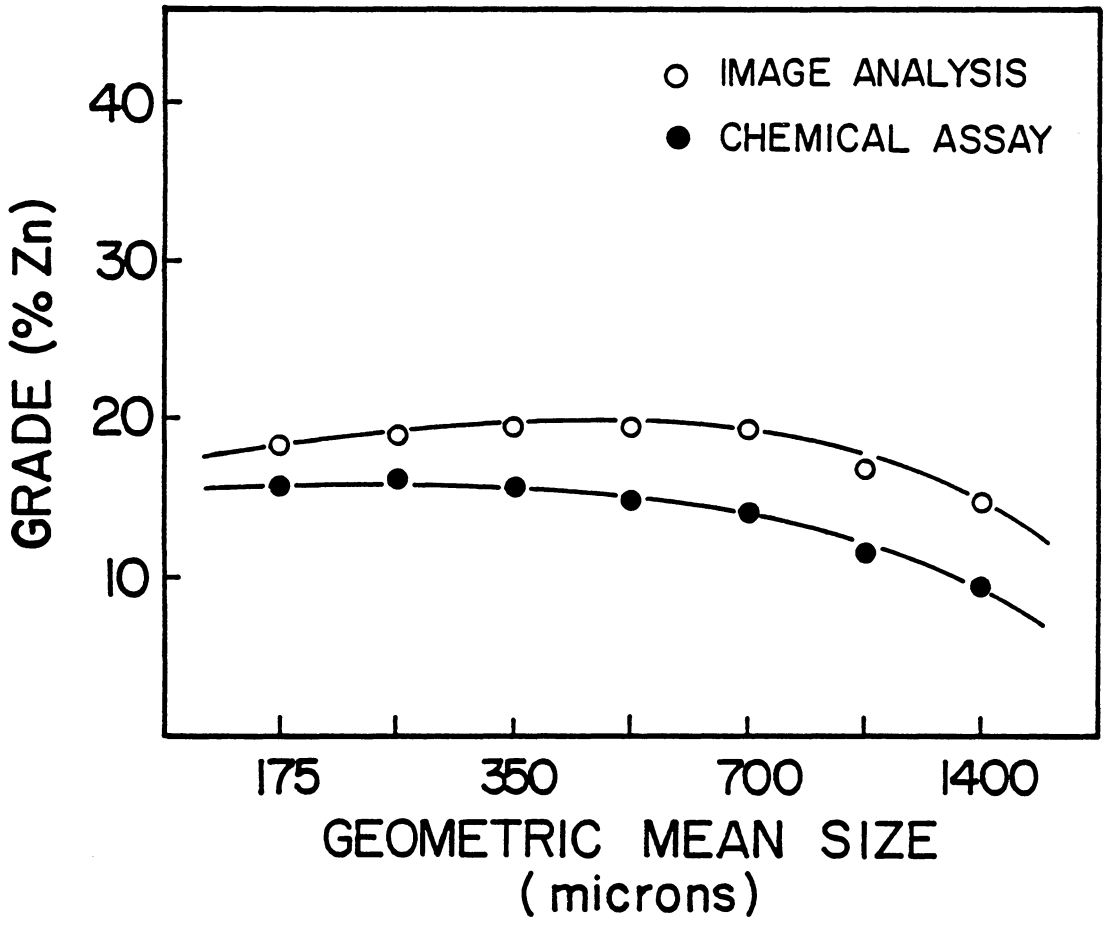

Figure 4.1 Comparison of zinc assay values determined by chemical analysis and image analysis showing orientation effect (monosized feed).

chemical assaying. Several factors may account for this overestimation of zinc content. These include the use of incorrect specific gravity values for the minerals (i.e., not accounting for porosity and impurities), the inherent tendency to overestimate free particles (Gaudin, 1939), and the orientation of heavier sphalerite particles at the bottom of the mold.

The porosity and the amount of impurities in the sphalerite was determined directly by using the SEM-IPS image analysis system. The procedure involved two steps. In the first step, the total area of the white regions representing sphalerite was measured and stored in memory channel 1. This area was taken to be equivalent to the solid volume occupied by the sphalerite. In the second step, the black regions encapsulated within the sphalerite were manually filled in using a digitizing pad, and then the procedure of the first step was repeated. This second value was stored in memory channel 2. This second area was taken to be equivalent to the total volume (i.e., solid volume + pore volume) of the sphalerite. Using this method, the amount of porosity of the sphalerite in the 20 x 28 mesh ore samples was found to be only 1.42%, as shown in Table 4.1. Therefore, the first two possibilities mentioned above cannot be responsible for the discrepancy between the assays determined by the image and chemical analyses. It appears,

Table 4.1 Amount of porosity and/or impurities in the sphalerite particles in the 20x28 mesh samples

Sample No.	1	2	3	4	5	6	Average
Percentage of porosity	1.9	1.2	1.1	1.4	1.2	1.7	1.42%

therefore, that the segregation effect is the most likely reason for this discrepancy.

Although sedimentation of particles can be minimized by careful sample preparation techniques, it is difficult to prevent the heavier portion of a composite particle, such as the sphalerite, from orientating itself in the downward position. This orientation effect is illustrated in Figure 4.2. Furthermore, since the bottom layer of particles in the briquette is restricted by the bottom of the briquette mold, an analysis of this bottom layer will further magnify the orientation effect as compared to an analysis of a horizontal cut taken somewhere above the bottom layer. In fact, a vertical cut through the sample should eliminate the orientation effect, leaving only the locking effect. A comparison of all three analysis methods is shown in Table 4.2 along with the chemical assay of the sample. Table 4.2 clearly shows that the orientation effect is a real phenomenon, and it can be greatly reduced or eliminated by proper analysis procedure.

The results shown in Figure 4.3 provide further evidence that the discrepancy is caused by the segregation effect. In this case, the particle mount was prepared by method B, and assayed by image analysis. There is excellent agreement between the two-dimensional image analysis and the chemical assay. The slight overestimation of the zinc value by the

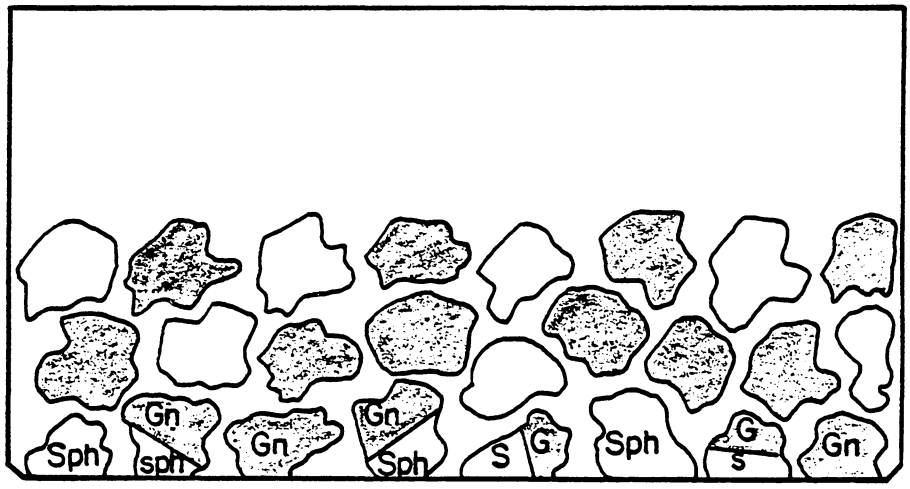

Figure 4.2 Orientation effect in sample briquette.

Table 4.2 Percent zinc in 10x14 mesh fraction determined by different methods.

Image Analysis			
Method A Bottom, no cut	Method B Horizontal cut	Method C Vertical cut	Chemical Assay
13.5%	11.9%	10.5%	8.4%

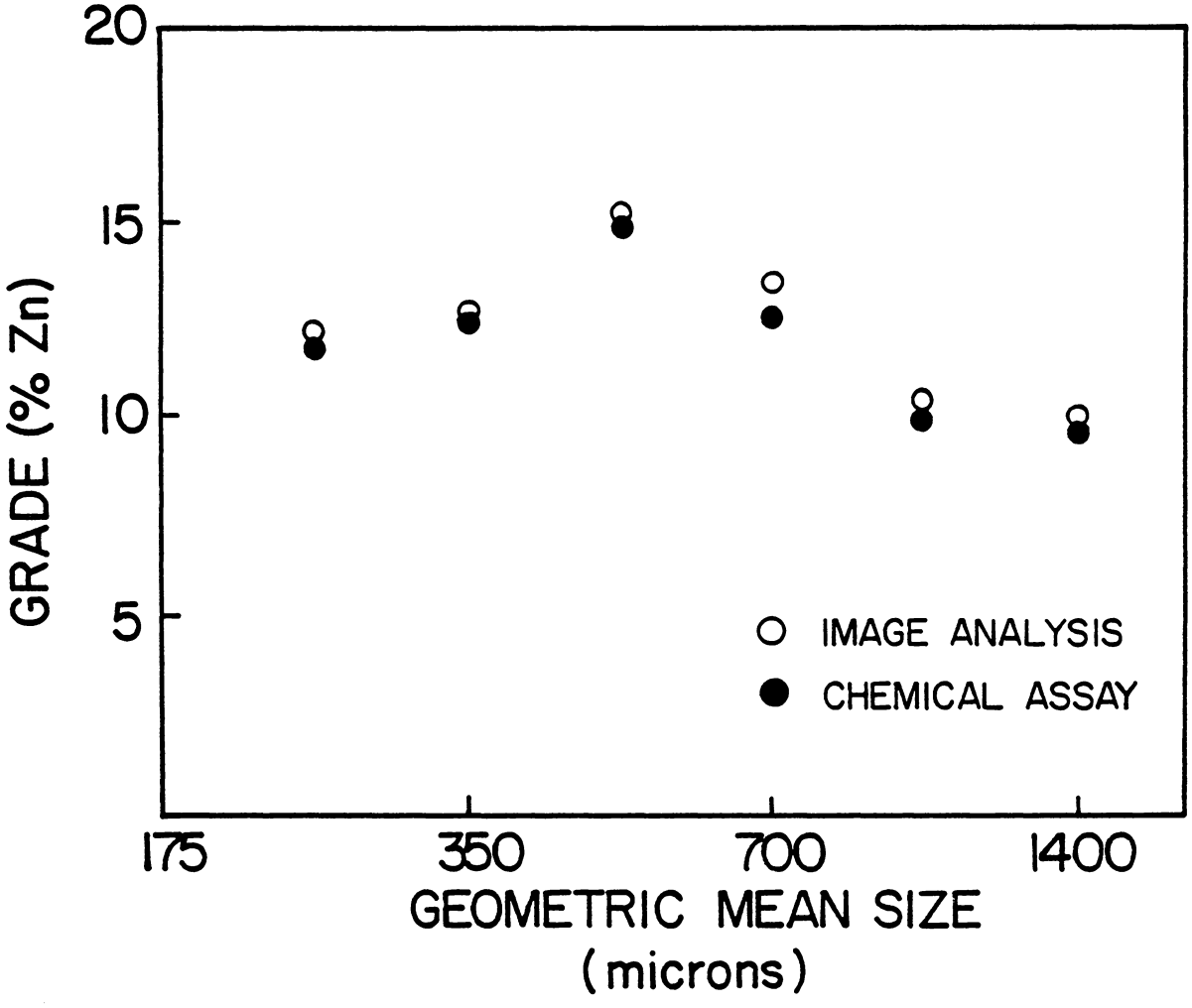

Figure 4.3 Comparison of zinc assay values determined by chemical analysis and image analysis without orientation effect (multisized feed).

image analysis might be attributed to the fact that locking factors were not considered. This observation may be explained by Table 4.3. The relative errors for coarse particles are relatively higher than for fine particles, indicating that the locking effect is less significant as particle size decreases. A major reason for this is probably that a majority of the materials in the fine size fractions was already in a liberated form. Nevertheless, the data presented here show that the areal grade can closely approximate the volume grade, provided that a proper care for sample preparation is taken for image analysis. Similar findings have been reported by Underwood (1970) showing that the mean linear grade, areal grade and volumetric grade are equivalent.

With the measurement technique verified, feed and product samples were characterized in order to determine model parameters. As mentioned previously, the ore sample used to experimentally verify the size reduction/liberation model was purposely chosen to have a relatively coarse liberation size. This helped minimize the experimental difficulty in obtaining fine size fractions, identifying minerals optically, and quantifying the amount of each mineral.

Table 4.3 Comparison of the zinc content determined by chemical assay and by image analysis.

Size (mesh)	Chemical Assay(x_1)	Image Analysis(x_2)	Relative Error*
10x14	9.5	10.1	6.2%
14x20	10.0	10.6	6.0%
20x28	12.6	13.6	7.9%
28x35	15.3	15.8	2.7%
35x48	12.1	12.4	2.4%
48x65	11.6	12.0	3.4%

$$*\text{Relative Error} = \frac{x_2 - x_1}{x_1}$$

4.1.2 Feed Characterization

a. Monosized feed: The image analysis characterization of the two monosized feeds tested is shown in Figures 4.4 and 4.5. The characterization is presented in the form of a histogram representing the weight percent of material present in the feed containing various amounts of sphalerite. Completely liberated particles are assumed to contain less than 2% sphalerite or greater than 98% sphalerite. It is clear from the two figures that a substantial portion of the feed material (77% for the 10x14 mesh feed and 81% for the 14x20 mesh feed) is already in a liberated form due to the coarse grain size of the mineral components. The coarse liberation size, however, makes the image analysis much easier since it avoids the need to analyze ultrafine particles. The liberation of sphalerite is also quite evident in going from the 10x14 mesh feed containing 14% free sphalerite to the 14x20 mesh feed containing 17% free sphalerite. Furthermore, breakage into the other composite particle classes appears to have a smoothing effect on the histogram in Figure 4.5.

b. Multisized feed: A three-dimensional representation of multisized feed distribution, showing the weight percent of material of a given size and having a given sphalerite composition, is shown in Figure 4.6.

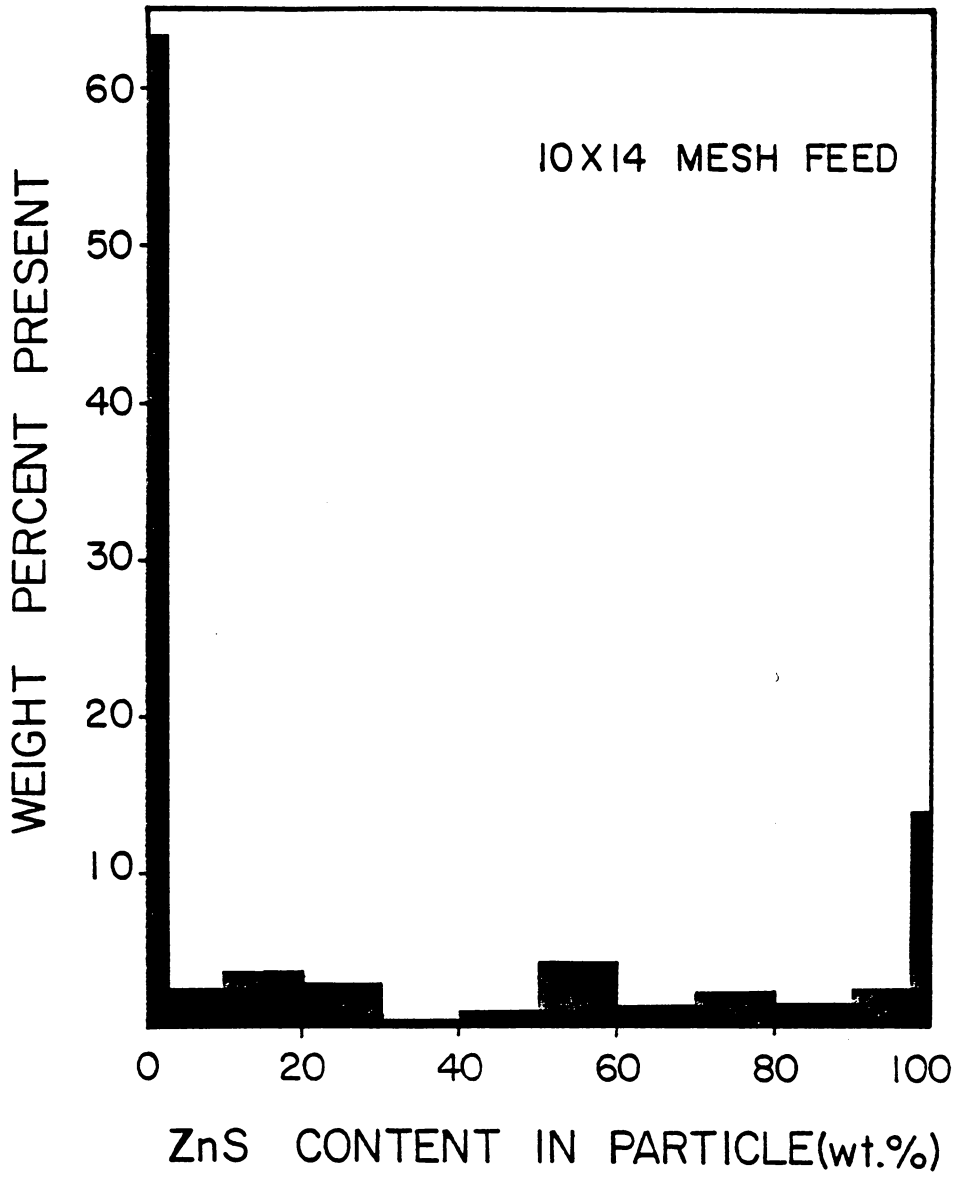

Figure 4.4 Sphalerite distribution in 10x14 mesh feed.

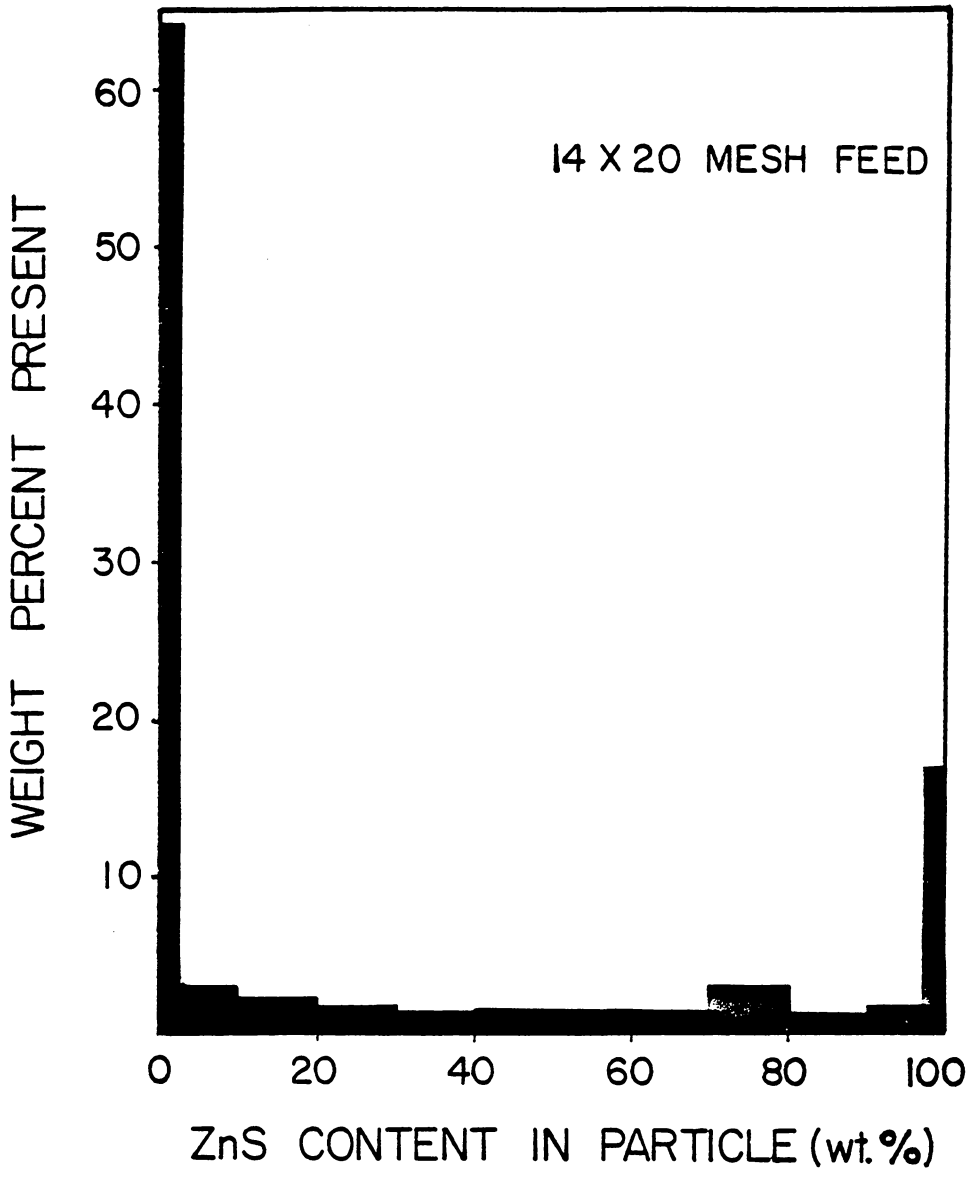

Figure 4.5 Sphalerite distribution in 14x20 mesh feed.

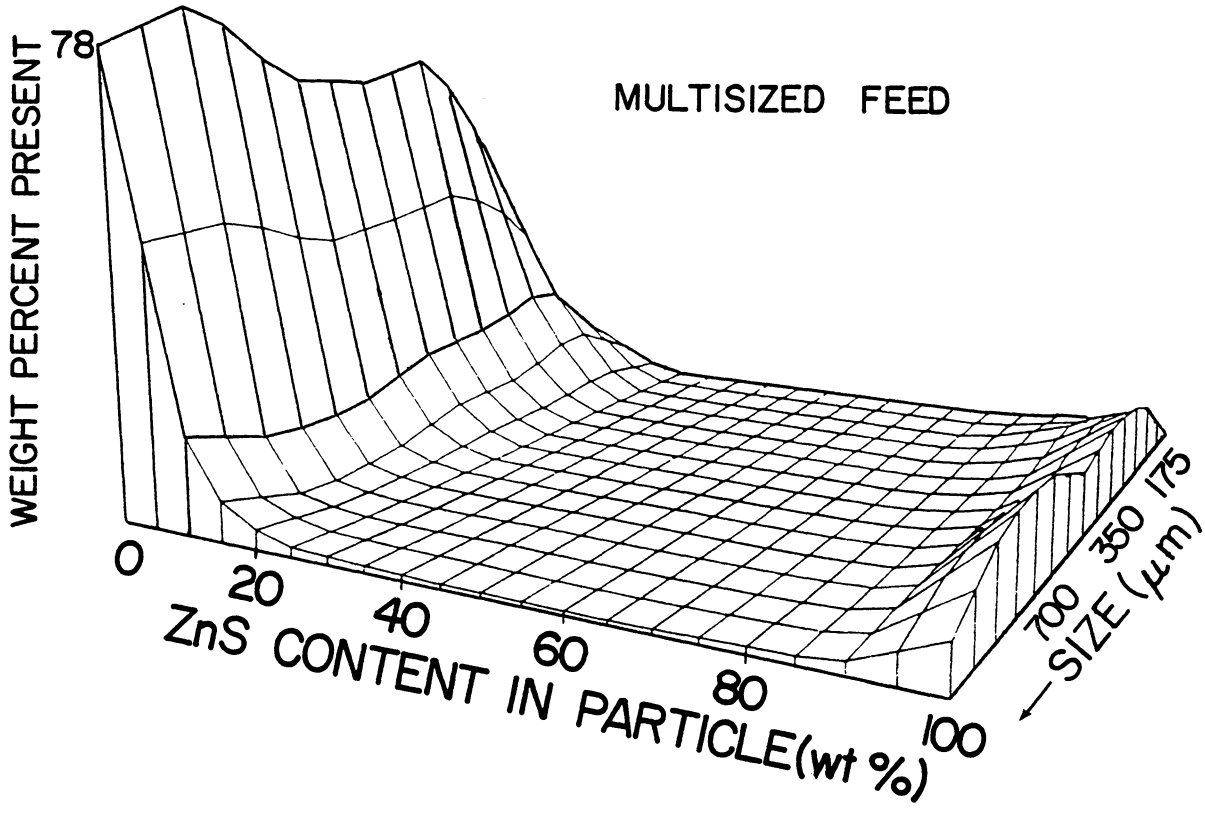

Figure 4.6 Three-dimensional plot of feed distribution showing the weight percent of material of a given size and sphalerite content.

This plot has been generated using Surface II (Sampson, 1978), a graphic software system developed by the Kansas Geological Survey. As mentioned previously, a material having a coarse liberation size was chosen for ease of analysis. Therefore, the amount of composite material in the feed was small compared to the free gangue and free sphalerite present. Figure 4.7 shows the product distribution after 4 minutes of grinding. The percentages of liberated particles are shown to have increased as compared to Figure 4.6.

4.2 Initial Parameter Estimation

4.2.1 Introduction

Several graphical methods (Herbst and Fuerstenau, 1968; Austin and Bhatia, 1972) are available to estimate selection and breakage function values for single component grinding. They are generally based on the measurement of initial slopes from plots of mass fraction versus time for a single size fraction being milled. This idea of "production plots" and "disappearance plots" has been extended to the two-component liberation model.

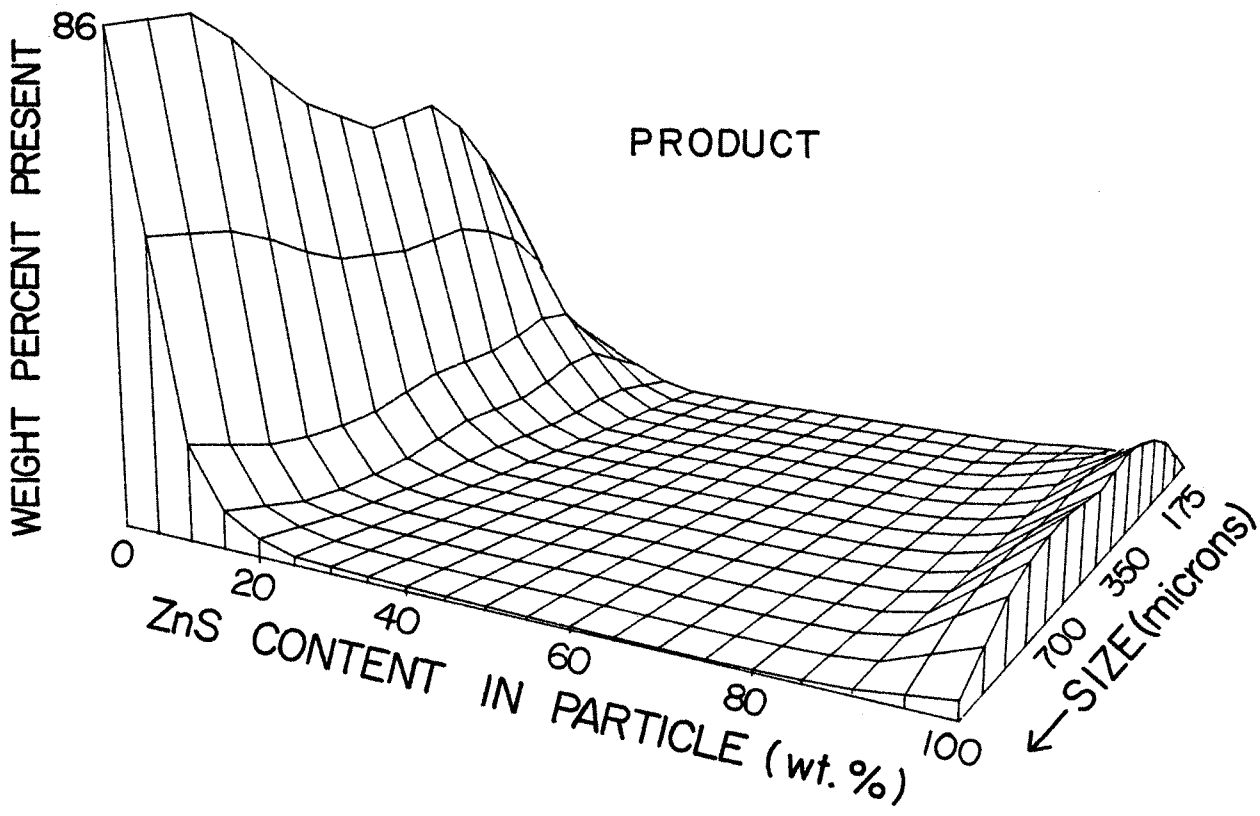

Figure 4.7 Three-dimensional plot of product distribution showing the weight percent of material of a given size and sphalerite content.

4.2.2 Determination of the Breakage Rates

The top size selection functions (breakage rates) for A, B, and AB particles can be determined by following the disappearance of these materials from monosized feed. Assuming that all material breaks to finer size classes, the slope of the fraction remaining vs. time plot gives the selection function values for a given feed size. Since the fraction of A, B, and AB particles in the feed can be determined by image analysis, all three selection functions can be estimated from the same series of grinding tests.

The top size selection function for pure component A, for example, can be determined by grinding the total ore in a batch mill. For this case, $m^a_1(0) = 1$ and $m^a_i = 0$ for i=2,....N. Equation [2.2] then becomes,

$$\frac{d}{dt}\,[m^a_1(t)] = -S^a_1(t)m^a_1(t). \qquad [4.1]$$

Rearranging Equation [4.1] yields

$$-S^a_1(t) = \frac{d\,[\ln m^a_1(t)]}{dt}. \qquad [4.2]$$

Thus, $S^a_1(t)$ is the slope of a plot of $\ln[m^a_1(t)]$ versus time (the so-called disappearance plot). The selection

functions for pure component B and composite particles AB can be found in the same manner.

4.2.3 Determination of the Breakage Distribution Functions

In the grinding of homogeneous materials, breakage distribution functions are often determined from the theory arising from the zero-order production of fines. Under this procedure, the cumulative mass fraction of product finer than a specified size is plotted against grind time and initial slope of the plot gives the zero-order production constant F_i, defined in Equation [1.2]. The cumulative breakage distribution functions for the minerals under the different mill operating conditions are then obtained using Equation [1.3]. For heterogeneous materials, however, this approach cannot be directly applied since Equations [2.2]-[2.4] show that, even as time approaches zero, fines are produced from the two components of homogeneous grinding and heterogeneous liberation. If, on the other hand, the amount of composite material present in the feed ore is small, the homogeneous grinding term will be much larger than the liberation term, and breakage distribution functions can be determined directly from the zero-order production plots in the standard manner, as mentioned earlier. In the present work, the breakage distribution functions for pure

components (A and B) have been determined by following the appearance of fine sizes of pure A and B produced from the batch grinding of a 28x35 mesh feed. The amount of composite material (8%) is small compared to the free gangue (80%) and free sphalerite (18%) present in this size fraction.

The method for obtaining cumulative breakage functions, $\bar{B}^a_{i1}$ (i=2, ...N), can be seen by writing the discretized equation in terms of the cumulative variable Y^a_i, as shown in Equation [2.11]

$$\frac{d[Y^a_i(t)]}{dt} = \sum_{j=1}^{i-1} [\bar{B}^a_{ij} S^a_j(t) m^a_j(t) + \bar{L}^a_{ij} S^{ab}_i(t) m^{ab}_i(t)]. \qquad [4.3]$$

By considering this expression in the limit as t approaches 0 and by assuming that m^{ab}_i is small,

$$\lim_{t\to 0} \frac{d[Y^a_i(t)]}{dt} = \lim_{t\to 0} \sum_{j=1}^{i-1} \bar{B}^a_{ij} S^a_j(t) m^a_j(t)$$

$$= \sum_{j=1}^{i-1} \bar{B}^a_{ij} S^a_j(0) m^a_j(0)$$

$$= \bar{B}^a_{i1} S^a_1(0) m^a_1(0). \qquad [4.4]$$

Solving for the breakage function value gives

$$\bar{B}^{a}_{i1} = \frac{1}{S^{a}_{1}(0)m^{a}_{1}(0)} \lim_{t\to 0} \frac{d[Y^{a}_{i}(t)]}{dt} \qquad [4.5]$$

Thus, $\bar{B}^{a}_{i1}$ (i=2,.....N) can be obtained by dividing the initial slope of the cumulative production rate plot for sizes finer than sieve size x_i by the initial breakage rate for the coarsest size fraction and the mass fraction of type A present in the feed. A similar argument for the type B material yields

$$\bar{B}^{b}_{i1} = \frac{1}{S^{b}_{1}(0)m^{b}_{1}(0)} \lim_{t\to 0} \frac{d[Y^{b}_{i}(t)]}{dt} \qquad [4.6]$$

Figure 4.8 shows that the composite material used in this investigation exhibits the same type of production plot as is seen for the grinding of homogeneous material. The zero-order production constant and the cumulative breakage function values for 10x14 and 14x20 mesh feeds are listed in Table 4.4. Figure 4.9 also shows zero-order production plots for gangue when gangue is ground as a component in the ore.

It should be noted that the composite particles may have compositions falling anywhere between the two extremes

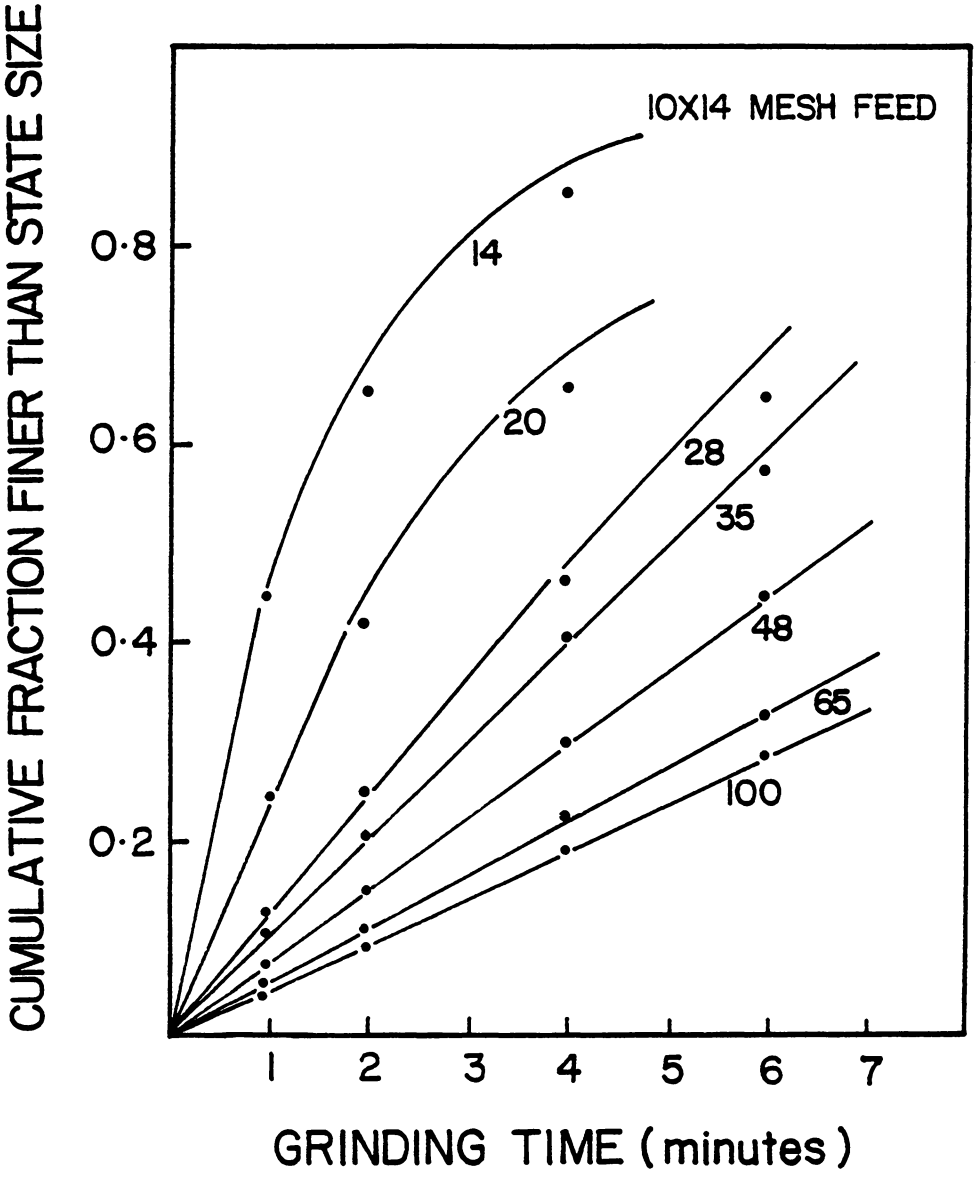

Figure 4.8. Zero-order production plot for 10x14 mesh feed.

Table 4.4 Zero-order production rates and cumulative breakage functions for the ore.

Size Interval	10x14 mesh feed		14x20 mesh feed	
	F_i	B_i^*	F_i	B_i^*
-14+20	0.425	0.906	--	1.000
-20+28	0.250	0.533	0.427	0.907
-28+35	0.125	0.267	0.190	0.413
-35+48	0.110	0.235	0.135	0.293
-48+65	0.075	0.160	0.095	0.207
-65+100	0.060	0.128	0.063	0.136
-100	0.048	0.102	0.053	0.114

$$B_i^* = \frac{F_i}{S_1}$$

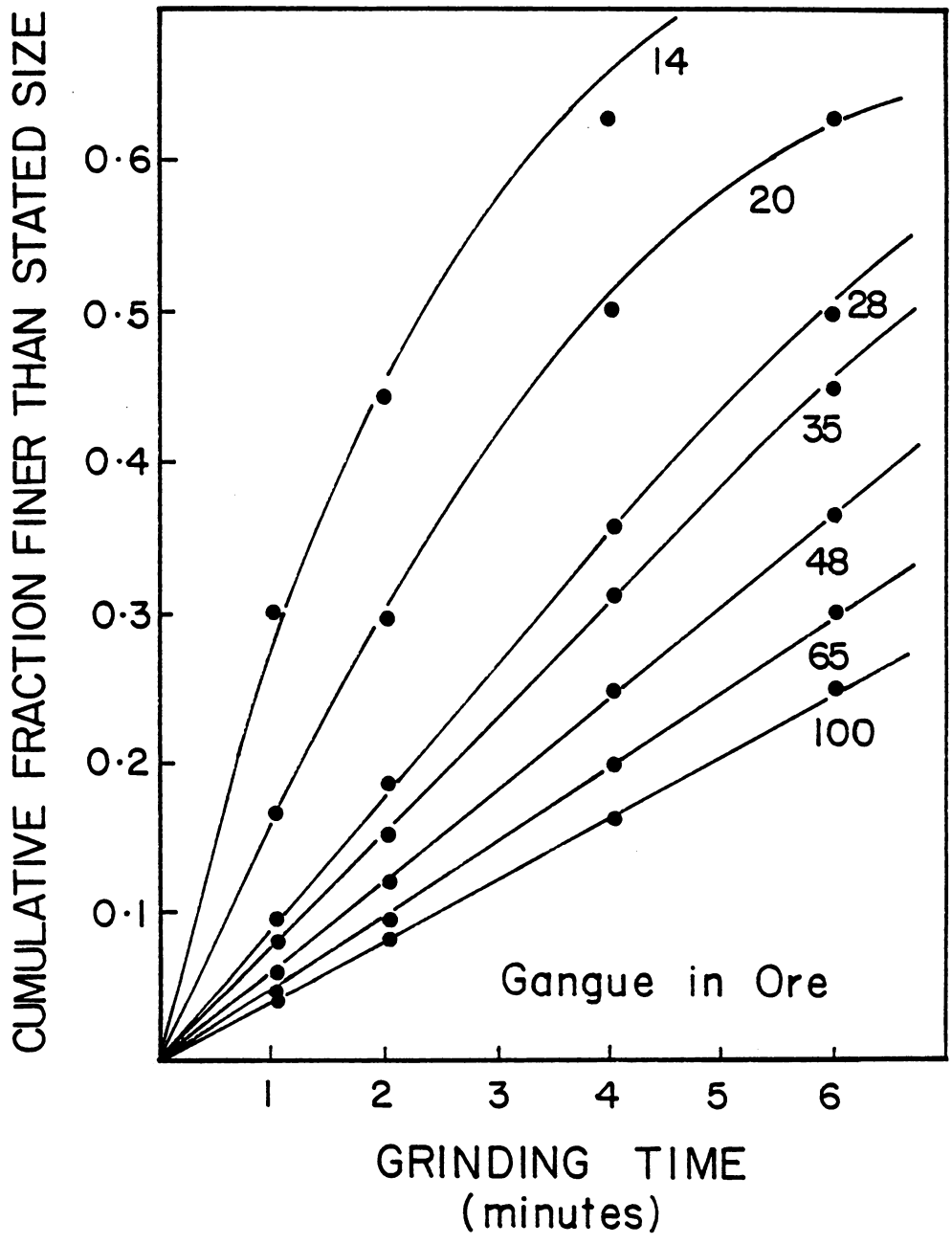

Figure 4.9 Zero-order production plot for gangue when ground with an ore.

represented by free valuable (A) and free gangue (B). Furthermore, it is realized that breakage properties could vary with mineralogical composition over the entire range of composite particles. An assumption has been made, here, that all composite particles belong to a single class characterized by a set of averaged breakage values.

4.3 Analysis of Model Parameters

4.3.1 Breakage Rates

Disappearance plots for various monosized feeds are shown in Figures 4.10 to 4.13. Included in these figures are plots for the total ore, free sphalerite, free gangue, and composite particles contained in the ore. It should be noted that in these plots, all composite (or locked) particles have been grouped in one class. Figure 4.10 also includes the disappearance plot for the gangue ground alone for comparison purposes. In all cases presented in Figures 4.10-4.13, first-order breakage behavior is observed. The breakage rates for the total ore itself are shown to fall between the breakage rates for free gangue and for free sphalerite. The ore breakage rate, however, is closer to that for free gangue. This may be attributed to the fact that the ore contains more gangue than sphalerite. Composite particles, on the other hand, tend to break at a rate closer to that of the sphalerite.

For the 10x14 mesh feed, free sphalerite is seen to exhibit the highest breakage rate. However, for the other mesh feeds, the composite material has a slightly higher breakage rate than the free sphalerite.

One method proposed for estimating the breakage rates for composite particles is to approximate these rates from a linear combination of the component minerals. If breakage

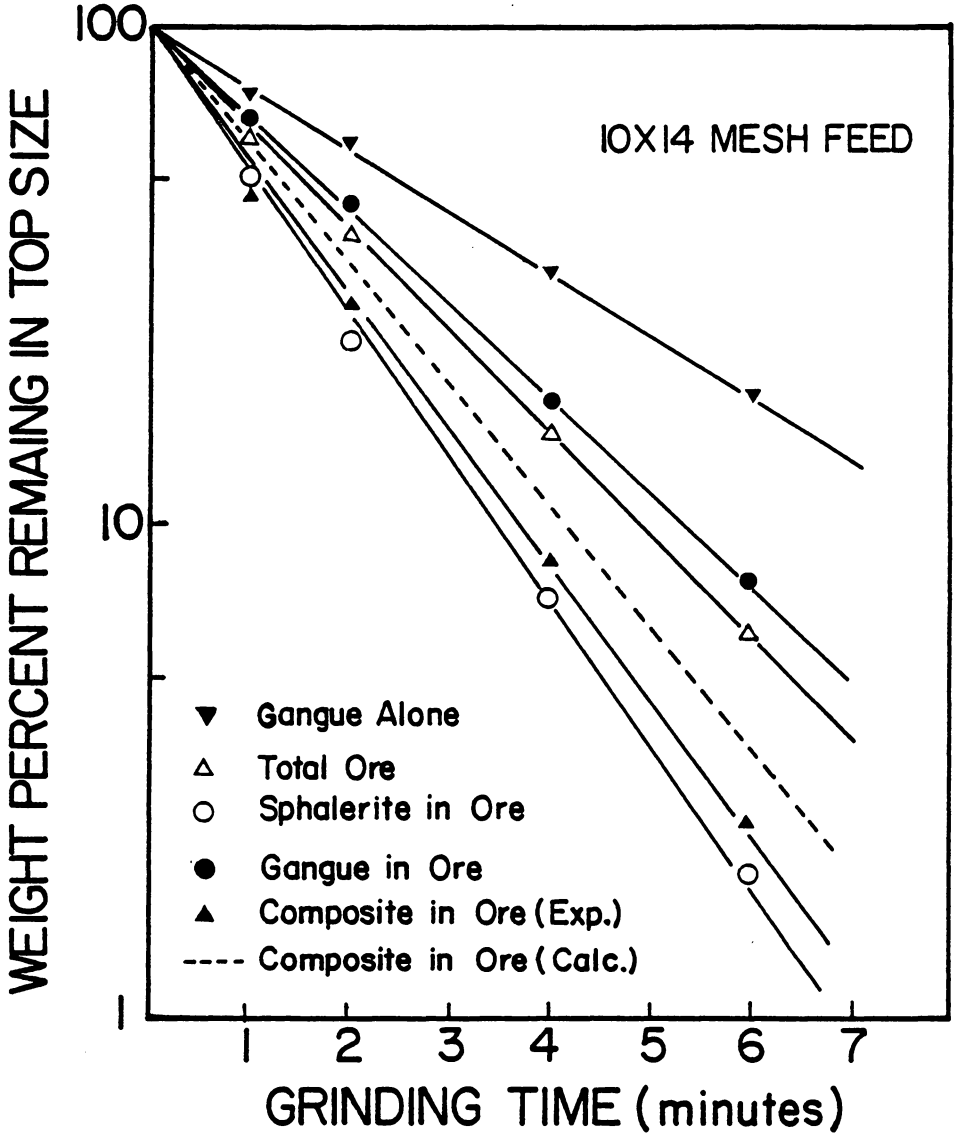

Figure 4.10 Disappearence plots for 10x14 mesh feed.

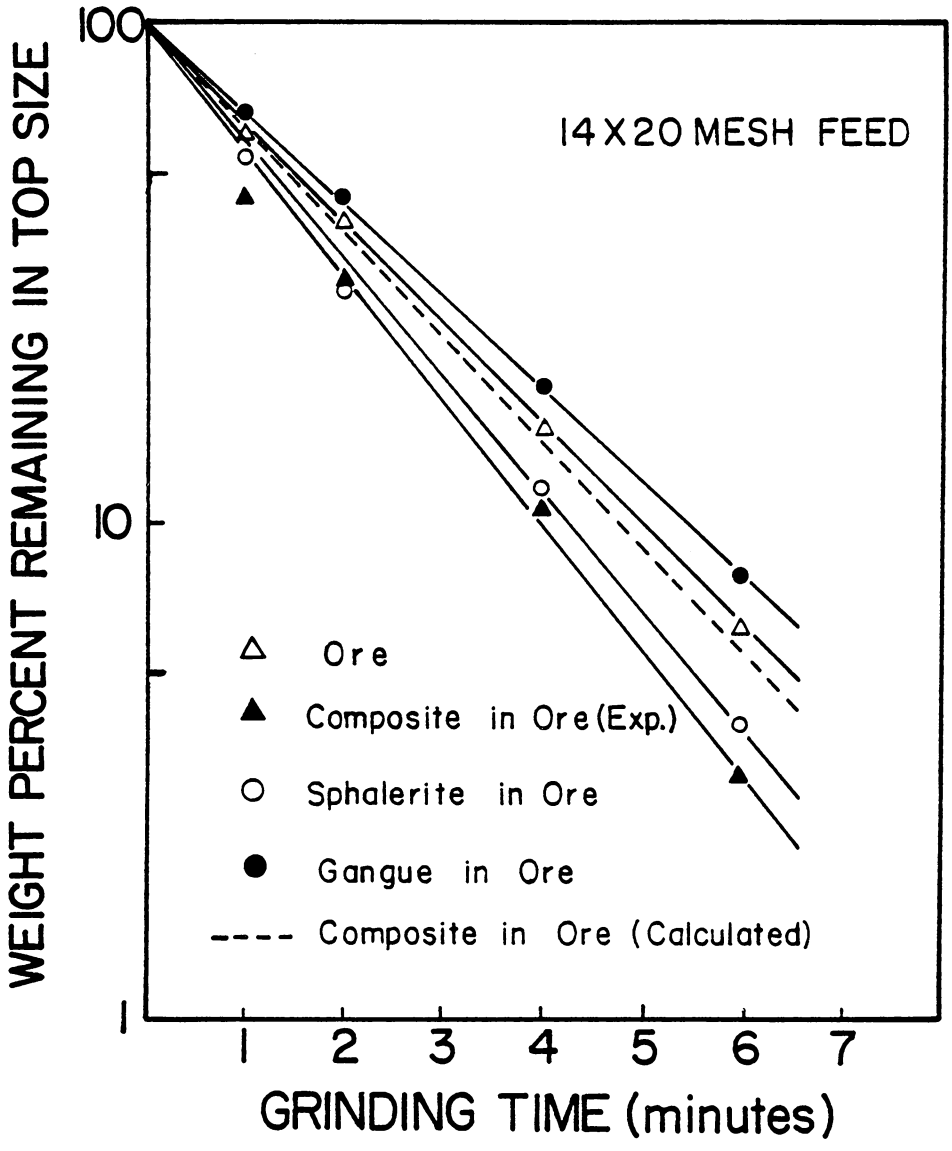

Figure 4.11 Disappearence plots for 14x20 mesh feed.

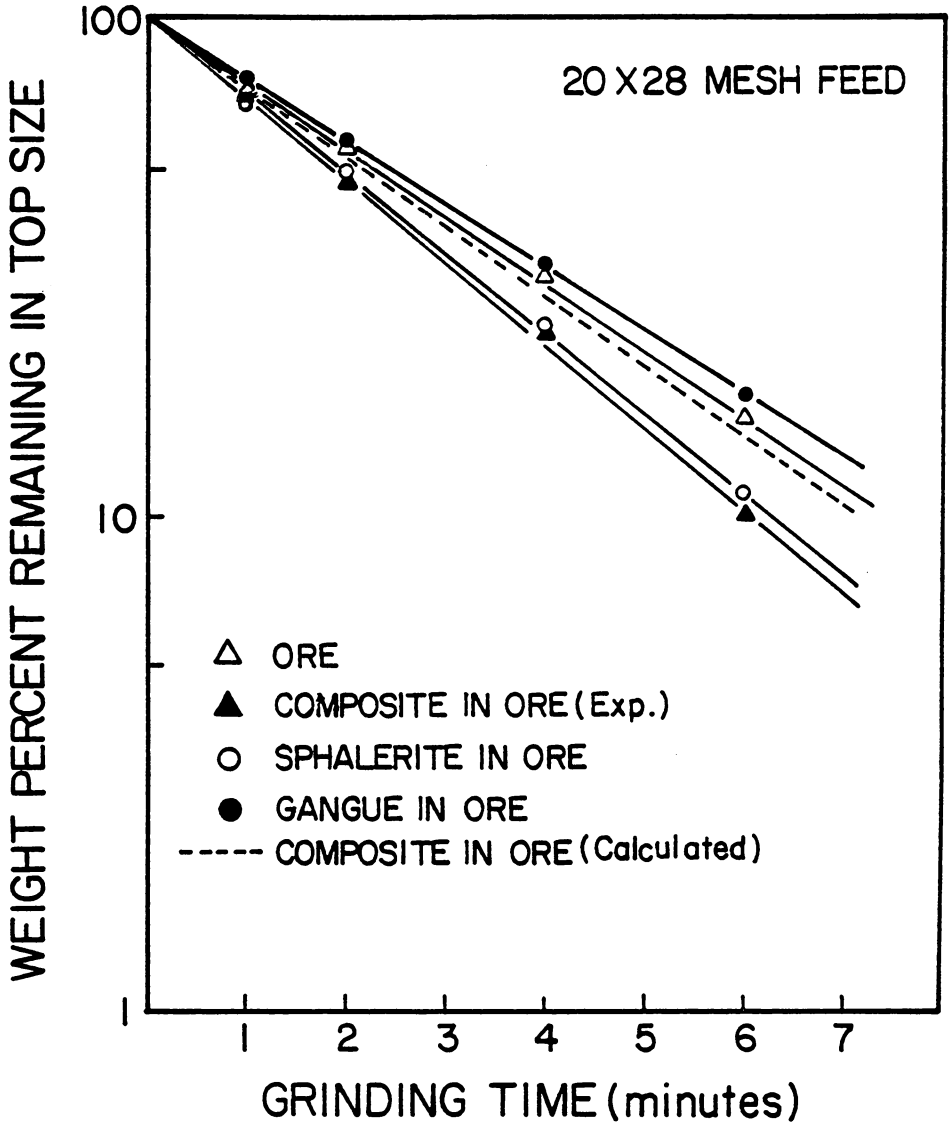

Figure 4.12 Disappearence plots for 20x28 mesh feed.

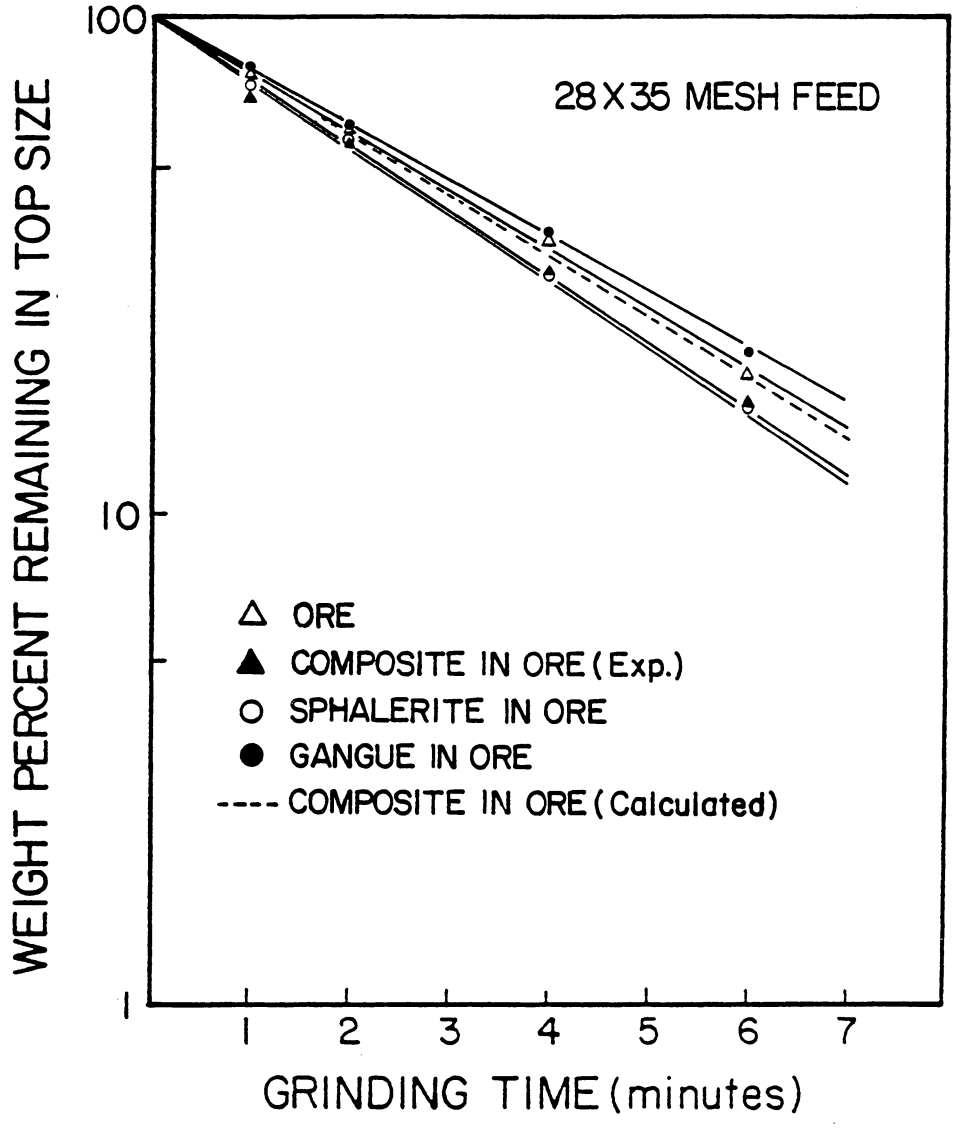

Figure 4.13 Disappearence plots for 28x35 mesh feed.

is completely random, it seems logical to assume that the breakage rate for a composite material should be a linear combination of the breakage rates for the component minerals, based on the mass fraction of each mineral present in the composite material. This relationship can be expressed as follows:

$$S_{ab} = \sum_{i=1}^{N} \frac{m_{ab,i}}{M_{ab}} \left\{ \frac{2i-1}{2N} S_a + \left(1 - \frac{2i-1}{2N}\right) S_b \right\}, \qquad [4.7]$$

where:

S_{ab} = the composite selection function for a given size class,

S_a, S_b = the selection functions for the free component minerals for a given size class,

$m_{ab,i}$ = mass of composite material in a given mineral content class for a given size class,

M_{ab} = total mass of composite material in a given size class,

N = number of mineral content classes.

The calculated disappearance plot obtained using this relationship for the composite material is also shown in Figure 4.10. It can be seen that the experimentally determined breakage rate for the composite material is

higher than the predicted value. This finding may suggest that some preferential breakage is taking place at the grain boundaries or through the sphalerite portion of the composite particle. In any case, it does not appear possible to approximate the breakage rates for composite materials directly from their component parts.

Another question which arises in determining breakage parameters for a composite ore is whether it is necessary to determine breakage parameters in the presence of the ore, or whether these parameters may be determined from grinding tests conducted on the individual components. Clearly, for the case of the breakage rate function, it is necessary to determine these parameters in-situ. As shown in Figure 4.10, the breakage rate for gangue ground alone is substantially lower than that for gangue ground in-situ. This finding agrees well with the work done with mixtures of minerals (Venkataraman and Fuerstenau, 1984).

The breakage rates obtained from the four size fractions considered in this work are plotted against mean size in Figure 4.14. As can be seen, the S_i values are smaller for smaller sizes. The decrease in these values indicates the difficulty in breaking finer particles. Except for a slight deviation at the coarsest size fraction, a linear trend is observed, making it possible to extrapolate the additional breakage rate values needed for

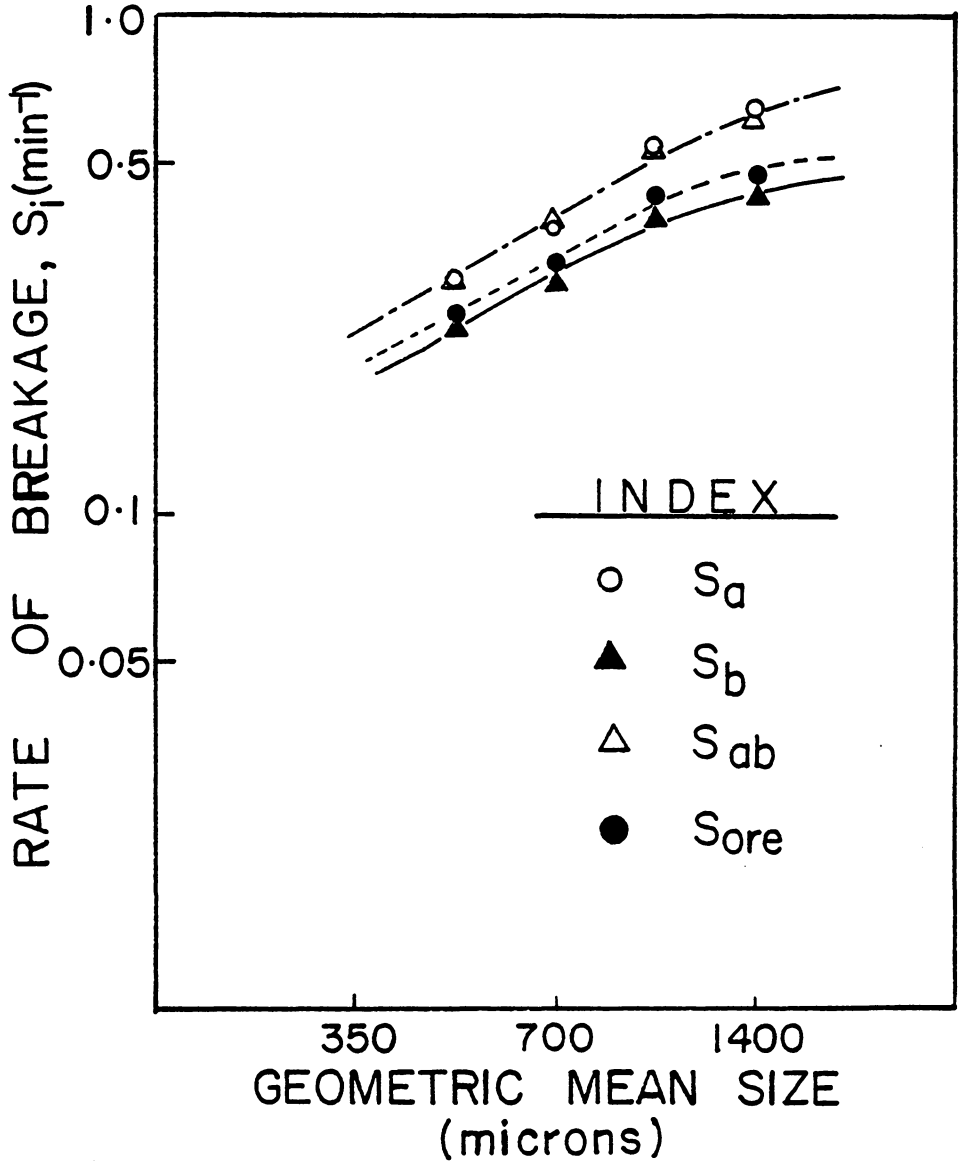

Figure 4.14 Breakage rates as functions of size for the various components in an ore.

computer simulation purposes. This trend is also normally observed for the grinding of homogeneous materials. The breakage rates obtained from the four size fractions, along with calculated S_{ab} values, are given in Table 4.5.

4.3.2 Breakage Distribution Functions

The cumulative breakage distribution functions for free gangue and free sphalerite were determined experimentally from standard zero-order production plots. As discussed previously, this measurement should be accurate, provided that the amount of material being liberated from composite particles is small. To test this hypothesis, cumulative breakage distribution functions have been determined for 10x14 mesh gangue ground alone and in the ore. These values are compared in Figure 4.15 and Table 4.6. It is clear from this figure that the cumulative breakage function for gangue is the same whether it is ground alone or in the presence of the ore. The same conclusion has been drawn from grinding mineral mixtures (Venkataraman and Fuerstenau, 1984). It also appears that since the 10x14 mesh ore fraction contained approximately 65% gangue and 20% composite material, this difference was sufficient to make the contribution of liberation to the zero-order production plot insignificant.

The assumption of breakage function normalizability

Table 4.5 Experimentally-determined breakage rates for free sphalerite, free gangue and composite material.

	S_a	S_b	S_{ab}^{*}	S_{ab}^{**}
S_1	0.656	0.434	0.622	0.560
S_2	0.541	0.410	0.560	0.480
S_3	0.368	0.293	0.384	0.324
S_4	0.305	0.244	0.300	0.268

*Experimental

**Calculated

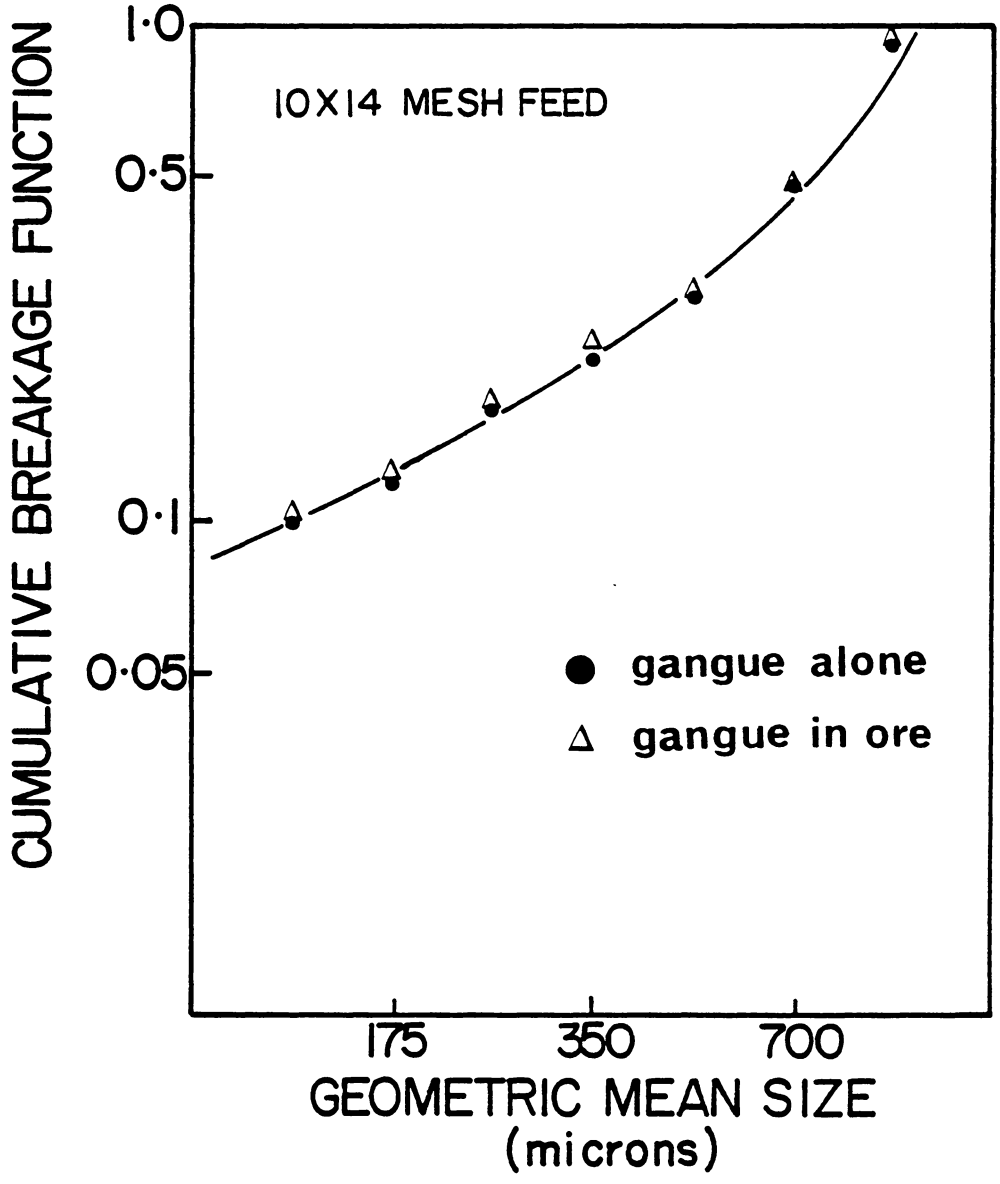

Figure 4.15 Cumulative breakage distribution function versus particle size for gangue ground alone and with an ore.

Table 4.6 Zero-order production rates and cumulative breakage functions when gangue is ground alone and as a component in a mixture.

Size Interval	Gangue Alone		Gangue in Ore	
	F_1	B_1	F_1	B_i
-14+20	0.260	0.910	0.400	0.920
-20+28	0.135	0.472	0.210	0.484
-28+35	0.075	0.263	0.120	0.275
-35+48	0.060	0.211	0.100	0.227
-48+65	0.048	0.168	0.075	0.173
-65+100	0.035	0.122	0.055	0.126
-100	0.030	0.107	0.046	0.106

with feed size was also tested, as shown in Figure 4.16. This figure clearly shows that the cumulative breakage distribution function for gangue is independent of feed size, thus reducing the number of parameters that must be estimated. Similar results were observed for the free sphalerite component in the ore (See Figure 4.17).

4.3.3 Liberation Distribution Functions

The remaining breakage parameters, $\underline{B}_{ab}$, $\underline{L}_a$, and $\underline{L}_b$, were estimated from the model equations as discussed earlier. The computer estimates of the liberation distribution functions for A and B materials are shown in Figure 4.18. It is quite clear from this figure that sphalerite has a greater tendency to liberate than does gangue. This may be due to the more friable nature of sphalerite, allowing it to be more easily broken away from a composite particle. This finding agrees well with the fact that the breakage rate of the composite particles is closer to that of sphalerite than to that of gangue (Figure 4.10). The manner in which the liberated particles distribute, however, appears to be similar for both materials since the curves parallel each other. It appears that the liberation function, along with other breakage parameters, provides a useful means for determining whether the fracture occurs randomly or preferentially.

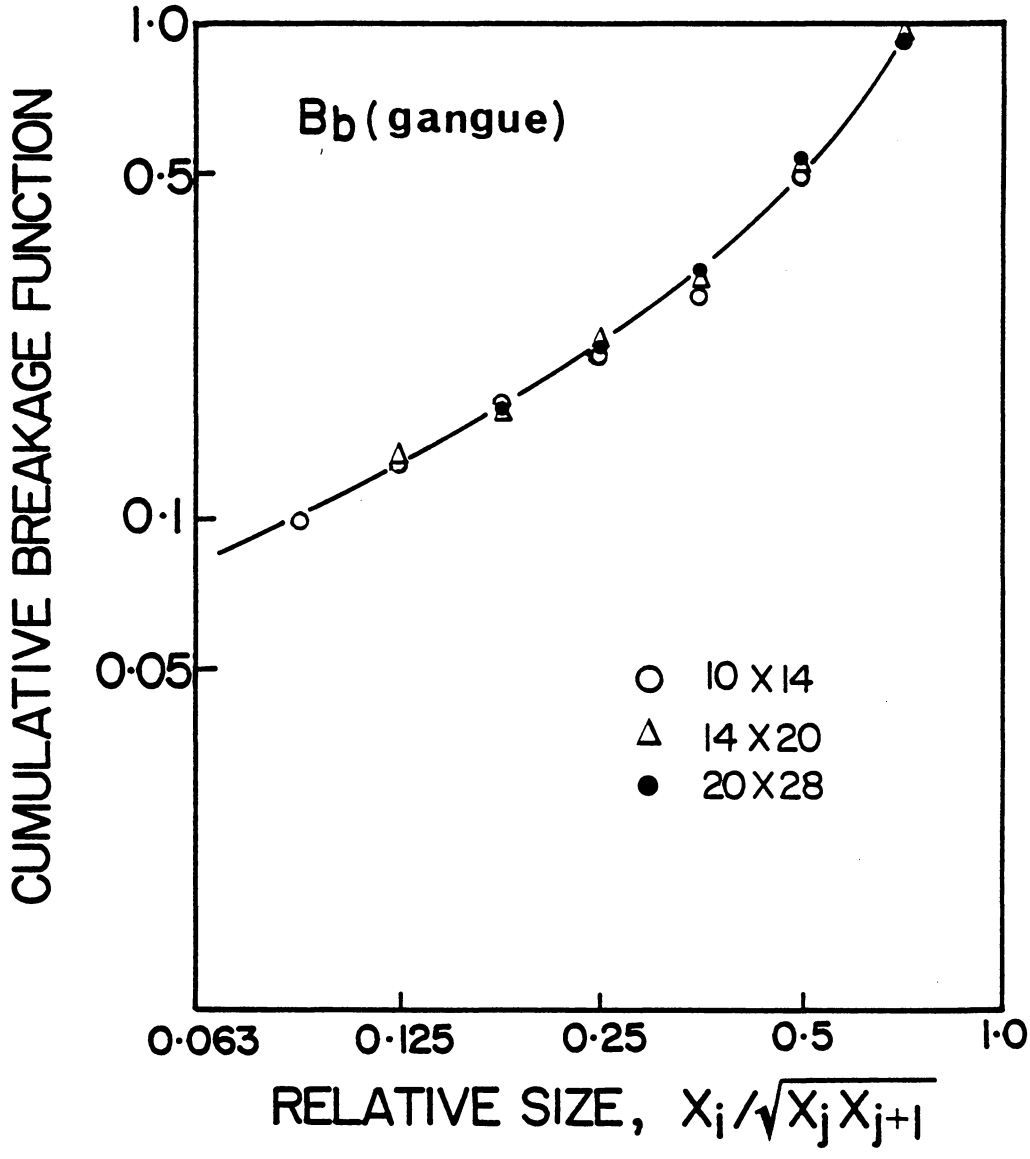

Figure 4.16 Cumulative breakage distribution function versus normalized size for B-type material.

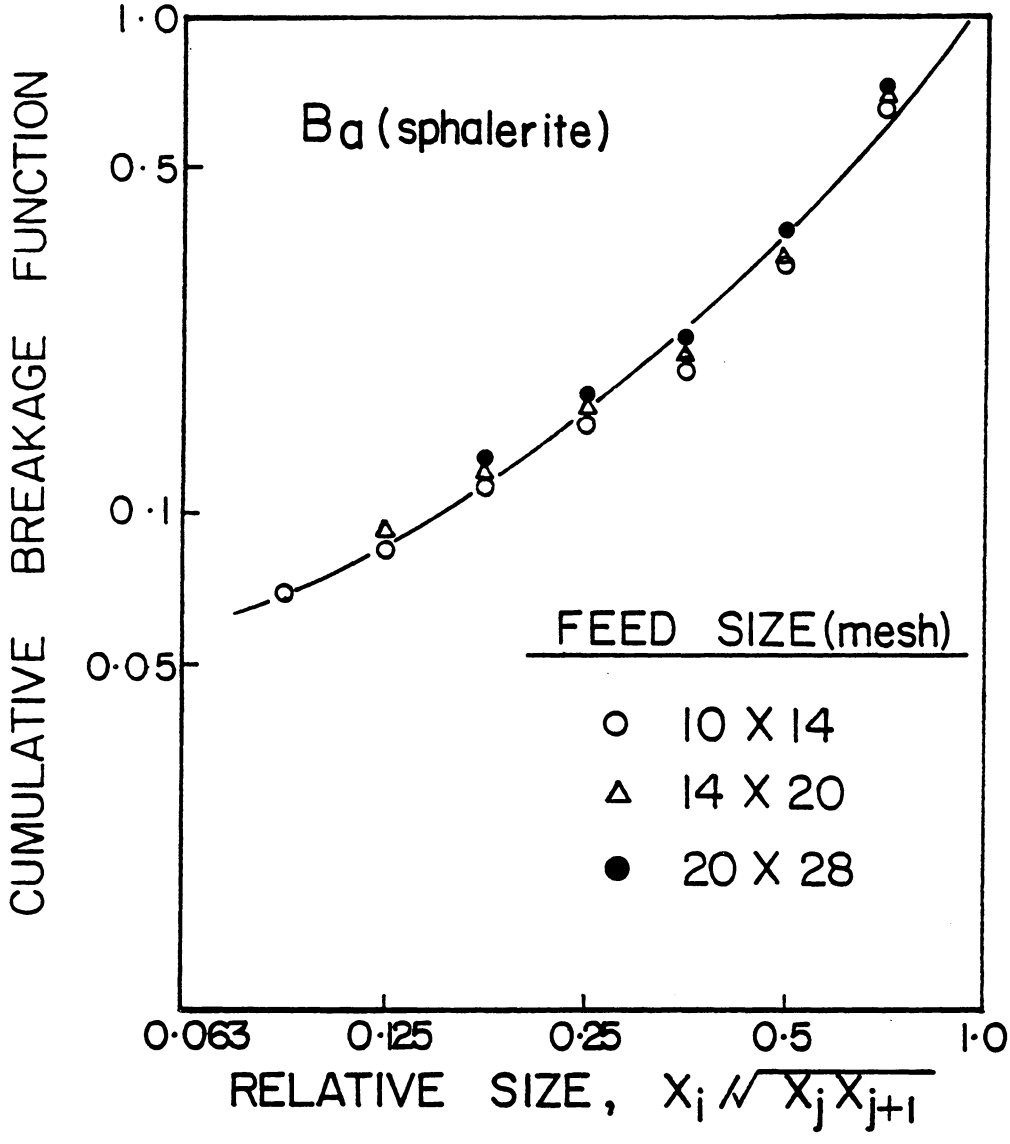

Figure 4.17 Cumulative breakage distribution function versus normalized size for A-type material.

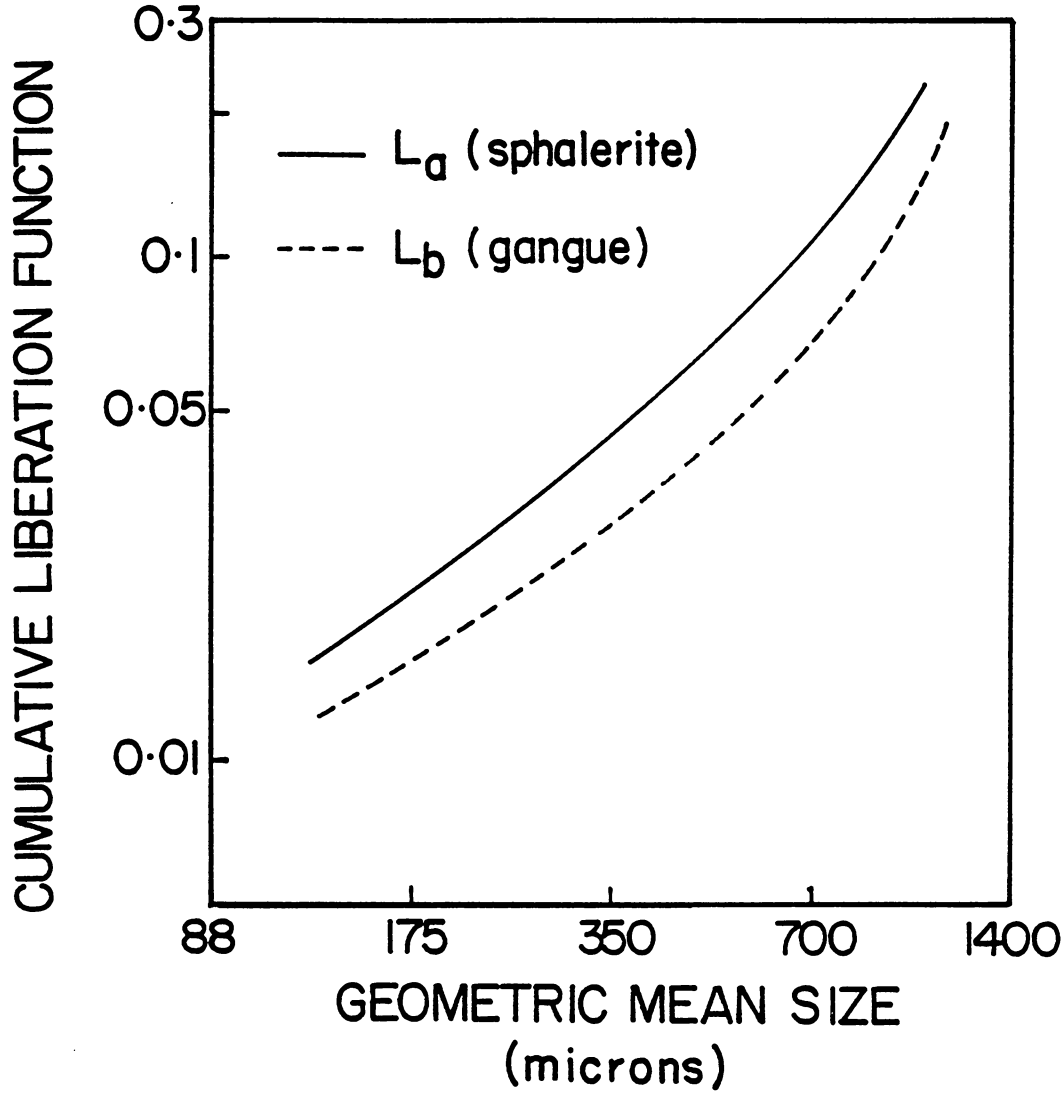

Figure 4.18 Computer simulated liberation functions for A- and B-type material.

4.4 Computer Simulation

4.4.1 Liberation from Batch Grinding of Monosized Feeds

Using the model parameters determined as described in the previous sections, computer simulations of dry batch ball milling were carried out to predict the product size distribution for each component in the ore. The results obtained with a 10x14 mesh sphalerite ore feed are given in Figure 4.19 and 4.20 along with the experimental values. From these figures, it is quite clear that simulation results agree quite closely with the experimentally determined size distributions for gangue, composite material, and the total product. In the case of free sphalerite, however, the computer-predicted values fall substantially above the experimentally-determined values. It appears that the discrepancy in the sphalerite is due to an overestimation of the sphalerite content in the feed material as determined by image analysis. This overestimation was shown in Figure 4.1, in which image analysis results were compared with the chemical assay.

In order to improve the simulation of the sphalerite product, a correction factor was introduced to adjust the free sphalerite in the feed based on the ratio of the chemical assay to the areal assay as follows:

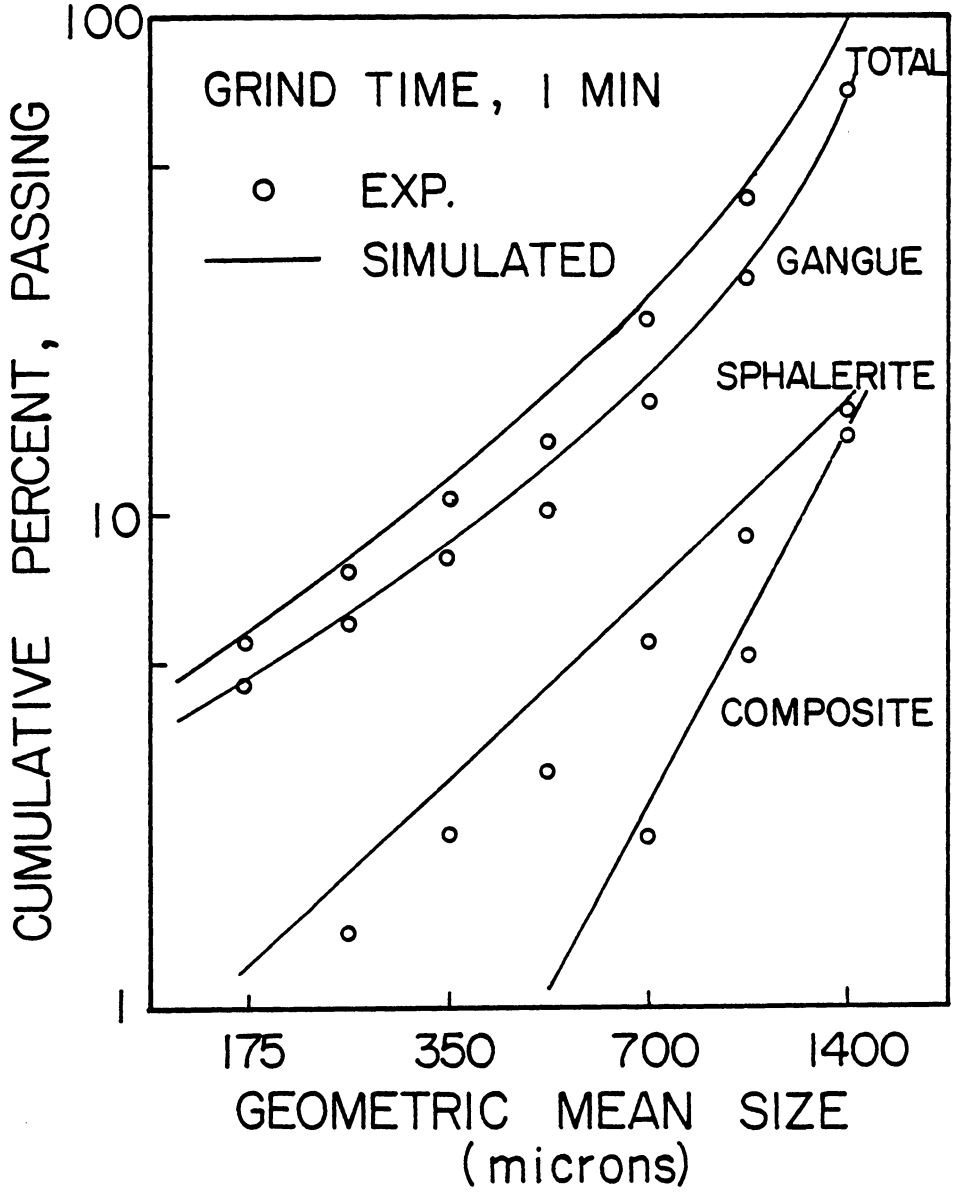

Figure 4.19. Comparison between the computer-simulated and the experimentally determined size distributions for each component produced in the batch ball milling of a 10 x 14 monosized feed.

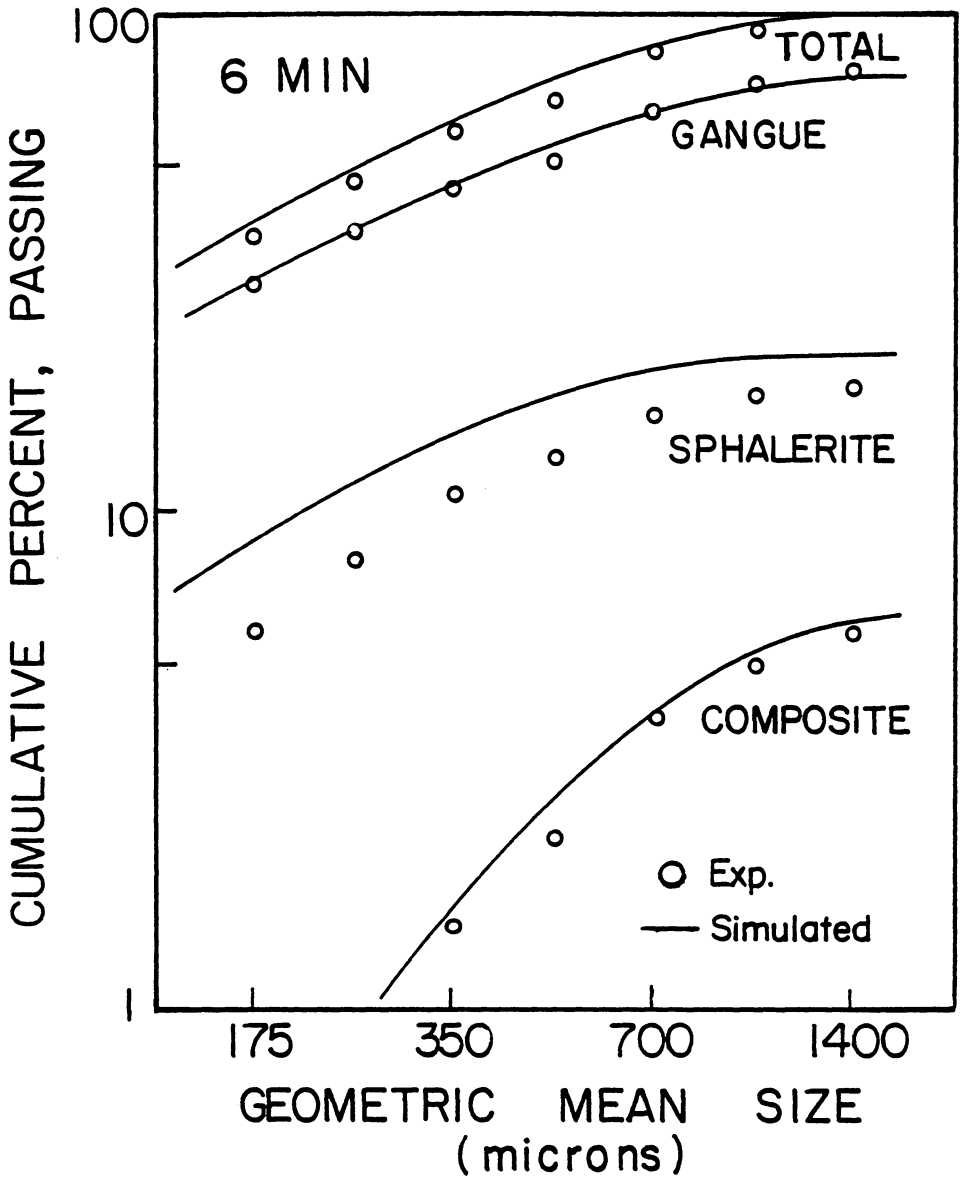

Figure 4.20. Comparison between the computer-simulated and the experimentally determined size distributions for each component produced in the batch ball milling of a 10 x 14 monosized feed.

$$\text{Correction Factor} = \frac{\text{\% Zn in the feed determined by chemical assay}}{\text{\% Zn in the feed determined by image analysis}} \qquad [4.8]$$

The results of the simulation using the corrected data are shown in Figure 4.21 and 4.22. A much better fit can be seen for free sphalerite, while the improvements are less pronounced for the other components. With the aid of this correction factor which accounts for the sampling bias, the model seems to successfully simulate the process of grinding and liberation simultaneously.

4.4.2 Liberation from a Multisized Feed

It has been shown in the previous section that the model predictions are in excellent agreement with the experimental data obtained from the batch grinding experiments in which a monosized feed was ground. It should be noted, however, that this may not be a rigorous test for the model, since the model parameters were determined from the monosized grinding experiments. Therefore, a computer simulation was run for the batch grinding of a multisized feed using the model parameters determined from monosized grinding experiments. Figure 4.23 shows the simulation results along with the experimental data. The results of the feed ore characterized have been shown in Figure 4.6.

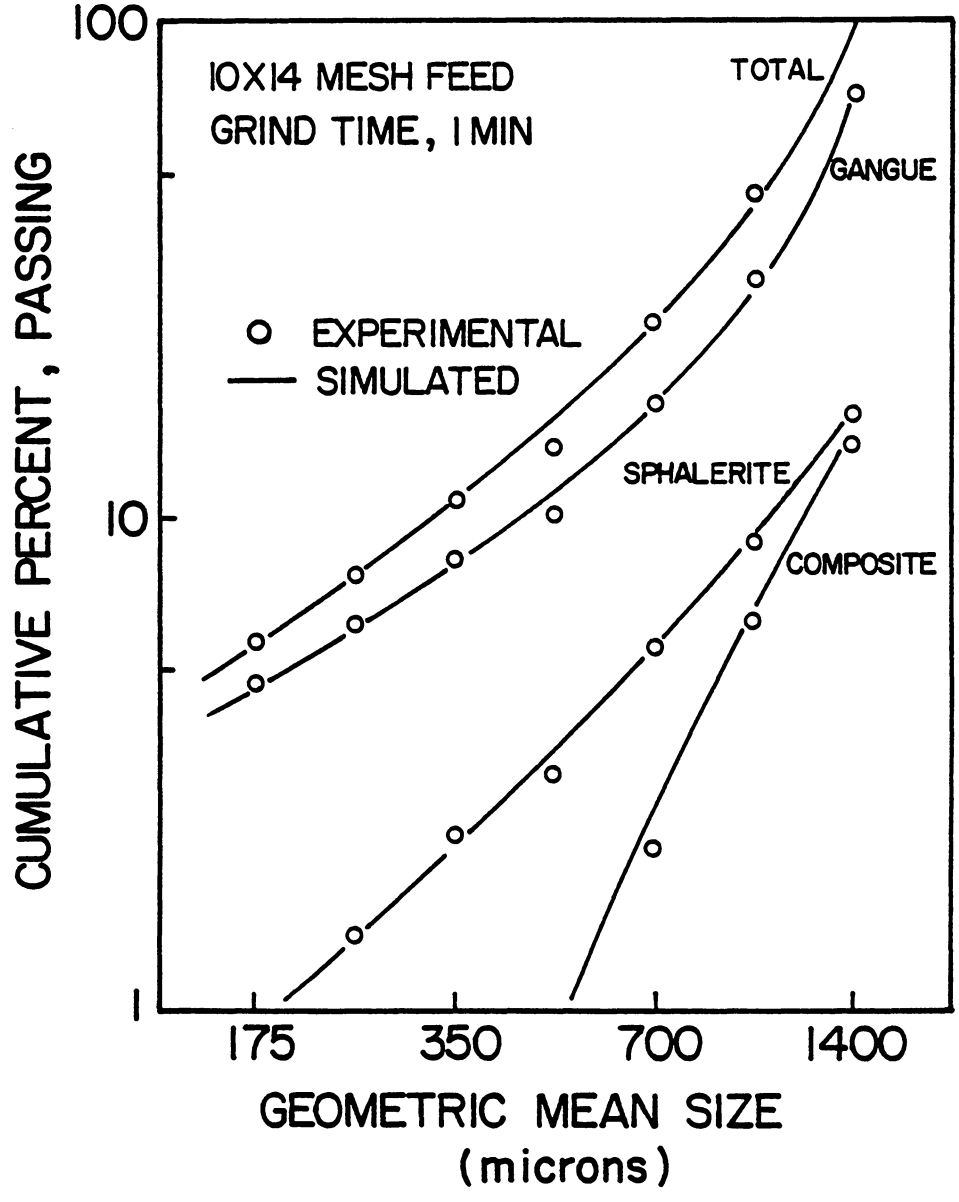

Figure 4.21 Comparison of experimentally determined and computer-simulated size distributions using corrected sphalerite assay.

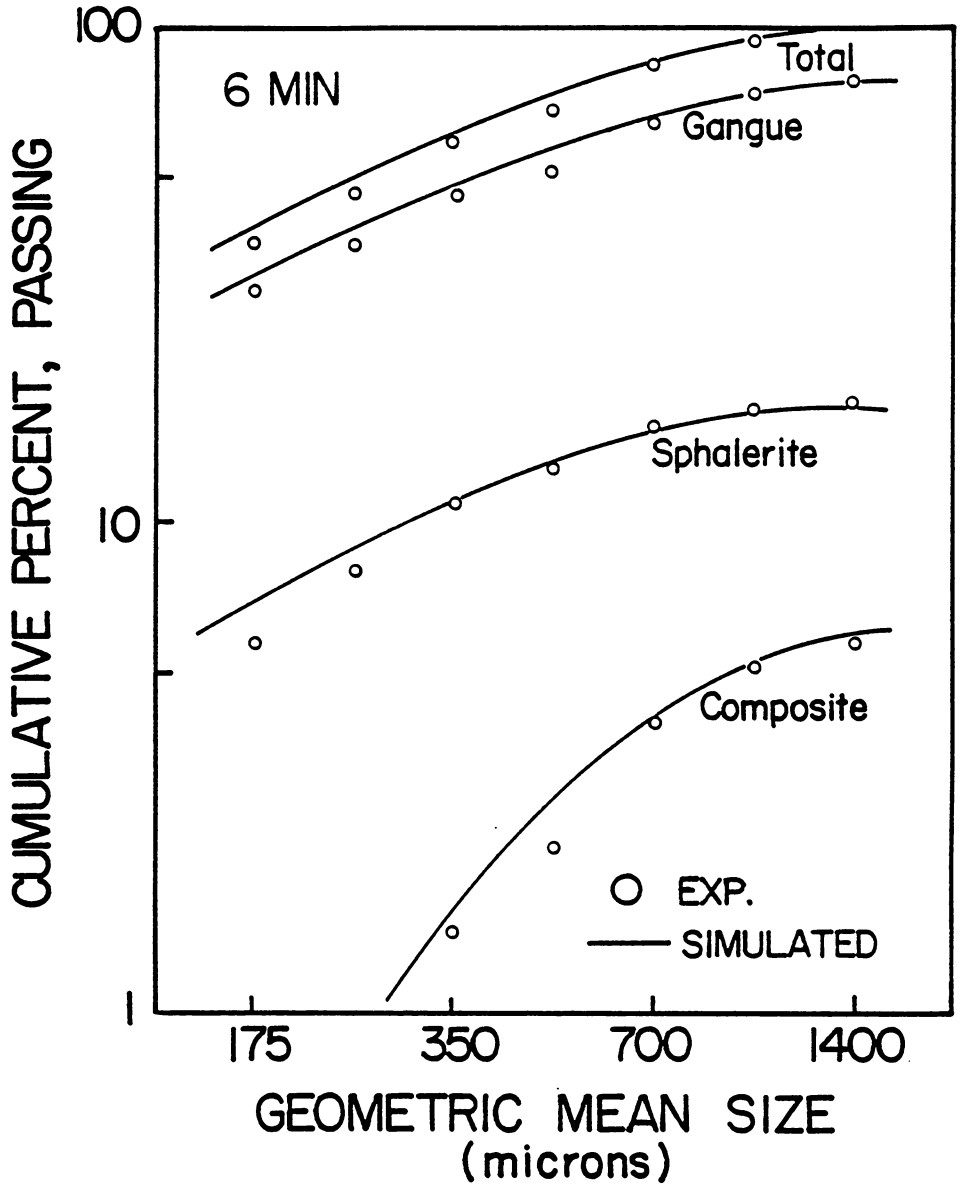

Figure 4.22 Comparison of experimentally determined and computer-simulated size distributions using corrected sphalerite assay.

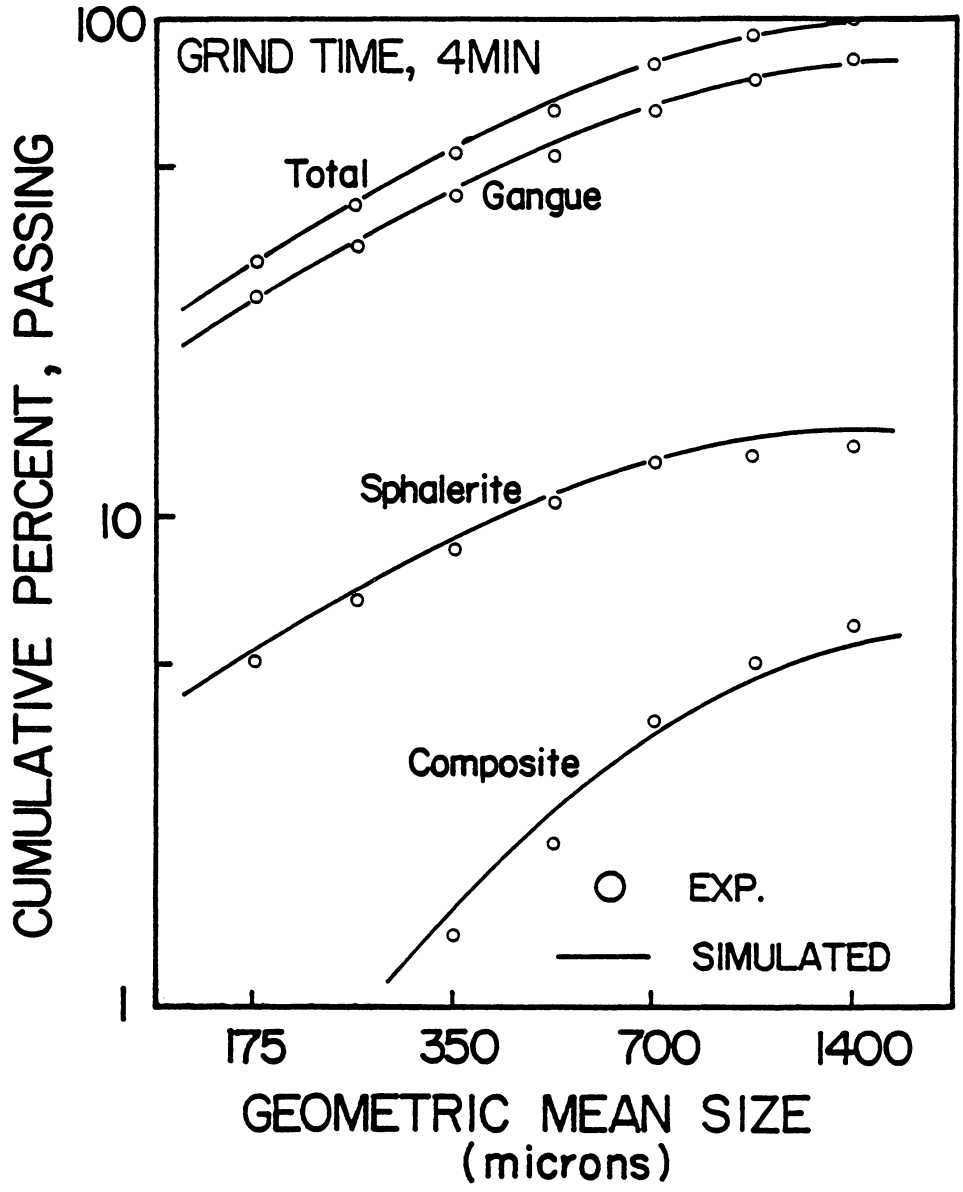

Figure 4.23. Comparison between the computer-simulated and the experimentally determined size distributions for each component produced in the batch ball milling of a multisized feed ore.

The feed size distribution for each component in the multisized feed is also shown in Figure 4.24. Once again, there is an excellent agreement between the experimental and computer simulated size distributions for all classes of particles including free gangue, free sphalerite, composite particles, and the total product. As has been noted, this simulation is a much more rigorous test of the validity of the model since the model parameters used in this simulation were determined independently from the monosized feeds.

4.4.3 Liberation with Two Composite Classes

As an initial attempt to expand the model to cases involving more than one class of composite particles, the composite particles were classified into two classes, namely: i) particles containing less than 50% sphalerite, and ii) particles containing more than 50% sphalerite.

The first-order disappearance plots for these two classes, along with the free gangue and free sphalerite, are shown in Figure 4.25. All parameters were determined in-situ, i.e., the fate of each class of particles was followed during breakage of the ore itself rather than through the breakage of isolated classes of particles. As shown, the breakage rate for free gangue material was clearly the slowest. This is followed by the material

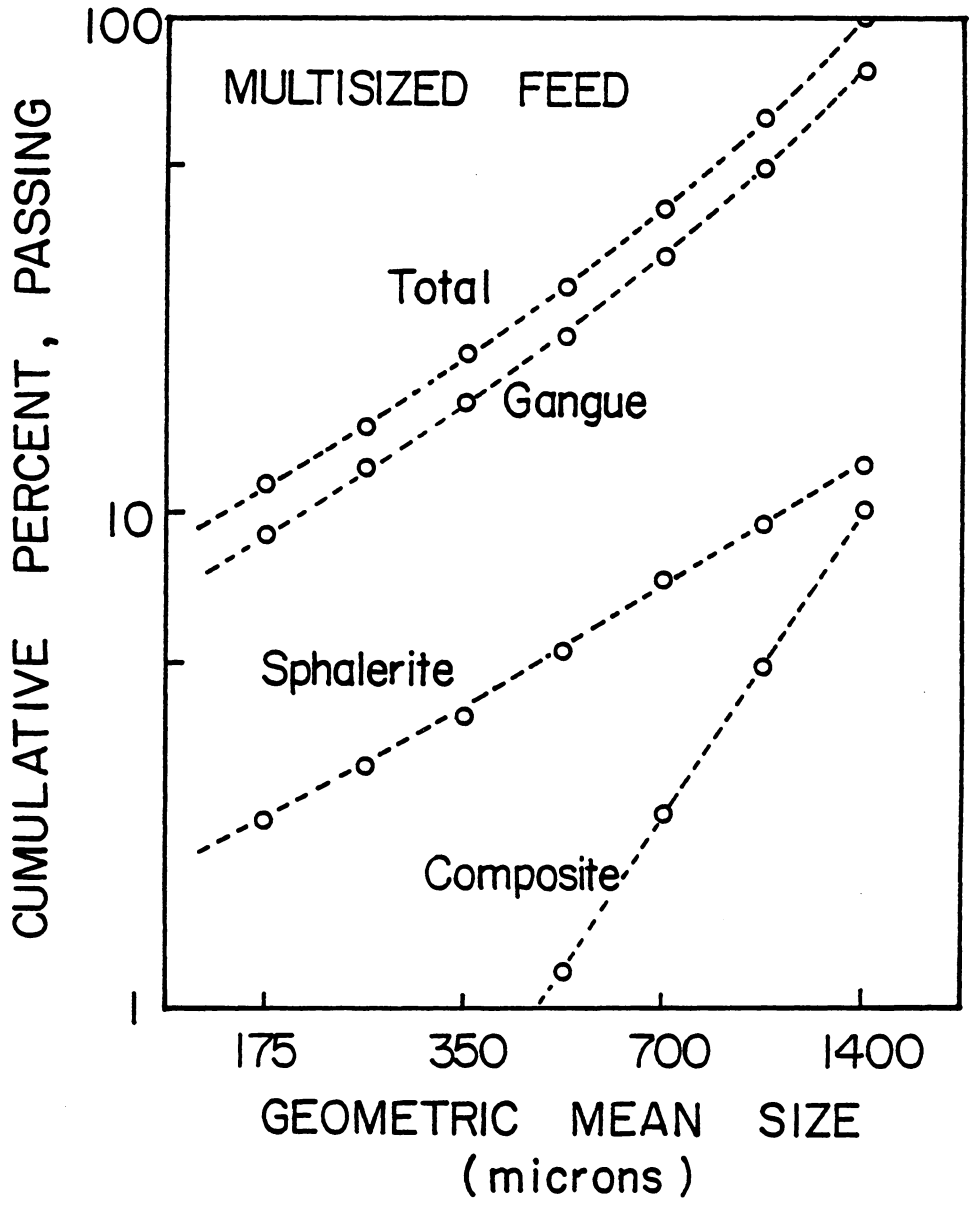

Figure 4.24 Size distributions for each component in the multisized feed.

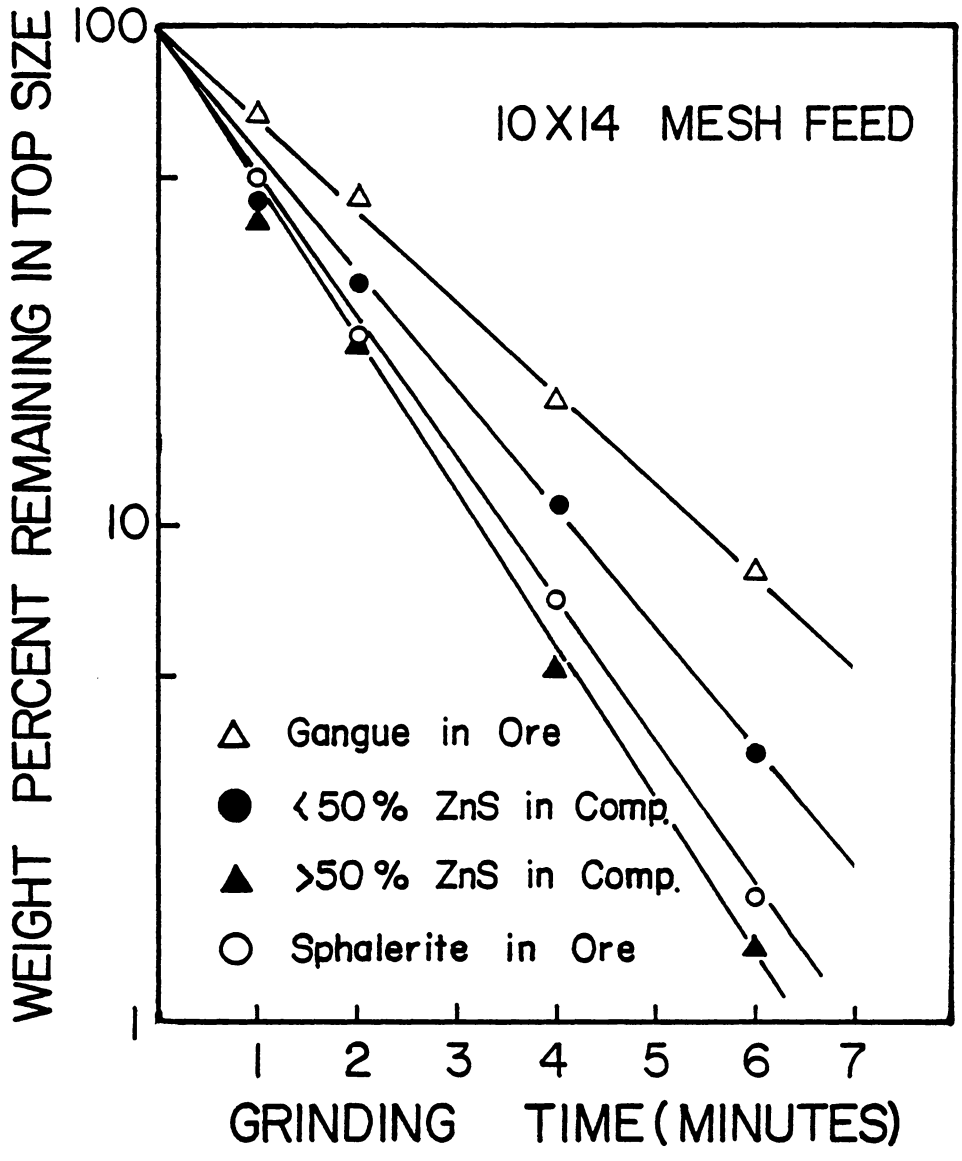

Figure 4.25 Disappearence plots for free sphalerite, free gangue and two cases of composite particle classes.

containing less than 50% sphalerite. It is interesting to note that particles containing a small amount of gangue actually grind faster than those containing pure sphalerite. These results may also suggest a preferential breakage along grain boundaries.

As mentioned previously, the cumulative liberation function ($\bar{\underline{L}}_{ab,1\leftarrow 2}$ and $\bar{\underline{L}}_{ab,2\leftarrow 1}$) and cumulative breakage function ($\bar{\underline{B}}_{ab,1}$ and $\bar{\underline{B}}_{ab,2}$) for the multi-component case were determined by proportioning the same parameters for the individual components on a volume fraction basis. Since no experimental values were available for either parameter, it was not possible to verify this assumption. However, for the case of a single composite particle class, $\underline{B}_{ab}$ was directly calculated from the model equations. Therefore, it is possible to compare this parameter to that determined from the individual components. This comparison is shown in Figure 4.26. Although there exists a considerable descrepancy, the difference between them is typically less than 15% of the value calculated from the model equations. It appears, therefore, that the method employed for estimating the $\underline{L}$ and $\underline{B}$ functions for the multicomponent case is not unreasonable as a first approximation.

Using the methods of determining the model parameters discussed above, the case of grinding with liberation into

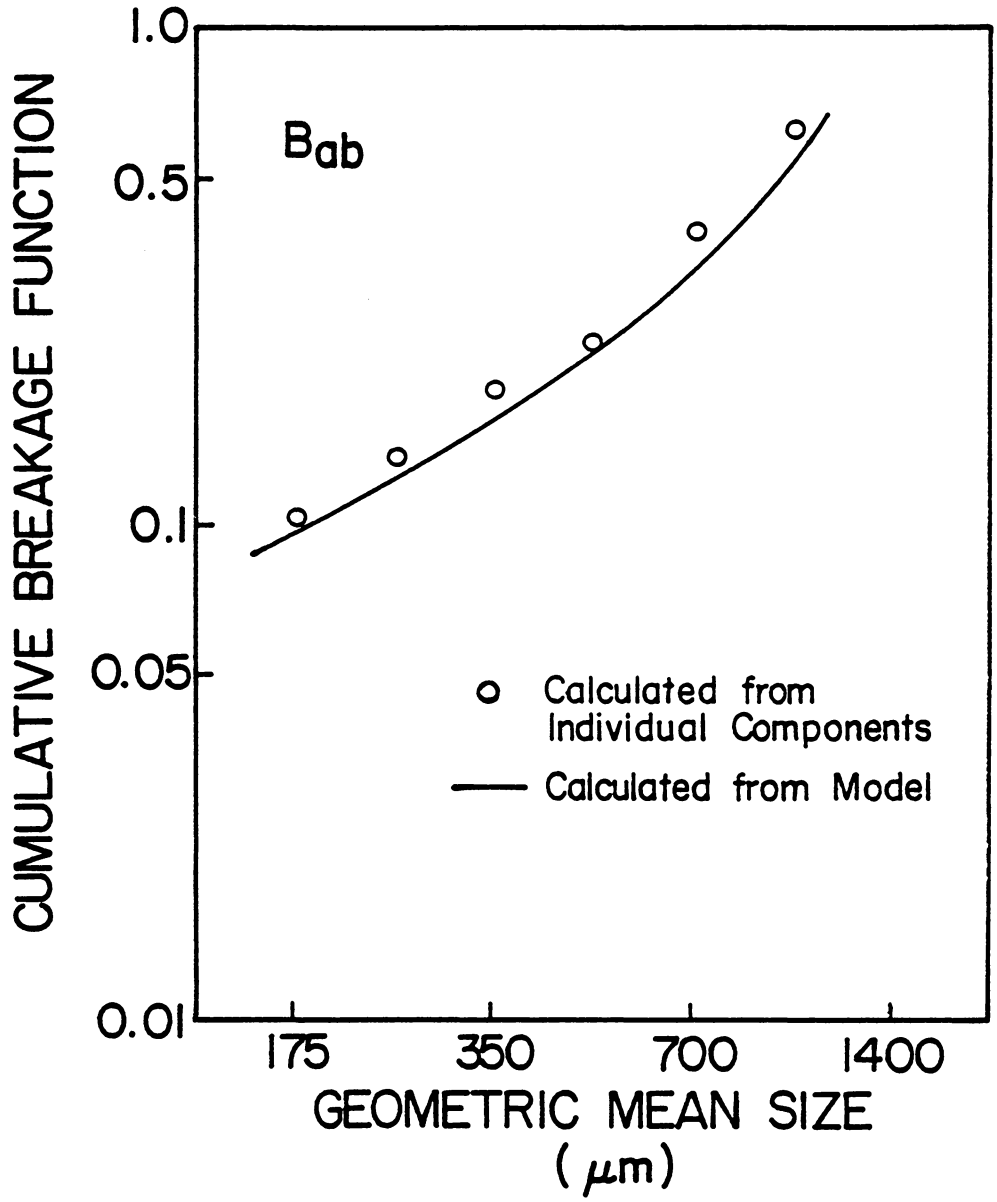

Figure 4.26 Comparison between estimated and model-predicted cumulative breakage distribution functions for the composite particles.

two classes of composite particles was simulated and compared to the experimental data, as shown in Figure 4.27. Once again, the model predictions are in an excellent agreement with the experimental data obtained for free gangue and free sphalerite. This was not unexpected since the equations describing this part of the liberation process remain essentially unchanged regardless of the number of components in the model. Also the model was found to describe the total product distribution quite well. This was also expected since most of the product consists of free components. For the two composite particle classes, the fit was not as good; however, this appears to be quite reasonable considering the simplifying assumption used in determining the unknown model parameters, particularly in estimating the $\underline{L}_{ab,j\leftarrow i}$ values.

When considering two composite classes, the estimation of the liberation functions becomes much more difficult. Therefore, a mathematical technique for estimating liberation functions for multiple classes of composite particles has been developed, as will be discussed in the next chapter.

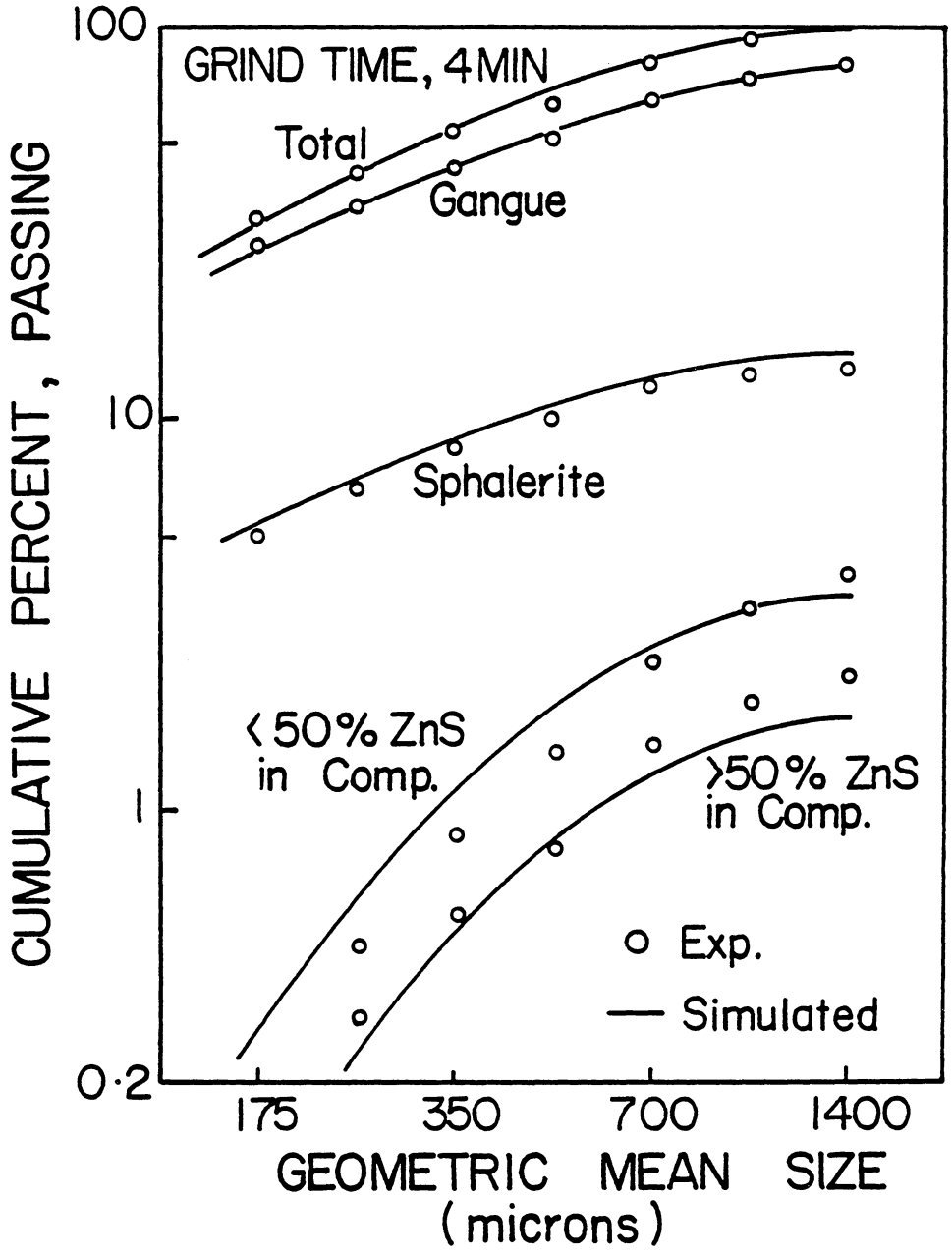

Figure 4.27. Comparison between the computer-simulated and the experimentally determined size distributions for the case of having two classes of composite particles.

CHAPTER V.

DISCUSSION

5.1 Quantification of Liberation Data Using Image Analysis

5.1.1 Evaluation of Areal Grade Measurements

Liberation analysis in its most complete form involves the determination of the volumetric abundance or volumetric grade distribution of a particular phase for each particle size. However, it is extremely difficult to determine the volumetric grade distribution of a specified mineral phase for a multi-component system by direct analysis. During the past few years, a common approach in liberation analysis involves an assumption that the areal grade distribution is a reasonable estimate of the volumetric grade distribution. In some cases, however, the areal grade distribution has been adjusted with an empirical factor to estimate the volumetric abundance. Although many attempts have been made to solve this problem, none of the proposed methods is entirely satisfactory.

It should be noted that in the present work the two-dimensional measurements have been used (without using any transformation functions) to estimate the volumetric grade distribution. Two major reasons are given for this:

Firstly, the transformation of two-dimensional data to three-dimensional information had little bearing on the model development itself. Since the parameter estimation and the computer simulations were conducted on the basis of two-dimensional data, the model development and validation are self-consistent. Secondly, the purpose of the present work was not to look at ways of transforming one- and two-dimensional measurements to three-dimensional data. This is an entire research area in itself which is being studied by other investigators (King, 1979; Stewart and Jones, 1982; Barbery et al., 1979; Lin et al., 1985). Therefore, this aspect has been bypassed in the present work in order to address the problem of directly combining size reduction with liberation.

Thus, there may be some inaccuracies involved in the measurement of volumetric grade distribution from the two-dimensional measurement. However, Lin and Miller's (1986) analysis seems to indicate that, in some cases, the amount of correction required to transform two-dimensional data to three-dimensional data can be minimal. These investigators have experimentally shown that when an ore has a dispersed phase volumetric grade of less than 10%, the areal grade distribution very nearly approximates the true volumetric grade distribution without adjustment (see Figure 5.1). The volumetric grade of the ore used in the present work

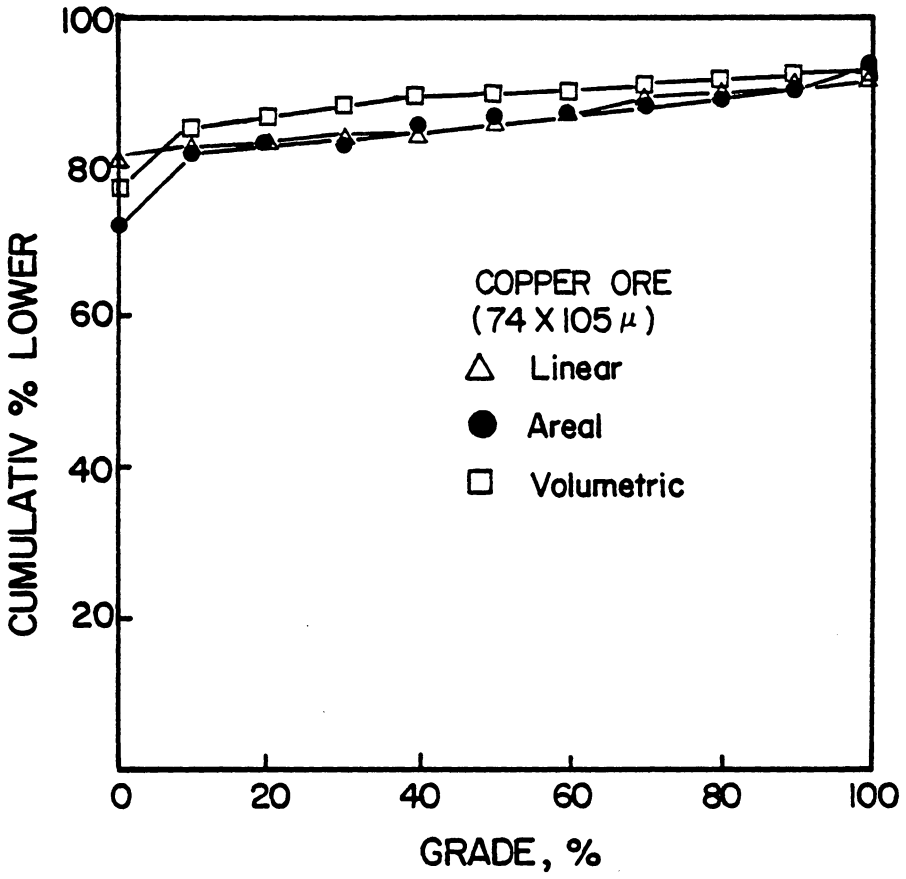

Figure 5.1 Comparison of linear, areal and volumetric grade distributions of copper ore (74x100 micron, 11% by volume of chalcopyrite) (Lin, 1986).

is approximately 13.4%. Therefore, the percent error caused by not using a transformation function may be insignificant.

It bas been shown in Figure 4.3 that there exists an excellent agreement between the areal assays and the chemical assays. One reason for this close agreement is that the results shown in this figure represent an average grade for each size fraction. Underwood (1970) has shown that

$$V_V = A_a = L_l = P_p \qquad [5.1]$$

where

V_V = mean volume fraction, volume of features per unit test volume,

A_a = mean area fraction, area of intercepted features per unit test area,

L_l = mean linear fraction, length of linear intercepts per unit test length,

P_p = mean point fraction, number of points (in areal features) per total test point.

Equation [5.1] holds irrespective of size, shape, particle composition, etc..

5.1.2 Statistical Analysis

Two kinds of error that may occur in areal grade measurements are: i) the error due to observation and image manipulation by the operator, and ii) the statistical error. The first type of error can be reduced to a negligible level with experience. In this regard, the reliability of the areal grade measurements was assessed by performing statistical analysis of the experimental results.

Based on the statistical analysis described by Jones (1982) and Lin et al. (1985), the number of particles required to obtain an unbiased representation of the linear or areal grade distribution of the sample can be estimated. The linear or areal grades of the particles which are randomly dispersed in the resin matrix can be broken down into discrete grade class intervals. Then the best estimate of the density in the i-th grade interval, $\hat{f}_i$, and the relative error, s_i, can be expressed as,

$$\hat{f}_i = \frac{\sum_{j=1}^{n_i} W_j'}{\sum_{j=1}^{n} W_j} \times 100 \qquad [5.2]$$

and

$$s_i = \frac{\hat{f}_i}{\sqrt{n}}, \qquad [5.3]$$

where

n = total number of observations,

n_i = number of observations in the i-th grade interval,

W_j = weighting factor for a given observation: $W_j = 1$ for the measurement based on number; $W_j = l_j$ for the measurement based on length where l_j is the intercepted length of particle j; etc.,

W_j' = same as above for a selected mineral in the i-th grade interval,

$\hat{f}_i$ = percentage in the i-th grade interval, and

s_i = standard deviation (i.e., the expected accuracy of the analysis) of $\hat{f}_i$.

Equation [5.3] can be used to establish the minimum number of measurements needed to determine accurate values of the volume fractions of the components. In general, the standard deviation is inversely proportional to the square root of the total number of observations ($1/\sqrt{n}$). Therefore, to halve the error, one must quadruple the sample size.

For example, if the composite particles amount to 15% of the total volume and are randomly distributed in ten grade intervals, $\hat{f}_i$ equals 1.5. For an expected accuracy of 3% i.e., s_i=0.03, the minimum number of

particles required can be calculated to be

$$n = \left(\frac{\hat{f}_i}{s_i} \right)^2 = \frac{2.25}{0.0009} = 2500.$$

It also follows from Equation [5.3] that for a given accuracy, the number of counts that are required increases as the number of composite particles increases.

Another method to determine the minimum number of measurements required is to plot the volumetric percent versus total number of particles examined, as shown in Figure 5.2. As can be seen, there are significant variations in the volumetric percent of composite particles when less than 2500 particles are examined. For a sample containing 15% composite particles, the expected accuracy after 2500 measurements is about 3%, according to the Equation [5.3]. From Figure 5.2, we can see that the corresponding value determined graphically is 15.3%, which is 2.5% relative error. The relative error was calculated from the difference between the volumetric percent of composite particles when 2500 particles were examined and when 3800 particles were examined. This analysis verified that the particles counted in the present work were large enough to provide an accurate representation of the product size distributions for each component in the ore.

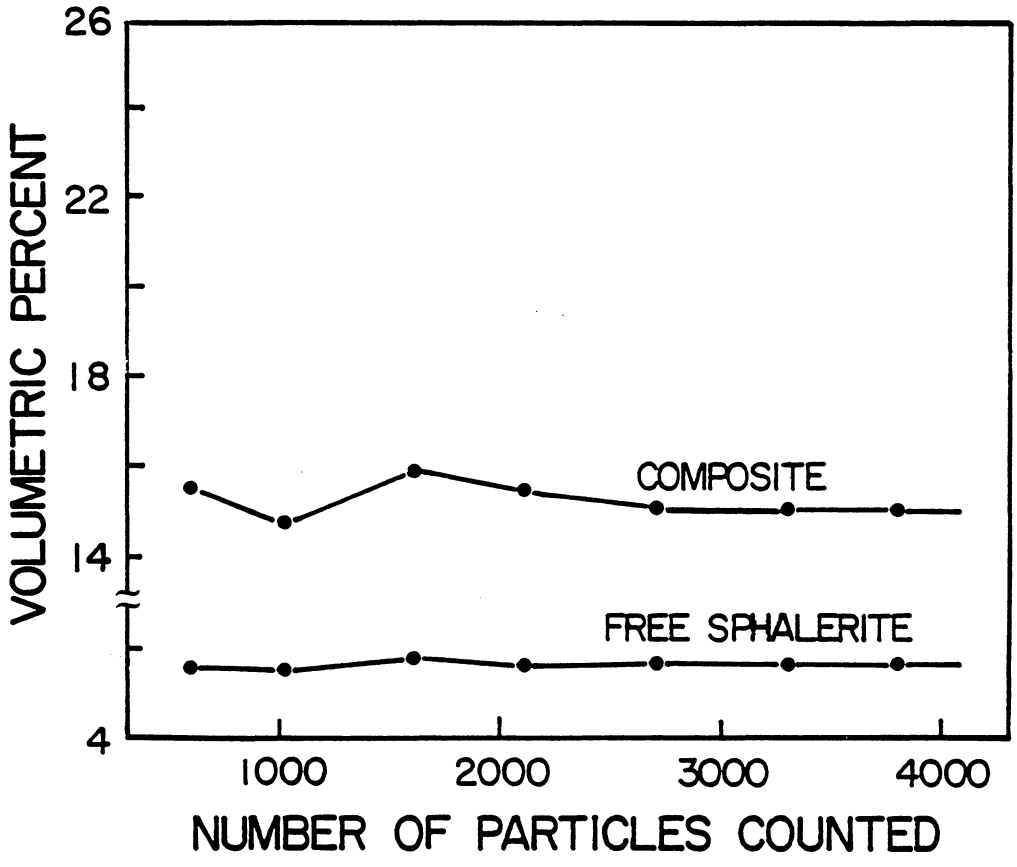

Figure 5.2 Variations in volumetric percent for free sphalerite and composite particles with number of particles examined.

5.2 Validity of the Parameter Estimation Scheme

5.2.1 Analysis of Model Parameter

The results given in the previous chapter show that the breakage rate functions of the components are highly dependent on the grinding environment and must be determined in-situ, i.e., in the presence of the total ore. As shown in Figure 4.10, the breakage rate for gangue ground alone is substantially lower than that for gangue ground in-situ. This might be expected because the absolute value of the breakage rate function is influenced by the hardness/ grindability of the components relative to each other. In order to get an accurate grinding rate for each component in the mill, the breakage rate must, therefore, be determined in-situ. This finding agrees well with the work done with mixtures of minerals (Venkataraman and Fuerstenau, 1984). They also concluded that the breakage rate function of a mineral in a dry ball mill under identical operating conditions was observed to be dependent on whether the minerals is ground alone or as a component in a mixture.

Figure 4.10 also verifies the validity of first-order disappearance kinetics for the minerals when ground alone or as components of a binary mixture. These plots show that, in all cases, the disappearence kinetics are time-independent. This has been the case for the grinding of mineral mixtures (Venkataraman, 1981). However, even though

the breakage rate values are time-independent, they are environment-dependent in that the absolute value of breakage rate depends upon the particles of the minerals constituting the mill charge.

The breakage rate values obtained from various size fractions are given in Table 4.5 and compared with the values calculated from Equation 4.7. For the 10x14 mesh feed, free sphalerite is seen to exhibit the highest breakage rate. During the cataracting (impact of falling balls) and cascading (abrasive action of balls when sliding past each other) of balls in the mill, if two different mineral particles are caught between grinding media, the one that is softer and easily breakable (sphalerite) will be comminuted before the stress threshold for rupture of the harder mineral (dolomite) is reached. Under the microscope, sphalerite particles appeared to be more cubical in shape than dolomite particles, which exhibited a more rounded or plate-like structure. Possibly this difference in the shape of the particles may also have contributed to the observed differences in the breakage rate functions. It can also be noted from Figure 4.10 and Table 4.5 that for the case of 10x14 mesh feed, free sphalerite had the highest breakage rate. However, for the other size fractions, the composite material had a slightly higher breakage rate than the free sphalerite. These results may suggest a preferential

breakage along grain boundaries.

Many investigators who worked on homogeneous materials have shown that the selection function, S(x), is a power function and can be described as $S(x)=ax^{\alpha}$, where x is the particle size and α is obtained from the slope of the log S(x) versus log x plot (Austin and Bhatia, 1971; Herbst and Fuerstenau, 1968). Figure 4.14 shows such a plot for various components in the ore. One can see that most of the experimental S_i values exhibit linear dependency with particle size except for the one for the coarsest fraction (10x14 mesh feed). As the feed particle size increases, the rate of breakage is found to increase up to a certain limit after which it starts going down. The decrease in the rate constant after a certain stage, however, may be due to insufficient nipping of the large particles between the impacting surfaces. The balls also may not have enough energy to break the large particles. This effect will be reduced if the mill and the ball size is increased, thus giving more impact energy for breakage (Austin et al., 1976).

It is very obvious from Figure 4.15 that the cumulative breakage functions for gangue are independent of whether it is ground alone or in the presence of the ore. This means that the manner in which mineral particles distribute into daughter fragments upon breakage is

independent of the grinding environment. This is one of the very important findings of the present investigation. Previously, it was found that the breakage distribution functions of individual minerals under normal mill operating conditions are independent of mill size, mill speed, ball charge and material charge (Herbst and Fuerstenau, 1973), although there is dependence on ball size (Malghan, 1976). More recently, a similar conclusion has been drawn for grinding mineral mixtures (Venkataraman and Fuerstenau, 1984). Furthermore, previous work has clearly shown that the breakage distribution function is normalizable; that is, it is independent of the absolute size of the parent material (Herbst and Fuerstenau, 1968). Figures 4.16 and 4.17 clearly show that the cumulative breakage distribution functions for sphalerite and gangue are independent of the feed size, thus reducing the number of parameters that must be estimated. Therefore, the normalizability of the breakage distribution functions has also simplified the computations in simulation studies in the case of heterogeneous grinding.

A significant point made in the present work is that all model parameters can be determined from grinding tests conducted on the total ore. It is not necessary to conduct separate grinding experiments on individual components. As shown previously, breakage rates are affected by the

grinding environment and must be determined in-situ. Breakage distribution functions, on the other hand, appear to be independent of the environment for the case studied here, and can be determined separately or with the total ore. In addition, the results of the model parameter analysis strongly suggest a preferential breakage of sphalerite over dolomite gangue. This finding is in apparent conflict with the concept of random fracture assumed in other models (Meloy,1984; Klimpel and Austin, 1983). It can be seen from Figure 4.10 that the experimentally determined breakage rates for the composite material are consistently higher than the calculated values and the rate is very close to that for free sphalerite. Furthermore, as shown in Figure 4-18, the liberation function for sphalerite is higher than that of gangue over all size ranges. These experimental findings may suggest that some preferential breakage is taking place at the grain boundaries or through the sphalerite portion of the composite particles. Because model parameters have been determined directly from experimental data, it has been possible to learn a great deal about the fundamental nature of liberation in a binary mineral system, particularly with regard to the controversy as to whether fracture occurs randomly or selectively.

5.2.2 Computer Simulation

As shown in Figures 4.19 and 4.20, the computer-simulated and experimentally determined size distributions for gangue, composite materials, and total product are in close agreement, whereas for the case of free sphalerite, the computer-predicted values fall substantially above the experimentally determined values. It has been found that the discrepancy in the sphalerite is due to an overestimation of the sphalerite content in the feed material as determined by image analysis. It can also be noted from Figures 4.19 and 4.20 that this discrepancy becomes even worse for longer grinding times. As discussed in the previous chapter, the major reason for this discrepancy is largely due to the orientation of heavier sphalerite particles at the bottom of the mold. The results of the simulation using corrected data, shown in Figures 4.21 and 4.22, demonstrate that the model predictions follow the experimental results quite well with the exception of small deviations at fine sizes for all components. This deviation may be ascribed to the experimental error associated with zinc assay values determined by image analysis.

As mentioned in the previous chapter, the model parameters were determined experimentally from the batch grinding of four different monosized feeds. Therefore,

Figures 4.21 and 4.22, which compare the model prediction to experimental data obtained from the batch grinding of monosized feed, are clearly a data fit. Figure 4.23, on the other hand, which compares the computer prediction to the experimental data obtained from the batch grinding of an arbitrary multisized feed, is an independent validation of the model since the parameters obtained from monosized grinding were used in this simulation without adjustment. Therefore, this result indicates that all the parameters in this model have a physical meaning and are physically real. The simulation results also prove the validity of the parameter estimation scheme and model proposed in the present work.

It can be noted from Figure 4.23, however, that the computer-predicted values fall slightly above the experimentally determined size distributions for total, free gangue and free sphalerite. This slight overestimation may be ascribed to the fact that breakage distribution functions for free A and B particles obtained from zero-order production plots have been used for the computer simulation. These experimentally determined breakage distribution values are somewhat higher than expected because, most likely, liberation from composite particles contributes to the zero-order production rate of free sphalerite and free gangue.

It is a well-established fact that the slope of the

size distribution curve for the locked particles is steep. Meloy (1984), for example, presented the concept of eight liberation theorems which are derived for locked particles. One of his theorems states that if the size distribution of the comminuted material follows a Gaudin-Schuhmann curve with a slope of "m", then the locked particles will follow the same curve but it will have a slope of m+1. The results obtained in the present work seem to support this theorem. As shown in Figure 5.3, the slope of the total ore is 0.68 while that of the composite particles is 1.52. This finding simply suggest that the composite particles are more easily found at larger sizes.

One of the major advantages of using the model proposed in the present work is that the degree of liberation for the minerals present in the ore can be predicted reasonably well. Figure 5.4 shows a comparison between the computer-predicted and the experimentally determined degree of liberation for the sphalerite present in the ore. The degree of liberation of sphalerite has been calculated from the Figure 4.23. There is reasonable agreement between the experimental and predicted degree of liberation for sphalerite. However, the computer-predicted values fall slightly above the experimentally determined values in the fine size range, the reverse being the case in the coarse size range. This may be due to the overestimation of the

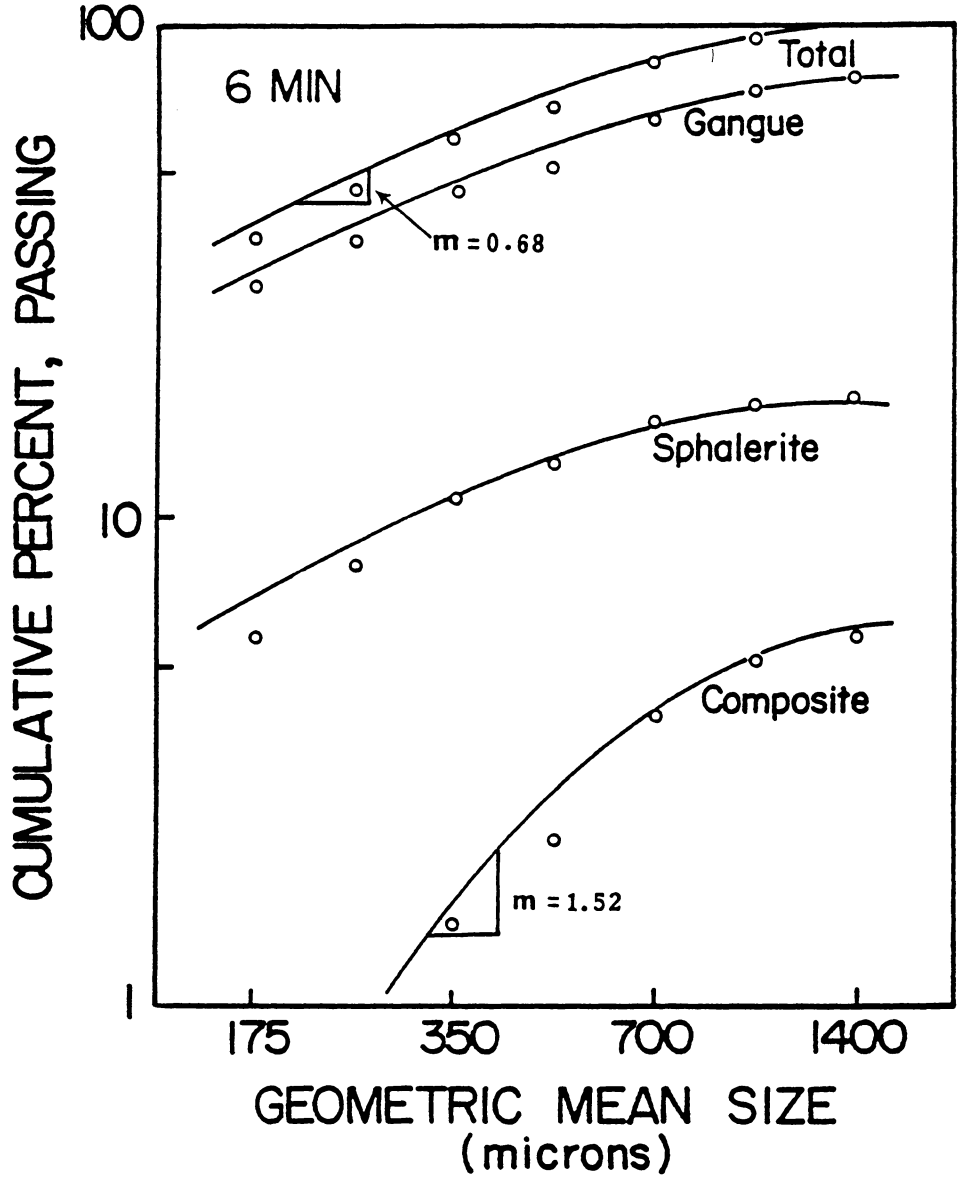

Figure 5.3 Comparison between the slope of the fine size distribution for the total ore (=0.68) and for composite particles (=1.52).

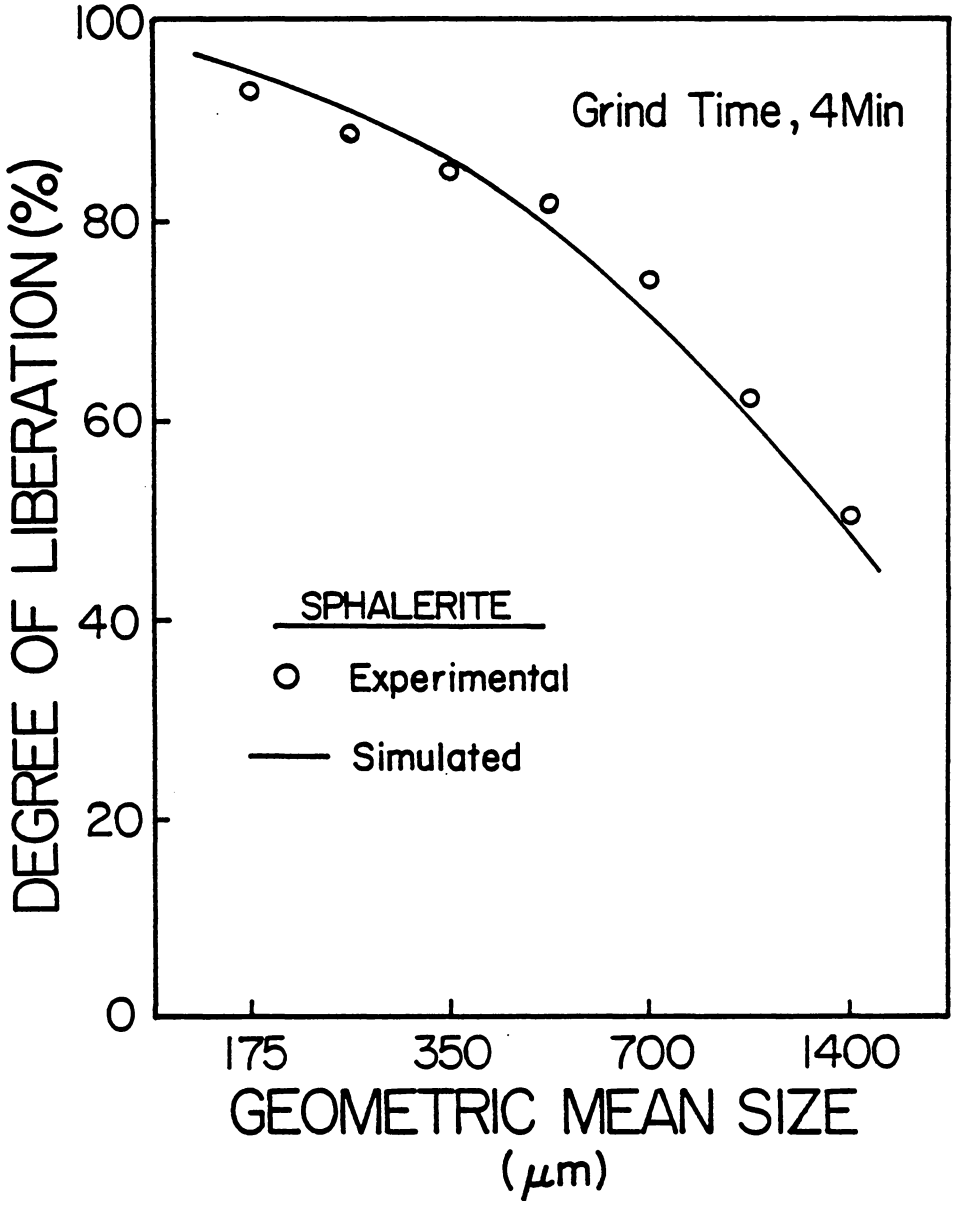

Figure 5.4 Comparison of experimentally determined and computer-simulated degree of liberation of sphalerite as a function of particle size.

experimentally determined size distribution in the coarse size range for the composite particles and the accompanying underestimation in the fine size range, as shown in Figure 4.23.

5.3 Improvement of Computer Simulation for the Case of Two Composite Classes

5.3.1 Model Equations for the Case of Two Composite Classes

As shown in the previous chapter, the model is capable of handling multiple classes of composite particles for a binary ore. However, the experimental verification of the model has been limited to a binary mineral system containing only one composite class. When considering multiple classes of composite particles, the estimation of some of the model parameters, such as the liberation function, becomes much more difficult because of the large number of model parameters to be estimated. For the case of two composite classes, the four matrix equations derived from Equations [2.7]-[2.9] become:

$$\frac{d\hat{M}_a}{dt} = (\underline{B}_a - \underline{I})\underline{S}_a\hat{M}_a + \underline{L}_a(\underline{S}_{ab,1}\hat{M}_{ab,1} + \underline{S}_{ab,2}\hat{M}_{ab,2}) \qquad [5.4]$$

$$\frac{d\hat{M}_b}{dt} = (\underline{B}_b - \underline{I})\underline{S}_b\hat{M}_b + \underline{L}_b(\underline{S}_{ab,1}\hat{M}_{ab,1} + \underline{S}_{ab,2}\hat{M}_{ab,2}) \qquad [5.5]$$

$$\frac{d\hat{M}_{ab,1}}{dt} = (\underline{B}_{ab,1} - \underline{I})\underline{S}_{ab,1}\hat{M}_{ab,1} + \underline{L}_{ab,1\leftarrow 2}\underline{S}_{ab,2}\hat{M}_{ab,2} \qquad [5.6]$$

$$\frac{d\hat{M}_{ab,2}}{dt} = (\underline{B}_{ab,2} - \underline{I})\underline{S}_{ab,2}\hat{M}_{ab,2} + \underline{L}_{ab,2\leftarrow 1}\underline{S}_{ab,1}\hat{M}_{ab,1} \qquad [5.7]$$

As can be seen in the above equations, there are four sets of unknown parameters, including two sets of liberation functions ($\underline{L}_{ab,2\leftarrow 1}$ and $\underline{L}_{ab,1\leftarrow 2}$) and two sets of breakage functions ($\underline{B}_{ab,1}$ and $\underline{B}_{ab,2}$). In the next section, an estimation method for the above parameters will be presented for a system containing two classes of composite particles.

5.3.2 Determination of the Liberation Functions

As discussed previously, the liberation functions for A and B type particles have been estimated from the model equations. For the case of two composite classes, the values determined previously for $\underline{L}_a$ and $\underline{L}_b$ are still valid. Initial estimates of the additional unknown parameters were determined as follows.

A constraining relationship exists between the liberation functions for the case of one composite particle and for the case of two composite classes. The total appearance term due to liberation from one composite particle must be equal to the sum of the liberation terms obtained from two different composite classes. Therefore, the following two equations can be written:

$$\underline{L}_a \underline{S}_{ab} \hat{M}_{ab} = \underline{L}_{a,1} \underline{S}_{ab,1} \hat{M}_{ab,1} + \underline{L}_{a,2} \underline{S}_{ab,2} \hat{M}_{ab,2} \qquad [5\text{-}8]$$

$$\underline{L}_b \underline{S}_{ab} \hat{M}_{ab} = \underline{L}_{b,1} \underline{S}_{ab,1} \hat{M}_{ab,1} + \underline{L}_{b,2} \underline{S}_{ab,2} \hat{M}_{ab,2} \qquad [5\text{-}9]$$

The right-hand side of the above equations includes liberation from two classes of composite particles, which introduced the additional unknown parameters, $\underline{L}_{a,1}$, $\underline{L}_{a,2}$, $\underline{L}_{b,1}$ and $\underline{L}_{b,2}$.

In order to solve the above equations, certain constraints can be imposed upon the breakage of composite AB particles. Figure 5.5 shows the process of breakage for a binary mineral system containing two classes of composite particles. In this case, the composite particles were divided into i) particles containing less than 50% sphalerite, and ii) particles containing more than 50% sphalerite. An assumption was made here that the average volumetric grade of sphalerite for each category of composite particles was 25% and 75%, respectively. When the first category of composite particles (AB_1) break, they cannot produce free valuable (A) in the next size class simply because the total volume of sphalerite in AB_1 type particles in the top size might be less than the volume of free valuable in the next size class. A similar limitation can be applied to AB_2 type particles. From this point of view, Equation [5.8] can be divided into two equations

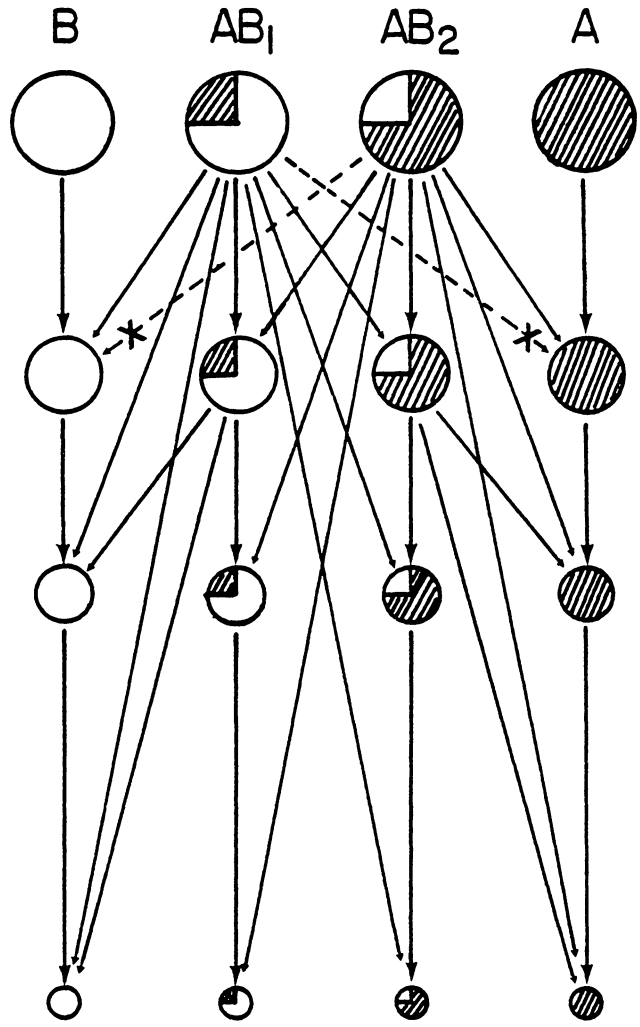

Figure 5.5 Schematic representation of the breakage of a binary ore for the case of two classes of composite particles showing the breakage limitation on composite particles.

using the proportionality constant, α.

$$\underline{L}_{a,2}\underline{S}_{ab,2}\hat{M}_{ab,2} = \hat{\alpha}\underline{L}_{a}\underline{S}_{ab}\hat{M}_{ab} \qquad [5.10]$$

$$\underline{L}_{a,1}\underline{S}_{ab,1}\hat{M}_{ab,1} = (1 - \hat{\alpha})\underline{L}_{a}\underline{S}_{ab}\hat{M}_{ab} \qquad [5.11]$$

Thus, $\hat{\alpha}$ is a vector and can be considered as a function of the particle size and liberation functions. The initial estimates of α_i can be made from the log-log plots of the experimentally determined liberation functions (see Figure 5.6). As shown in Figure 5.6, the experimentally determined liberation functions decrease linearly as particle sizes decrease. If the initial and final α values are known, then the remaining α values can be calculated directly from the linear function. From the breakage limitation on composite particles shown in Figure 5.5, the α_2 (size class, i=2) value can be assumed to be 1 and the α_8 (size class, i=8) value must be equal to 0. The remaining α values can therefore be determined as mentioned above. The initial estimates of the α_i values for free sphalerite and free gangue determined by the above methods are given in Table 5.1.

As mentioned previously, it has been assumed that the cumulative breakage functions for composite particles ($\underline{\overline{B}}_{ab,1}$ and $\overline{\underline{B}}_{ab,2}$) can be estimated from their component parts in proportion to the volume fraction of each part present in

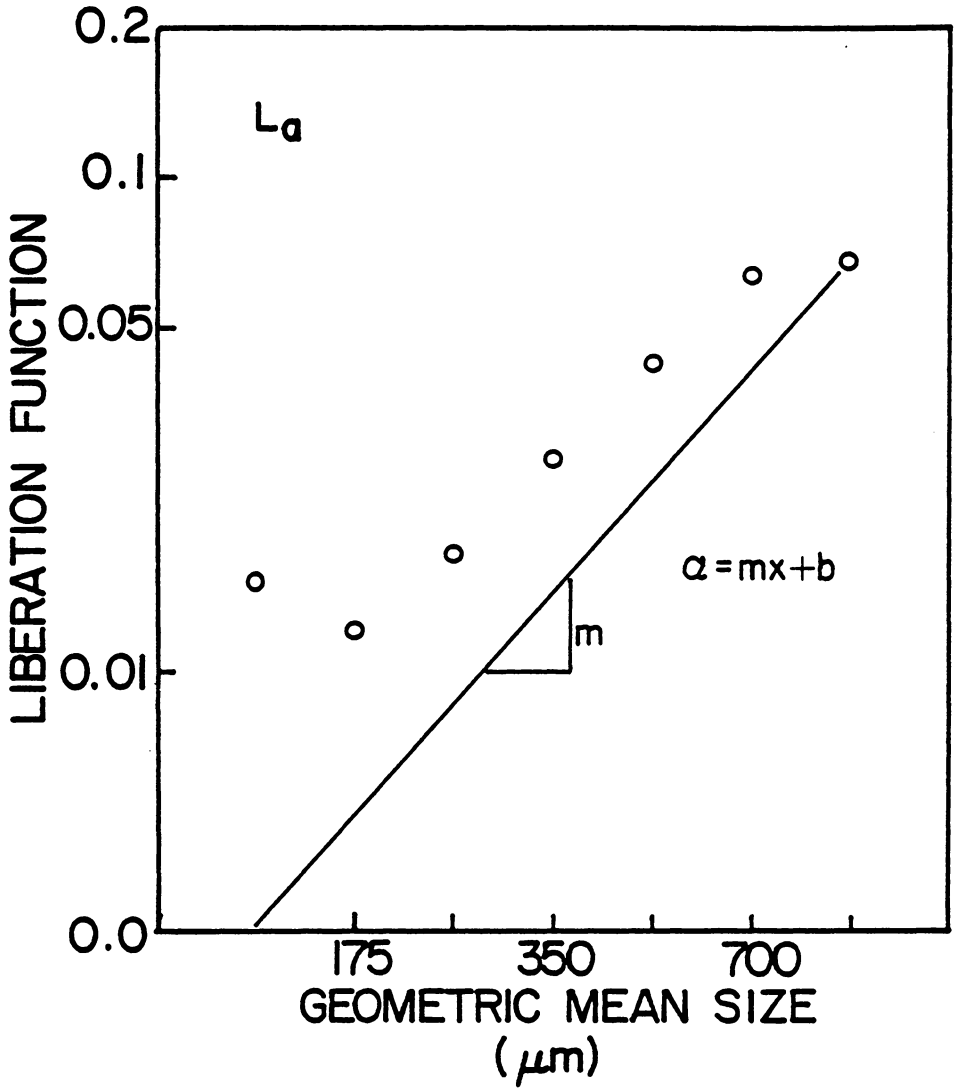

Figure 5.6 Method for determining α_1 values from liberation function data.

Table 5.1 Comparison of initial estimates of α_i values for liberation functions.

α_i	Sphalerite	Gangue
2	1.00	1.00
3	0.70	0.66
4	0.58	0.50
5	0.38	0.38
6	0.24	0.26
7	0.16	0.15
8	0.10	0.07

the composite particle. This leaves two parameters, $\underline{\underline{L}}_{ab,1\leftarrow 2}$ and $\underline{\underline{L}}_{ab,2\leftarrow 1}$, which are unknown.

One final constraint on the breakage and liberation functions which must be met is that the total of the AB_1 (or AB_2) particle breakage and liberation functions must add up to unity, or:

$$\sum_{i=j+1}^{N} (b^{ab,1}{}_{ij} + l^{a,1}{}_{ij} + l^{b,1}{}_{ij} + l^{ab,2\leftarrow 1}{}_{ij}) = 1 \qquad [5.12]$$

$$\sum_{i=j+1}^{N} (b^{ab,2}{}_{ij} + l^{a,2}{}_{ij} + l^{b,2}{}_{ij} + l^{ab,1\leftarrow 2}{}_{ij}) = 1 \qquad [5.13]$$

For each j, $1 \leq j \leq N-1$

In the above notation, $b^{ab,1}{}_{ij}$, $l^{a,1}{}_{ij}$, $l^{b,1}{}_{ij}$, $l^{ab,1\leftarrow 2}{}_{ij}$ and $l^{ab,2\leftarrow 1}{}_{ij}$ represent the size-discretized breakage and liberation functions for AB_1, A_1, B_1 and AB_1 material, respectively. In order to determine the individual components of the matrices for $\underline{\underline{L}}_{ab,2\leftarrow 1}$ and $\underline{\underline{L}}_{ab,1\leftarrow 2}$, it is necessary to run the computer program several times using different values of $\underline{\underline{L}}_{ab,2\leftarrow 1}$ and $\underline{\underline{L}}_{ab,1\leftarrow 2}$, which must meet the above-mentioned condition. The computer estimates of the liberation functions for A, AB_1, and AB_2 materials are shown in Table 5.2.

Table 5.2 Computer-estimated cumulative liberation functions for free sphalerite and composite particles.

Size	Free Sphalerite		Composite Particles	
	$L_{a,1}$	$L_{a,2}$	$L_{ab,2\leftarrow1}$	$L_{ab,1\leftarrow2}$
10x14	--	--	--	--
14x20	--	0.265	0.105	0.216
20x28	0.111	0.159	0.094	0.112
28x35	0.065	0.088	0.052	0.037
35x48	0.016	0.027	0.020	0.023
48x65	0.008	0.009	0.004	0.013
65x100	0.004	0.005	0.001	0.005
-100	0.001	0.002	0.000	0.000

5.3.3 Computer Simulation

Using the model parameters determined as described above, computer simulations were carried out to predict the product size distributions for each component in the batch mill grinding of multisized feeds. Figure 5.7 shows the model predictions and the actual experimental results. The model predictions follow the experimental results quite well with the exception of a small deviation for two composite classes. While this fit is not as good as can be obtained for the case of one class of composite particles, the model appears to be reasonably successful. The average error is approximately 5.7%, which is within experimental limits of error.

The goal of this investigation was to develop an experimental technique to estimate parameters for the two-component grinding-liberation model and then to verify its validity. This has been accomplished. The major problem for the population balance model is how to estimate the exceedingly large number of parameters, especially when the second variable (composition) is introduced.

The work done at the University of Utah has clearly demonstrated the use of numerical parameter estimation techniques to determine the parameters for a such a model. However, there was a lack of experimental data to justify some of the simplifying assumptions which are typically

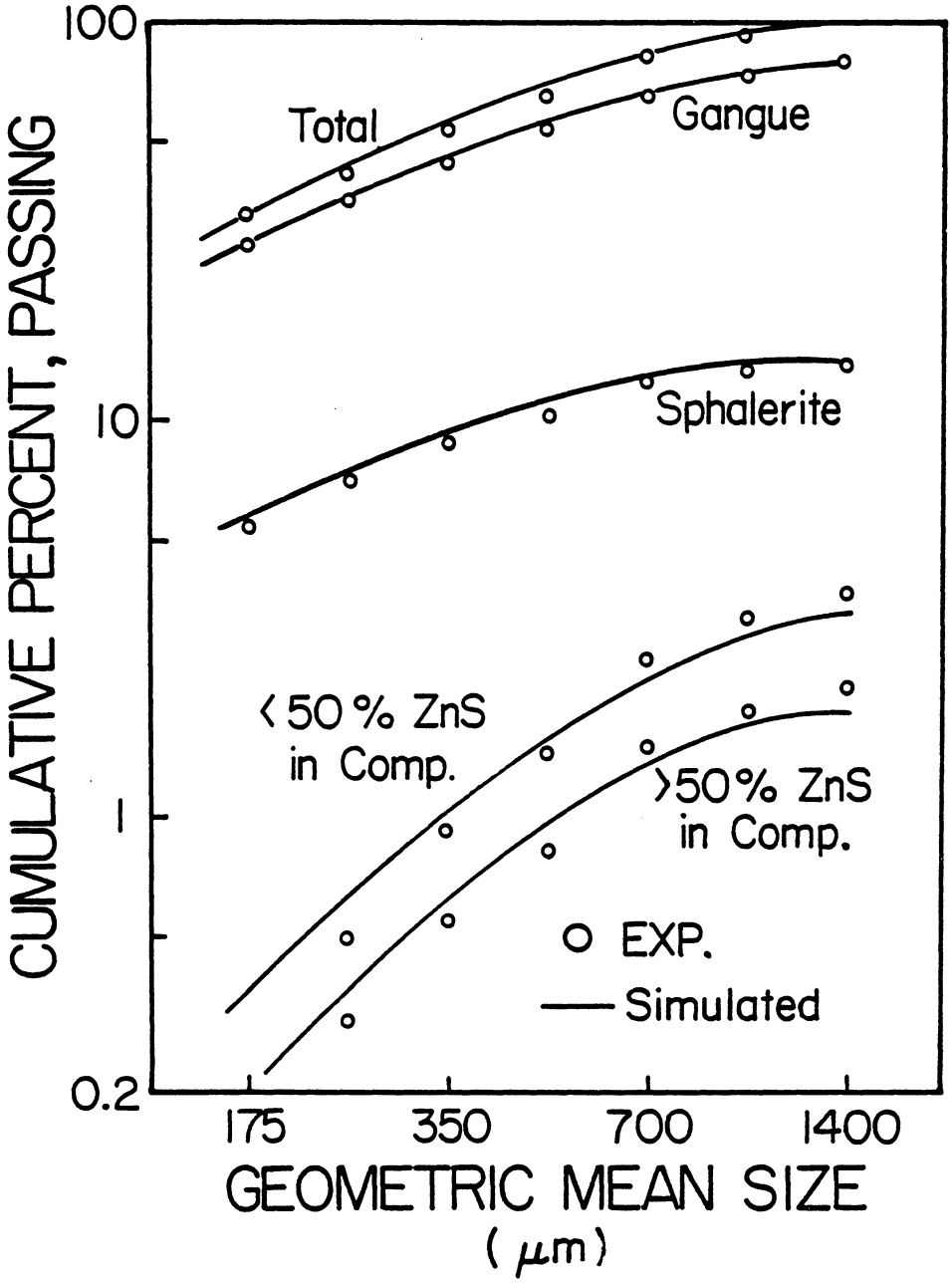

Figure 5.7. Comparison between the computer-simulated and the experimentally determined size distributions for the case of having two classes of composite particles.

needed in this type of parameter estimation. Therefore, our approach has been to determine the model parameters, wherever possible, directly from experimental data. It should be noted, however, that a number of suggestions can be made which may improve the simulation with more than one class of composite particles.

CHAPTER VI.

SUMMARY AND CONCLUSIONS

The major findings of the present work may be summarized as follows:

1. A combined size reduction-liberation model of grinding has been developed to predict size distributions for both free and composite particles. The model is based on an extension of the population balance model for grinding to include the liberation behavior of a binary ore. Separate model equations have been used to describe the breakage and production of A, B, and AB type material. Along with the conventional breakage rate and breakage distribution function values required for all component minerals and composite particles, a new parameter, the liberation function, has been introduced. This function describes the fraction of primary breakage product of type AB which reports to another size and composition class.

2. In order to verify the proposed model and parameter estimation scheme, a series of batch grinding tests was performed on a coarse-grained sphalerite ore obtained from ASARCO's Young Mine in eastern Tennessee. In this

work, a computerized optical image processing system (SEM-IPS) was used to quantify the mineral liberation as a function of the extent of size reduction. This system provided an areal assay of each particle which was assumed to directly correspond to the volumetric assay. Areal assays, obtained from image analysis of monosized particle mounts, have been found to correspond quite closely to the actual chemical assays. Therefore, the data presented here suggest that the mean areal grade can closely approximate the mean volumetric grade, provided that representative and random samples are presented for the image analysis. Recent work presented by C. L. Lin (1986) also seems to indicate that, in some cases, the areal grade distribution very nearly approximates the true volumetric grade distribution without any adjustment. In the present work, it has also been found that the method used to prepare particle mounts is critical in achieving accuracy.

3. In the present work, a detailed parameter estimation scheme has also been developed which utilizes image analysis data obtained from the batch grinding of monosized feed materials. Heavy emphasis has been placed on the experimental determination of the model parameters, as opposed to mathematically fitting the

parameters, in order to gain a better fundamental understanding of the liberation process. Therefore, breakage distribution and rate functions for A and B type particles have been determined directly from dry, batch grinding experiments on the ore. Breakage parameters for the AB material and for the liberation of A and B type particles have been estimated from the model equations.

4. As a result of the model parameter analysis, breakage rate functions are found to be highly sensitive to the grinding environment and must be determined in the presence of the ore in order to get accurate representation of the grinding rate for each component. On the other hand, breakage distribution functions appear to be independent of the grinding environment and, therefore, can be determined either by grinding pure components or in situ. It also appears that breakage distribution functions can be determined accurately from the standard zero-order production plots obtained from grinding the total ore, provided that the amount of composite material present in the feed ore is small. Furthermore, these breakage distribution functions obtained as such are found to be normalizable with respect to feed size, thus reducing the number of parameters which must be determined.

5. The major advantage of the parameter estimation method described above is that it emphasizes the direct experimental determination of breakage parameters rather than using functional forms adjusted by a computer package to fit a product distribution. Since model parameters have been determined directly from experimental data, it has been possible to learn a great deal about the fundamental nature of liberation in a binary mineral system, particularly with regard to the controversy as to whether fracture occurs randomly or selectively. In fact, both the breakage rate and liberation functions suggest a preferential breakage of sphalerite over dolomite gangue. This may be due to the more friable nature of sphalerite, allowing it to be more easily broken away from composite particles. The liberation function is found to be useful for analyzing the breakage mechanisms of composite particles.

6. The model has been tested successfully for the batch grinding of a monosized sphalerite ore, assuming that all composite particles can be lumped into one class. It can predict the size distributions for the total ore and its components, including gangue, sphalerite, and composite particles. In order to independently validate the model, the same parameters determined from monosized

feed grinding data were used to simulate the batch grinding and liberation of an arbitrary multisized feed. Excellent agreement between the model predictions and the experimental results was also observed for multi-sized feed material. This may serve as an independent verification of the model. Furthermore, the model has been shown to successfully predict the degree of liberation of sphalerite as a function of particle size.

7. The model is capable of handling multiple classes of composite particles. When considering multiple classes of composite particles, however, the estimation of some of the model parameters, such as the liberation function, becomes much more difficult. In the present work, a mathematical technique for estimating the liberation function for two composite classes has been developed. The experimental verification of the model for the case of two composite classes was found to be reasonably successful. It should be noted, however, that a more efficient way to estimate the liberation function is possible. Additional work is necessary to develop a mathematical solution and parameter estimation scheme for the case of more than one class of composite particles.

CHAPTER VII.

SUGGESTIONS FOR FUTURE WORK

Based upon the experience and information obtained during the course of the present work, additional research in the following areas is suggested:

1. In the present work, the model has been tested successfully for the batch grinding of a simple binary ore, but has not been tested with complex ores. Since multicomponent systems are much more common than binary systems, fundamental information on the liberation characteristics of multicomponent systems will be of practical use in a variety of ore processing applications. Therefore, additional work is necessary to further develop the model to describe the breakage of multicomponent complex ores. To model a multicomponent system, the model may be applied, in turn, to each component contained in the ore with the rest of the ore lumped as the second component of the binary model. This requires only a minor adaptation of the existing model form.

2. A liberation model developed for complex ores may also be useful in describing the breakage characteristics

of coal. Using the image analysis technique employed in the present work, it is possible to develop techniques for characterizing coal and to study the liberation and breakage properties of coal macerals and mineral matter during grinding. The breakage and liberation of macerals and mineral matter can be modeled and used for simulation. Therefore, the automatic image analysis techniques developed may also be useful in coal blending technology.

3. The model has been verified against experimental results by considering only two composite classes. Further study is needed to make the liberation model more general. This future work includes the development of mathematical solutions and parameter estimation schemes for the case of more than one class of composite particles.

4. In the present work, the breakage parameters for the AB material and the liberation function of A and B type particles have been estimated from the model equations. However, it may possible to directly measure the liberation functions if the amount of free material in the monosized feed material is small. Therefore, in the future work, the feed material will be chosen in such a way that it will contain a very small amount

of free particles, or the free particles will be removed from the feed by a suitable method in order to directly measure the liberation function. The liberation functions, determined as such, will be compared to the calculated values, which will facilitate understanding of the liberation process regarding random or preferential fracture.

5. It would be useful to characterize liberation in different grinding environments. The effect of such variables as ball size, ball load, mill speed and solids load on the liberation properties of the ore should be studied through the use of the model parameters. A torque sensor on the drive shaft of the mill can be used to report on the basis of specific energy input. It is hoped that this analysis will lead to some insight as to whether grinding conditions can affecthe liberation process.

REFERENCES

Andrews, J.R.G. and Mika, T.S., 1976. "Comminution of a Heterogeneous Material: Development of a Model for Liberation Phenomena." Proc. 11th Int. Miner. Process. Congr., Cagliari, pp. 59-88

Anon., "Comminution and Energy Consumption, 1981. " Report of the Committee on Comminution and Energy Consumption, National Materials Advisory Board, Publication NMAB - 364, National Academy Press, Washington, D.C.

Austin, L.G. and Bhatia, V., 1971. "Experimental Methods for Grinding Studies in Laboratory Mills," Powder Technology, V. 5, pp. 261.

Austin, L.G., Shoji, K., Luckie, P.T., 1976. "The Effect of Ball Size on Mill Performance," Powder Technology, V. 14, pp. 71-79.

Austin, L.G., Klimpel, R.R. and Luckie, P.T., 1984. Process Engineering of Size Reduction: Ball Milling Published by SME-AIME, New York.

Baba, K., Miller, J.D. and Herbst, J.A., 1985. "A General Transformation Function for the Prediction of Volumetric from Linear Grade Distributions", presented at the 114th AIME Annual Meeting, New York.

Bagga, P.S. and Luckie, P.T., 1983. "A Monte Carlo Simulation of Liberation Phenomena." Proceedings of First Conference on Use of Computers in Coal Industry, Y.J. Wang and R.L. Sanford, ed., AIME, New York, pp. 247-250.

Barbery, G., 1974. "Determination of Particle Size Distribution from Measurements on Sections," Powder Technology, V. 9, pp. 231-240.

Barbery, G., Huyet, G., and Gateau, C., 1979. "Liberation Anaysis with the Help of Image Analysis: Theory and Application", XIII IMPC, Toronto, VIII 1.1-1.18.

Barbery, G., 1985. "Mineral Liberation Analysis Using Stereological Methods: A Review of Concepts and Problems", ICAM '84, Applied Mineralogy, ed. by W.C. Park et al., AIME, pp 171-190.

Barbery, G., 1985. "Random Sets and Integral Geometry in Comminution and Liberation of Minerals", presented at the 114th AIME Annual Meeting, New York.

Berube, M.A., Berube, Y. and LeHouillier, R., 1979. "A Comparison of Dry and Wet Grinding of a Quarzite in a Small Batch Mill," Powder Technology, V. 23, pp. 169-178.

Berube, M.A. and Marchand, J.C., 1984. "Evolution of the mineral liberation characteristics of an iron ore grinding," International Journal of Mineral Processing, V. 13, pp. 223-237.

Bloise, R., Gateau, G. and Broussund, A., 1984. "Determination of Mineral Liberation in Ore Dressing", Eighteenth International Symposium of Application of Computers and Mathmatics in the Mineral Industries, London, pp. 427-439.

Bond, F.C., 1952. "The Third Theory of Comminution," Trans. AIME, V. 193, pp. 484-494.

Broadbent, S.R. and Calcott, T.G., 1956. "Coal Breakage Process - 1 and 2," J. Inst. Fuel, V. 29, pp. 524.

Burt, R.O., 1984. Gravity Concentration Technology, Elsevier Scientific Pub. Co., Amsterdam.

Carnahan, B., Luther, H.A. and Wilkes, J.O., 1969. Applied Numerical Methods, John Wiley & Sons, New York.

Choi, W.Z., 1982. "Comminution and Liberation Studies of Complex Sulfide Ores," M.S. Thesis, Dept. of Mining and Minerals Engineering, Virginia Polytechnic Institute and State University, Blacksburg, Virginia.

Choi, W.Z., Adel, G.T. and Yoon, R.H., 1985. "A combined size reduction and liberation model of grinding," 114th AIME Annual Meeting, February 24-27, New York, Preprint No. 85-3.

Choi, W.Z., Adel, G.T. and Yoon, R.H., 1985. "Liberation analysis using a simple image processing system," Proceedings, 16th Annual Meeting of the Fine Particle Society, April, Miami Beach, Florida. (in press)

Choi, W.Z., Yoon, R.H., Craig, J.R. and Haralick, R.M., 1985. "Application of Population Balance Model to Comminution of Complex Sulfide Ores," Proceedings, 16th Annual Meeting of the Fine Particle Society, April, Miami Beach, Florida. (in press)

Choi, W.Z., Adel, G.T. and Yoon, R.H., 1986. "Liberation Modeling using automated image analysis." Presented at the Engineering Foundation Conference on Recent development in Comminution, Cona, Hawaii, December, 1985; Accepted for publication in International Journal of Mineral Processing.

Choi, W.Z., Adel, G.T. and Yoon, R.H., 1986. "A Size Reduction/Liberation Model of Grinding Including Multiple Classes of Composite Particles," 115th AIME Annual Meeting, New Orleans, Preprint No. 86-104, Accepted for publication in Minerals and Metallurgical Engineering.

Choi, W.Z., Adel, G.T. and Yoon, R.H., 1986. "Modelling of Size Reduction and Liberation," Presented at the 25th Annual Conference of Metallurgists, Toronto, Ontario, Canada, August 17-20, 1986.

Choi, W.Z., Adel, G.T. and Yoon, R.H., 1987. "Estimation of Model Parameters for Liberation and Size Reduction," 116th AIME Annual Meeting, Denver, Colorado, February 24-27, 1987. (In preparation)

Connelly, T.G., 1985. "A basic guide to the use of the ZEISS image analysis systems," IBAS/SEM-IPS User Guide V. 1-6 Published by Carl Zeiss, Inc., New York.

Craig, J.R., Yoon, R.H., Haralick, R.M., Choi, W.Z. and Pong, T.C., 1982. "The Application of the General Image Processing System (GIPSY) to Mineral Beneficiation Studies," Process Mineralogy II, edited by R. Hangi, The Metallurgical Society of AIME, Pennsylvania, pp. 55-67.

Craig, J.R., Yoon, R.H., Haralick, R.M., Choi, W.Z. and Pong, T.C., 1984. "Mineralogical Variations During Comminution of Complex Sulfide Ores," Process Mineralogy III, edited by W. Petruk, SME-AIME, New York, pp. 51-63.

Craig, J.R., Haralick, R.M., Yoon, R.H., Choi, W.Z. and Pong, T.C., 1986. "Ore Microscopic Studies Using the General Image Processing System (GIPSY)," Physics of Minerals and Ore Microscopy, Proceedings of the 13th General Meeting of the International Mineralogical Association, Varna, Bulgaria, September 19th-25th, 1982.

Davy, P.J., 1984. "Probability Models for Liberation," Journal of Applied Probability, V.21, pp. 160-169.

Delesse, A., 1848. "Procede mecanique pour determiner la composition des roches," Ann. Mines, (iv) 13,pp. 139.

Finch, J.A. and Petruk, W., 1984. "Testing a Solution to the King Liberation Model", International Journal of Mineral Processing, V.12, pp. 305-311.

Finlayson, R.M. and Hulbert, D.G., 1980. "The simulation of the behavior of individual minerals in a closed grinding circuit," Proceeding, 3rd IFAC Symposium, Montreal, pp. 323-332.

Forssberg, E. and Zhai, H., 1985. "Liberation Modelling of Base Metal Ores in Autogenous Grinding," Scandinavian Journal of Metallurgy, V. 14, pp. 9-17.

Fuerstenau, D.W. and Sullivan, D.A., 1962. "Analysis of the comminution of mixtures in ball mills," Can. of Chem. Engrs., V. 40, pp. 43-50.

Fuerstenau, D.W. and Sullivan, D.A., 1962. "Comminution of mixtures in ball mill," Trans. SME-AIME V. 223, No.1, pp. 152-157.

Gardner, R.P. and Austin, L.G., 1962, "The use of a radioactive tracer technique and a computer in the study of the batch grinding of coal." J. Inst. Fuel, V. 35, p. 173.

Gaudin, A.M., 1939. Principles of Mineral Dressing. MaGraw-Hill, New York, pp. 70-91.

Grandy, G.A. and Fueratenau, D.W., 1970. "Simulation of nonlinear grinding systems: rod mill grinding," Trans. AIME, V.247, pp. 348-354.

Gupta, K. A., Hodouin, D., Berube, M.A., and Everell, M. D., 1981. "The Estimation of Rate and Breakage Parameters from Batch Grinding Data for a Complex Pyritic Ore Using Back-Calculation Method," Powder Technology V. 28, pp. 97-106.

Halasyamani, P., Venkatachalam, S. and Mallikarjunan, R., 1966. "Heterogeneous Comminution," Mining Mag., V. 115(3), pp. 184-194.

Haralik, R.M., Yoon, R.H., Craig, J.R., Pong, T.C. and Choi, W.Z., 1982, "The application of the general image processing system (GIPSY) to mineral beneficiation studies." Process Mineralogy Symposium: Application to Extractive Metallurgy I, Dallas, Texas.

Herbst, J.A. and Fuerstenau, D.W., 1968. "The zero order production of fine sizes in comminution and its implications in simulation." Trans. SME-AIME, V.241, pp. 538-548.

Herbst, J.A. and Fuerstenau, D.W., 1972. "Influence of mill speed and ball loading on the parameters of the batch grinding equation," Trans. AIME, V. 252, pp. 169-176.

Herbst, J.A., Rajamani, K., Lin, C.L. and Miller, J.D., 1985. "Development of a Multicomponent - Multisize Mineral Liberation Model," Presented at the 114th AIME Annual Meeting, New York.

Herbst, J.A. and Mika, T.S., 1973. "Linearization of tumbling mill models involving non-linear breakage phenomena," 11th International Symposium on Computer Applications in Minerals Industries, Tucson, Ariz., pp. E78-E124.

Herbst, J.A., Fuerstenau, D.W., 1973. "Mathematical simulation of dry ball milling using specific power information," Trans AIME, V. 254, pp. 343-348.

Herbst, J.A. and Fuerstenau, D.W., 1980, "A Scale-Up Procedure for Continuous Grinding Mill Design Using Population Balance Models", International Journal of Mineral Processing, V. 7, pp. 1-31.

Holland-Batt, A.B., 1983. "Liberation analysis," Trans. Instn. Min. Metall., The Institution of Mining and Metallurgy, V. 92, pp. C129-C137.

Holmes, J.A. and Patching, S.W.F., 1957. "A preliminary investigation of differential grinding-grinding of quartz/limestone mixtures," Trans. Instn. of Chem. Engineers, V. 35, pp.111-124.

Hukki, R., 1961. "Proposal for a Solominic Settlement Between the Theories of von Rittinger, Kick and Bond," Trans. AIME, V. 220, pp. 403.

Jones, M.P. and Shaw, J.L., 1973. "Autometic measurement and stereological assessment of mineral data for use in mineral technology." 10th International Mineral Processing Congress, London.

Jones, M.P., 1977. "Automatic Image Analysis," Physical Methods of Determinative Mineralogy, Zussman, J., ed., Academic Press, pp. 167-200.

Jones, M.P. and Horton, R., 1978, "Recent developments in the stereological assessment of composite (middling) particle by linear measurements", Procesdings of the 11th Commonweath Mining and Metallurgical Congress, Hong Kong, pp. 113-122.

Jones, M.P., 1979, "Automatic Mineralogical Measurements in Mineral Processing", Proceeding, XIII IMPC, J. Laskowski, ed., Elsevier Scientific Pub. Co., Amsterdam, pp. 533-567.

Jones, M.P., 1982, "Designing an X-Ray Image Analyzer for Measuring Mineralogical Data", XIV IMPC, Toronto, Canada, paper 4.

Kelsall, D. and Reid, K., 1965. "The Derivation of Mathematical Model for Breakage in a Small Continuous Wet Ball Mill," AIChE Symp. Series 4, 14.

Kelly, E.G. and Spottiswood, D.J., 1982. Introduction to Mineral Processing, John Wiley & Sons, New York.

King, R.P., 1975. "A quantitative model for mineral liberation," Journal of the South African Institute of Mining and Metallurgy, October, pp. 170-172.

King, R.P., 1978. "Determination of Particle Size Distribution from Measurements on Sections," Powder Technology, V. 21, pp. 147-150.

King, R.P., 1979. "A Model for the Quantitative Estimation of Mineral Liberation by Grinding." International Journal of Mineral Processing. V.6, pp. 207-220.

King, R.P., 1982. "The Prediction of Mineral Liberation from Mineral Texture", XIV IMPC, Toronto, VIII 1.1-1.18.

King, R.P., 1982. "Determination of the Distribution of Size of Irregularly Shaped Particles from Measurements on Sections or Projected Areas," Powder Technology, V.32, pp. 87-100.

Kinneberg, D.J. and Herbst, J.A., 1984. "A Comparison of Linear and Nonlinear Models for Open-Circuits Ball Mill Grinding," International Journal of Mineral Processing, V. 13, pp. 143-165.

Klimpel, R.R. and Austin L.G., 1970. "Determination of Selection-for-Breakage Functions in the Batch Grinding Equation by Non-Linear Optimization," IEC Fund., V. 9, pp. 230.

Klimpel, R.R. and Austin, L.G., 1977. "The Back-Calculation of Specific Rates of Breakage and Non-Normalizable Breakage Distribution Parameters from Batch Grinding Data," International Journal of Mineral Processing, V. 4, pp. 7-32.

Klimpel, R.R. and Austin, L.G., 1983. "A preliminary model of liberation from a binary system." Powder Technology, V. 34, pp. 121-130.

Klimpel, R.R., 1984. "Applications of a Model for the Analysis of Liberation from a Binary System," Powder Technology, V. 39, pp. 117-128.

Li, T.M., 1976. The new look at Asarco's Tennessee Mines, Min. Eng. V. 27, pp. 37-41.

Lin, C.L., Miller, J.D., Herbst, J.A., Sepulveda, J.E., and Prisbrey, K.A., 1984. "Prediction of volumetric abundance from two-dimensional mineral images," ICAM 84, 15 pp.

Lin, C.L., Miller, J.D., Herbst, J.A. and Rajamani, K., 1985. "An evaluation of procedures for the measurement of linear grade distributions in liberation analysis," Presented at the 114th AIME Annual Meeting, February 24-27, New York.

Lin, C.L., 1986. "Measurement and Prediction of Mineral Liberation During Grinding," Ph.D. Thesis, Dept. of Metallurgy and Metallurgical Engineering, Univ. of Utah, Salt Lake City, Utah, pp. 184.

Luckie, P. and Austin, L.G., 1972. "A Review Introduction to the Solution of the Grinding Equations by Digital Computation," Minerals Sci. Engng., V. 4 (2).

Lynch, A., Whiten, W. and Draper, N., 1967. "Developing the Optimum Performance of a Multi-Stage Grinding Circuit," Trans. IMM, V. 76, pp. C169.

Lynch, A., 1977. Mineral Crushing and Grinding Circuits, Elsvier Scientific Pub. Co., Amsterdam.

Malghan, S.G., 1976. "The Scale-up of Ball Mills Using Population Balance Models," Ph.D. Thesis, Univ. of Calif., Berkeley, Calif., pp. 271.

Malvik, T., 1982. "An Empirical Model to Establish the Liberation Properties of Minerals," Proceedings XIV International Mineral Processing Congress, October 17-23, Toronto, Canada.

Maxon, W.L., Cadena, F. and Bond, F.C., 1934. Trans. AIME, V. 112, pp. 130.

McKee, D.J., 1984. "The use of scanning electron microscopy in evaluating metallurgical plant performance," ICAM '84, Los Angeles, California.

Meloy, T.P., 1984. "Liberation theory - eight modern, usable theorems", International Journal of Mineral Processing, V. 13, pp. 313-324.

Meloy, T.P. and Gotoh, K., 1985. "Liberation in a Homogeneous Two-Phase Ore," International Journal of Mineral Processing, V. 14, pp. 45-57.

Miller, P.R., Reid, A.F. and Zuiderwyk, M.A., 1982. "QEM*SEM image analysis in the determination of model assays, mineral associations and mineral liberation," XIV International Mineral Processing Congress, Toronto, Canada.

Mular, A.L. and Jergensen, G.V., 1982. "Design and Installation of Comminution Circuits," A.L. Mular and G.V. Jergensen, Co-Editors, SME of the AIME, New York, New York.

Oosthuyzen, E.J., 1980. "An Elementary Introduction to Image Analysis - A New Field of Interest at the National Institute for Metallurgy," NIM Report No. 2508, South Africa.

Oosthuyzen, E.J., 1983. "The Application of Automatic Image Analysis to Mineralogy and Extractive Metallugy," Spec. Publ. Geol. Soc. S. Afr., V.7, pp. 449-464.

Peterson, R.D., 1983. "Estimation of Parameters for Verification of an Integrated Model for Grinding and Flotation Circuit Simulation," M.S. Thesis, Dept. of Metallurgy and Metallurgical Engineering, University of Utah.

Peterson, R.D. and Herbst, J.A., 1985. "Estimation of kinetic parameters of a grinding-liberation model," International Journal of Mineral Processing, V. 14, pp. 111-126.

Petruk, W., 1976. "The Application of Quantitative Mineralogical Analysis of Ores to Ore Dressing," CIM Bulletin, V. 69, pp. 146-153.

Petruk, W., 1978. "Image analysis study of mill products from batch tests on Brunswick Mining and Smelting Mill tailings," CANMET Report 78-23.

Petruk, W., 1982. "Image Analysis in Process Mineralogy," Process Mineralogy II: Application in Metallurgy, Warrendale, Pennsylvania, pp. 39-53.

Petruk, W., Pinard, R.G. and Finch J., 1985. "Relationship between observed mineral liberations in screened fractions and in composite particles," Presented at the SME-AIME Annual Meeting, February 24-28, 1985, Preprint No. 85-111.

Petruk, W., 1986. "Predicting and measuring mineral liberations in ores and mill products, and effect of mineral textures and grinding methods on mineral liberations," Mineral Sciences Laboratory, Division Report MSL 86-37, CANMET.

Pong, T.C., Haralick, R.M., Craig, J.R., Yoon, R.H. and Choi, W.Z., 1983. "The application of image analysis techniques to mineral processing," Pattern Recognition Letters, V. 2, pp. 117-123.

Rajamani, K. and Herbst, J.A., 1984. "Simultaneous estimation of selection and breakage functions from batch and continious grinding data," Trans. Instn Min. Metall. pp. C74-C85.

Reid, K., 1965. "A Solution to the Grinding Equation," Chem. Eng. Sci., V. 20, pp. 953.

Rose, H.E. and Matsumura, S., 1985. "Simultaneous grinding of two materials in a batch ball mill," Trans. Instn. Min. Metall., V. 94, pp. C40-C46.

Rosiwol, A., 1898. "On geometric rock analysis: A simple surface measurement to determine the quantitative content of mineral constituents of a stoney aggregate," Verdhandl. K.K., Geol. Reich. Wien, V. 5-6, pp. 143.

Ruebush, J.C., Herbst, J.A. and Rajamani, K., 1980. "SIMPLANT-A Program for the simulation of individual mineral behavior in an integrated grinding and flotation circuit," Dept. of Metallurgy and Metallurgical Engineering, Univ. of Utah, Salt Lake City, Utah.

Ruebush, J.C., 1982. "Simulator for Individual Mineral Liberation Behavior in an Integrated Grinding and Flotation Plant," M.S. Thesis, Dept. of Metallurgy and Metallugical Engineerig, University of Utah, Salt Lake City, Utah.

Sampson, R., 1978. Surface II Graphics System. Lawrence, Kansas.

Shoji, K. and Austin, L.G., 1974. "A Model for Batch Rod Milling," Powder Technology, V. 20, pp. 29-35.

Siddique, M., 1977. "A Kinetic Approach to Ball Mill Scale-Up for Dry and Wet Systems," M.S. Thesis, Dept. of Mining, Metallurgical, and Fuels Engineering, Univ. of Utah, Salt Lake City, Utah.

Somasundaran, P. and Fuerstenau, D.W., 1963. "Preferential energy consumption in tumbling mills," Trans. AIME, V. 226, pp. 132-134.

Somasundaran, P., 1986. "Advances in Mineral Processing," Proceedings, Symposium honoring Nathaniel Arbiter on his 75th birthday, New Orleans, Louisiana, March 3-5, 1986, ed. by P. Somasundaran, Published by the SME, Littleton, Colorado.

Steiner, H.J., 1975. "Liberation Kinetics in Grinding Operations," Proceedings, XI International Mineral Processing Congress, Cagliari.

Stewart, P.S.B. and Jones, M.P., 1977. "Determining the Amount and Composite (Middling) Particle," XII IMPC, Sao Paulo, Brasil, V. 3, pp. 91-116.

Tanaka, T. and Selby, D.W., 1976. Austral. Inst. of Mining and Metall., V. 258, pp. 41-45.

Thompson, E., 1930. "Quantitative microscopic analysis." J. Geol., V. 27, pp. 276.

Underwood, E.E., 1970. Quantitative Stereology, Addison-Wesley, Reading, Mass.

Venkataraman, K.S., 1981. "Specific Energy Considerations in the Kinetics of Mixture Grinding," M.S. Thesis, Dept. of Materials Science and Mineral Engineering, Univ. of California, Berkeley.

Venkataraman, K.S. and Fuerstenau, D.W., 1984. "Application of the population balance model to the grinding of mixtures of minerals," Power Technology, V. 39, pp. 133-142.

Weiss, N.L., 1985. "SME Mineral Processing Handbook," N.L. Weiss, Editor-in-Chief, Published by SME of the AIME, New York, New York.

Wiegel, R.L., 1964. "A Mathmatical Model for Mineral Liberation by Size Reduction," M.S. Thesis, Chemical Engineering Dept., Carnegie Inst. of Technology, Pittsburgh, Pa.

Wiegel, R.L., and Li, K., 1967. "A random model for mineral liberation by size reduction." Trans. SME-AIME, V. 238, pp. 179-189.

Wiegel, R.L., 1975. "Liberation in Magnetic Iron Formations," Trans. SME-AIME, V. 258, pp. 247-256.

Wiegel, R.L., 1976. "Integrated size reduction-mineral liberation model," Trans. SME-AIME V. 260, pp. 147-152.

Wills, B.A., 1981. Mineral Processing Technology, 2nd edition, Pergamon Press.

Yang, D., Mempel, G. and Fuerstenau, D.W., 1967. "A Laboratory Mill for Batch Grinding Experimentation," Trans. SME-AIME, V. 238, pp. 273-275.

APPENDIX I

NOMENCLATURE

NOMENCLATURE

A,B - two individual materials types in a two component system

A_a - mean area fraction, area of intercepted features per unit test area

AB - composite (locked middling) of materials A and B, which is present in that two component system

b_{ij} - fraction of primary breakage product initially of the j-th size interval that appears in the i-th size interval

$b^{ab}{}_{ij}$ - fraction oftheprimarybreakage product of composite AB material of size j that remains as composite AB material in size i

$b^{ab,1}{}_{ij}$ - same as above for type AB_1

$b^{ab,2}{}_{ij}$ - same as above for type AB_2

$\underline{B}_a$ - fraction of primary breakage product of type A reporting to each size class (matrix)

$\underline{B}_b$ - same as above for type B

$\underline{B}_{ab}$ - same as above for type AB

$\underline{B}_k$ - same as above for the general case of composition class k

$\overline{\underline{B}}_a$ - fraction of primary breakage product of type A reporting finer than a given size (matrix)

$\overline{\underline{B}}_b$ - same as above for type B

$\overline{\underline{B}}_{ab}$ - same as above for type AB

$\overline{\underline{B}}_{ab,j}$ - same as above for type AB_j

Du - largest intercept length across any particle of mesh size D

$\hat{f}_i$ - percentage in the i-th grade interval

F_i - zero-order rate constant for the production of fines smaller than that stated size

$F(l)$ - distribution of linear intercept length for the mineral

i - a specific composition class

k - same as above

K - total number of composition classes

l^{a}_{ij} - fraction of primary breakage product of type AB of size j which reports to liberated A material in size i

$l^{a,1}_{ij}$ - same as above, but composite type AB_1 appearing as liberated A

$l^{a,2}_{ij}$ - same as above, but composite type AB_2 appearing as liberated A

l^{b}_{ij} - same as above for liberation into type B

$l^{b,1}_{ij}$ - same as above, but composite type AB_1 appearing as liberated B

$l^{b,2}_{ij}$ - same as above, but composite type AB_2 appearing as liberated B

$l^{ab,2\leftarrow1}_{ij}$ - same as above, but composite type AB_1 appearing as composite AB_2 material

$l^{ab,1\leftarrow2}_{ij}$ - same as above, but composite type AB_2 appearing as composite AB_1 material

$\underline{L}_a$ - fraction of primary breakage product of type AB which reports to each size class as free A (matrix)

$\underline{L}_b$ - same as above for liberation into type B

$\underline{L}_{ab,j\leftarrow i}$ - fraction of primary breakage product of type AB_i which liberates into the j-th composition class

$\underline{L}_{k\leftarrow i}$ - same as above for the general case of liberation into composition class k

$\underline{L}_a$ - fraction of primary breakage product of type AB reporting as free A to all sizes finer than a given size (matrix)

$\bar{L}_b$ - same as above for liberation into type B

$L(D)$ - fractional liberation of the mineral at mesh size D

L_l - mean linear fraction, length of linear intercepts per unit test length

m^a_i - mass fraction of material A in the i-th size interval

m^b_i - same as above for type B

m^{ab}_i - same as above for type AB

$m_{ab,i}$ - mass of composite material in a given mineral content class for a given size class

$m_i(t)$ - mass fraction of total mass present in size i at time t

M_{ab} - total mass of composite material in a given size class

$\hat{M}_a$ - mass fraction of particle type A contained in each size class (vector)

$\hat{M}_b$ - same as above for type B

$\hat{M}_{ab}$ - same as above for type AB

$\hat{M}_{ab,j}$ - same as above for type AB_j

$\hat{M}_k$ - same as above for the general composition class k

n - total number of observations

n_i - number of observations in the i-th grade interval

N - number of size intervals

N - number of mineral content classes; see equation [4.7]

$N(l/D)$ - linear intercept distribution function for particles of mesh size D

QA - "directional coefficients" describing the quantity of AB from size class i-1 which appears as component A in size i

QB - same as above for type B

QAB - same as above for type AB

S^a_i - breakage rate function for type A in the i-th interval

S^b_i - same as above for type B

S^{ab}_i - same as above for type AB

$S_i(t)$ - breakage rate function at time t for material in the i-th size class

$\underline{S}_a$ - the rate at which material breaks out of composition class A (matrix)

$\underline{S}_b$ - same as above for type B

$\underline{S}_{ab}$ - same as above for type AB

$\underline{S}_{ab,j}$ -same as above for type AB_j

$\underline{S}_k$ - same as above for the general composition class k

SA - selection function for A component

SB - same as above for B component

SAB - same as above for AB component

s_i - standard deviation (i.e., the expected accuracy of the analysis) of $\hat{f}_i$

t - time

V_v - mean volume fraction, volume of features per unit test volume

WA - quantities of species A

WB - same as above for species B

WAB - same as above for species AB

W_j - weighting factor for a given observation, $W_j = 1$ for the measurement based on number, $W_j = l_j$ for the measurement based on length where l_j is the intercepted length of particle j, etc.

W_j' - same as above for a selected mineral in the i-th grade interval

Y_i - cumulative mass fraction smaller than size class i

$\hat{Y}_a$ - cumulative mass fraction of particle type A finer than a given size (vector)

$\hat{Y}_b$ - same as above for type B

$\hat{Y}_{ab}$ - same as above for type AB

$\hat{Y}_{ab,j}$ - same as above for type AB_j

$\hat{\alpha}$ - proportionality constant, see Equation [5-10]

μ - mean linear intercept length

APPENDIX II

ASSAY PROCEDURE

ASSAY PROCEDURE: Representative portions of each size fraction were ground for 10 minutes using a mechanically operated agate motor and a pestle. After grinding, 0.5g of each finely ground sample was riffled and accurately weighed into a 125-ml Erlenmeyer flask. Ten ml each of concentrated HCl and HNO_3 were added to each flask and placed on a hotplate. A reflux boiling funnel was placed in the mouth of the flask to prevent excessive splashing of the solution and to wash down the sides of the flask. Sufficient heat was applied to maintain a slight boiling condition and the samples were evaporated almost to dryness. The sides of each beaker were rinsed with warm double-distilled water to prevent precipitation of metal ions and to maximize the extraction of soluble metal into solution.

The samples were then allowed to cool and filtered through Whatman No. 2 filter paper into appropriated volumetric flasks. The remaining volumes were filled with double-distilled water. Samples were further diluted according to their respective metal concentrations to fit within the range of calibration the standards.

The zinc content of each sample was determined with a Spectraspan IV Plasma Emission Spectrometer. The wavelength used to detect zinc metal was 2052.52 Angstroms.

All glassware used throughout sample assaying procedures was cleaned in Micro cleaning solution,

thoroughly rinsed with tap water, and finally rinsed with distilled water.

APPENDIX III

IMAGE ANALYSIS DATA

TABLE III-1. Percent zinc in various size fractions determined by chemical analysis and image analysis (monosized feed).*

Size (mesh)	Chemical Assay	Image Analysis
10x14	9.8	14.9
14x20	12.2	16.8
20x28	14.5	20.2
28x35	15.1	19.5
35x48	15.6	19.9
48x65	16.9	19.3
65x100	15.8	18.7

*This data is plotted in Figure 4.1.

TABLE III-2. Percent zinc in various size fractions determined by chemical analysis and image analysis (multisized feed).*

Size (mesh)	Chemical Assay	Image Analysis
10x14	9.5	10.1
14x20	10.0	10.6
20x28	12.6	13.6
28x35	15.4	15.8
35x48	12.1	12.4
48x65	11.6	12.1
65x100	12.3	14.3

*This data is plotted in Figure 4.3.

TABLE III-3. Sphalerite distribution in 10x14 mesh and 14x20 mesh feeds.*

ZnS Content (wt%)	10x14 mesh	14x20 mesh
0-2	62.8	64.0
2-10	2.5	3.0
10-20	3.6	2.3
20-30	2.8	1.8
30-40	0.4	1.3
40-50	1.5	1.5
50-60	4.2	1.5
60-70	1.6	1.5
70-80	2.4	3.2
80-90	1.7	1.3
90-98	2.6	1.6
98-100	14.0	17.0

*This data is plotted in Figure 4.4 and 4.5.

TABLE III-4. Sphalerite distributions in 20x28 mesh and 28x35 mesh feeds.

ZnS Content (wt%)	20x28 mesh	28x35 mesh
0-2	69.4	74.3
2-10	2.2	1.3
10-20	1.6	1.5
20-30	1.3	0.8
30-40	1.2	0.6
40-50	1.0	0.7
50-60	0.8	0.9
60-70	0.7	0.6
70-80	0.9	0.6
80-90	1.0	0.8
90-98	0.9	0.2
98-100	19.0	17.7

TABLE III-5. Sphalerite distribution of multisized feed determined by image analysis.*

ZnS Content (wt%)	10x14	14x20	20x28	28x35	35x48	48x65	65x100
0-2	77.6	78.3	74.7	72.6	81.9	80.2	77.0
2-10	3.0	2.6	1.9	1.4	1.1	0.9	0.7
10-20	2.6	0.8	1.2	1.0	0.7	0.5	0.3
20-30	1.6	1.3	0.8	0.8	0.7	0.5	0.2
30-40	1.3	1.0	0.7	0.7	0.5	0.4	0.3
40-50	1.0	1.1	1.0	0.7	0.4	0.3	0.3
50-60	1.0	1.1	0.7	0.8	0.4	0.4	0.3
60-70	0.9	0.8	0.8	0.6	0.5	0.3	0.3
70-80	1.4	0.9	0.7	0.7	0.3	0.3	0.2
80-90	1.1	1.1	1.2	0.7	0.5	0.4	0.4
90-98	0.8	0.9	0.9	0.6	0.4	0.2	0.2
98-100	7.7	10.1	15.4	19.4	12.6	15.6	19.8

*This data is plotted in Figure 4.6.

TABLE III-6. Sphalerite distribution of product determined by image analysis.*

ZnS Content (wt%)	10x14	14x20	20x28	28x35	35x48	48x65	65x100
0-2	81.6	83.0	77.5	75.8	78.1	77.0	77.7
2-10	2.8	2.9	2.2	1.7	1.1	1.0	0.8
10-20	1.5	1.9	1.2	0.8	1.0	0.5	0.5
20-30	1.6	1.3	1.0	0.8	0.7	0.5	0.4
30-40	1.1	1.0	0.8	0.7	0.7	0.3	0.3
40-50	0.9	0.8	0.7	0.8	0.5	0.6	0.3
50-60	0.7	0.8	1.0	0.8	0.5	0.6	0.3
60-70	0.6	0.8	0.6	0.5	0.4	0.4	0.3
70-80	0.5	0.5	0.6	0.6	0.4	0.3	0.3
80-90	0.9	0.8	1.0	0.6	0.6	0.5	0.3
90-98	0.3	0.6	0.7	0.4	0.3	0.4	0.2
98-100	3.0	5.6	12.7	16.5	15.7	17.9	18.6

*This data is plotted in Figure 4.7.

TABLE III-7. Sphalerite distributions in 10x14 mesh for various grinding times.

ZnS Content (wt%)	Grind, Time, minutes			
	1.00	2.00	4.00	6.00
0-2	69.8	72.9	80.2	85.6
2-10	2.7	1.8	2.7	1.9
10-20	1.2	2.3	2.2	1.8
20-30	1.3	2.7	0.6	1.4
30-40	2.1	2.4	1.4	0.4
40-50	0.9	1.0	1.5	1.1
50-60	1.3	2.6	0.4	0.5
60-70	1.9	0.9	0.4	1.0
70-80	1.0	1.9	1.2	0.4
80-90	2.5	1.0	1.2	0.5
90-98	1.5	2.0	1.2	0.9
98-100	12.9	9.5	7.0	4.9

TABLE III-8. Sphalerite distributions in 14x20 mesh for various grinding times.

ZnS Content (wt%)	Grind, Time, minutes			
	1.00	2.00	4.00	6.00
0-2	70.6	72.9	70.5	77.2
2-10	2.5	1.8	2.5	2.1
10-20	1.4	1.1	2.0	1.6
20-30	1.5	1.2	0.9	1.1
30-40	2.3	0.6	1.4	1.9
40-50	1.0	0.7	1.2	1.0
50-60	0.7	1.3	0.6	0.4
60-70	1.1	1.2	0.8	0.7
70-80	0.6	1.6	1.3	0.6
80-90	1.8	1.7	1.2	0.4
90-98	0.8	1.2	1.5	1.1
98-100	15.7	13.1	15.0	11.9

TABLE III-9. Sphalerite distributions in 20x28 mesh for various grinding times.

ZnS Content (wt%)	Grind, Time, minutes			
	1.00	2.00	4.00	6.00
0-2	69.5	72.3	73.5	79.2
2-10	1.2	1.9	1.6	1.6
10-20	2.0	1.4	1.6	0.9
20-30	1.6	0.8	1.3	0.8
30-40	1.1	0.8	1.0	0.3
40-50	1.0	1.0	1.0	0.4
50-60	1.1	0.4	0.6	0.4
60-70	0.7	1.2	0.5	0.3
70-80	0.7	1.4	1.3	0.4
80-90	1.4	0.9	0.9	0.9
90-98	1.3	0.5	0.2	0.3
98-100	18.4	17.7	16.5	14.5

TABLE III-10. Sphalerite distributions in 28x35 mesh for various grinding times.

ZnS Content (wt%)	Grind, Time, minutes			
	1.00	2.00	4.00	6.00
0-2	75.3	74.1	77.0	78.3
2-10	2.0	1.2	1.6	0.9
10-20	1.0	1.5	1.3	0.9
20-30	0.7	1.1	1.0	0.8
30-40	0.4	1.2	0.5	0.8
40-50	0.7	0.6	0.7	0.6
50-60	0.4	0.6	0.7	1.0
60-70	0.3	0.5	0.2	0.2
70-80	0.5	0.5	0.5	0.7
80-90	0.4	0.3	0.6	0.5
90-98	0.3	0.2	0.3	0.1
98-100	18.0	18.1	15.6	14.9

APPENDIX IV

EXPERIMENTAL AND COMPUTER SIMULATED SIZE DISTRIBUTIONS

TABLE IV-1.

EXPERIMENTAL PRODUCT SIZE DISTRIBUTIONS
(10 x 14 mesh feed)

Cumulative Size Fraction Passing Stated Size

Size (mesh)	Grind Time, minutes			
	1.00	2.00	4.00	6.00
10	1.000	1.000	1.000	1.000
14	0.444	0.643	0.852	0.941
20	0.246	0.420	0.680	0.835
28	0.134	0.252	0.471	0.649
35	0.109	0.208	0.404	0.574
48	0.077	0.153	0.308	0.452
65	0.057	0.116	0.238	0.357
100	0.045	0.092	0.191	0.288
150	0.033	0.069	0.145	0.220
200	0.025	0.054	0.113	0.172
270	0.018	0.039	0.082	0.123
400	0.015	0.032	0.066	0.095

TABLE IV-2.

EXPERIMENTAL PRODUCT SIZE DISTRIBUTIONS
(14 x 20 mesh feed)

Cumulative Size Fraction Passing Stated Size

Size (mesh)	Grind Time, minutes			
	1.00	2.00	4.00	6.00
14	1.000	1.000	1.000	1.000
20	0.427	0.631	0.851	0.940
28	0.190	0.336	0.585	0.750
35	0.148	0.270	0.499	0.666
48	0.100	0.188	0.368	0.513
65	0.070	0.135	0.279	0.402
100	0.053	0.102	0.219	0.312
150	0.038	0.073	0.162	0.234
200	0.028	0.054	0.123	0.179
270	0.020	0.039	0.085	0.121
400	0.016	0.029	0.065	0.091

TABLE IV-3.

EXPERIMENTAL PRODUCT SIZE DISTRIBUTIONS
(20 x 28 mesh feed)

Cumulative Size Fraction Passing Stated Size

Size (mesh)	Grind Time, minutes			
	1.00	2.00	4.00	6.00
20	1.000	1.000	1.000	1.000
28	0.287	0.471	0.703	0.848
35	0.212	0.371	0.597	0.760
48	0.131	0.241	0.416	0.573
65	0.091	0.175	0.315	0.450
100	0.058	0.115	0.212	0.305
150	0.041	0.085	0.162	0.240
200	0.027	0.057	0.105	0.154
270	0.018	0.039	0.073	0.103
400	0.011	0.025	0.049	0.069

TABLE IV-4.

EXPERIMENTAL PRODUCT SIZE DISTRIBUTIONS
(28 x 35 mesh feed)

Cumulative Size Fraction Passing Stated Size

Size (mesh)	Grind Time, minutes			
	1.00	2.00	4.00	6.00
28	1.000	1.000	1.000	1.000
35	0.395	0.543	0.762	0.887
48	0.143	0.252	0.442	0.591
65	0.089	0.170	0.321	0.445
100	0.056	0.144	0.218	0.318
150	0.040	0.115	0.164	0.244
200	0.028	0.090	0.115	0.176
270	0.021	0.076	0.090	0.138
400	0.015	0.065	0.069	0.105

TABLE IV-5.

EXPERIMENTAL PRODUCT SIZE DISTRIBUTIONS
(10 x 14 mesh feed, Gangue)

Cumulative Size Fraction Passing Stated Size

Size (mesh)	Grind Time, minutes			
	1.00	2.00	4.00	6.00
10	1.000	1.000	1.000	1.000
14	0.285	0.405	0.684	0.819
20	0.122	0.197	0.440	0.605
28	0.063	0.106	0.265	0.395
35	0.055	0.089	0.226	0.343
48	0.040	0.067	0.175	0.269
65	0.034	0.057	0.151	0.223
100	0.025	0.044	0.113	0.175
150	0.020	0.036	0.092	0.143
200	0.015	0.028	0.072	0.112
270	0.012	0.022	0.056	0.086
400	0.009	0.016	0.039	0.062

TABLE IV-6.

EXPERIMENTAL PRODUCT SIZE DISTRIBUTIONS
(multisized feed)

Cumulative Size Fraction Passing Stated Size

Size (mesh)	Feed	Grind Time (4 minutes)
10	1.000	1.000
14	0.637	0.922
20	0.423	0.805
28	0.291	0.625
35	0.209	0.530
48	0.157	0.418
65	0.115	0.324
100	0.088	0.253

TABLE IV-7. Experimental product size distributions for each component produced in the batch ball milling of a 10x14 monosized feed (Grind time, 1minutes).

Cumulative Size Fraction Passing Stated Size*

Size (mesh)	Total	Free Sphalerite	Free Gangue	Binary
10	1.000	0.164	0.693	0.143
14	0.444	0.089	0.305	0.052
20	0.246	0.055	0.169	0.052
28	0.134	0.029	0.099	0.023
35	0.109	0.023	0.082	0.007
48	0.077	0.014	0.061	0.005
65	0.057	0.009	0.048	0.002
100	0.045	0.006	0.039	0.000

*This data is plotted in Figures 4.19 and 4.21.

TABLE IV-8. Experimental product size distributions for each component produced in the batch ball milling of a 10x14 monosized feed (Grind time, 2 minutes).

Cumulative Size Fraction Passing Stated Size

Size (mesh)	Total	Free Sphalerite	Free Gangue	Binary
10	1.000	0.170	0.715	0.115
14	0.643	0.118	0.455	0.075
20	0.420	0.085	0.300	0.036
28	0.252	0.051	0.187	0.015
35	0.208	0.039	0.156	0.013
48	0.153	0.026	0.120	0.009
65	0.116	0.018	0.096	0.004
100	0.092	0.012	0.080	0.000

TABLE IV-9. Experimental product size distributions for each component produced in the batch ball milling of a 10x14 monosized feed (Grind time, 4 minutes).

Cumulative Size Fraction Passing Stated Size

Size (mesh)	Total	Free Sphalerite	Free Gangue	Binary
10	1.000	0.173	0.745	0.082
14	0.852	0.161	0.624	0.072
20	0.680	0.136	0.500	0.048
28	0.471	0.098	0.356	0.018
35	0.404	0.081	0.314	0.013
48	0.308	0.056	0.249	0.007
65	0.238	0.038	0.200	0.005
100	0.191	0.024	0.167	0.000

TABLE IV-10. Experimental product size distributions for each component produced in the batch ball milling of a 10x14 monosized feed (Grind time, 6 minutes).

Cumulative Size Fraction Passing Stated Size*

Size (mesh)	Total	Free Sphalerite	Free Gangue	Binary
10	1.000	0.180	0.768	0.052
14	0.941	0.174	0.724	0.051
20	0.835	0.165	0.630	0.045
28	0.649	0.130	0.498	0.028
35	0.574	0.112	0.447	0.021
48	0.452	0.081	0.364	0.013
65	0.357	0.058	0.298	0.008
100	0.288	0.036	0.252	0.000

*This data is plotted in Figures 4.20 and 4.22.

TABLE IV-11. Experimental product size distributions for each component in the multisized feed.

Cumulative Size Fraction Passing Stated Size*

Size (mesh)	Total	Free Sphalerite	Free Gangue	Binary
10	1.000	0.125	0.773	0.102
14	0.637	0.097	0.491	0.049
20	0.423	0.075	0.323	0.025
28	0.291	0.055	0.224	0.012
35	0.209	0.039	0.164	0.006
48	0.157	0.032	0.122	0.003
65	0.115	0.026	0.088	0.001
100	0.088	0.021	0.067	0.000

*This data is plotted in Figure 4.24.

TABLE IV-12. Experimental product size distributions for each component produced in the batch ball milling of a multisized feed (Grind time, 4 minutes).

Cumulative Size Fraction Passing Stated Size*

Size (mesh)	Total	Free Sphalerite	Free Gangue	Binary
10	1.000	0.132	0.808	0.060
14	0.922	0.129	0.741	0.052
20	0.805	0.123	0.644	0.038
28	0.625	0.099	0.504	0.021
35	0.530	0.084	0.432	0.014
48	0.418	0.067	0.344	0.007
65	0.324	0.050	0.272	0.003
100	0.253	0.037	0.217	0.000

*This data is plotted in Figure 4.23.

TABLE IV-13. Experimental product size distributions for each component in the multisized feed (for the case of having two classes of composite particles).

Cumulative Size Fraction Passing Stated Size*

Size (mesh)	Free Sphalerite	Free Gangue	Binary (<50% ZnS)	Binary (>50% ZnS)
10	0.125	0.773	0.063	0.039
14	0.097	0.491	0.029	0.021
20	0.075	0.323	0.014	0.011
28	0.055	0.224	0.007	0.005
35	0.039	0.164	0.004	0.002
48	0.032	0.122	0.002	0.001
65	0.026	0.088	0.001	0.001
100	0.021	0.067	0.000	0.000

TABLE IV-14. Experimental product size distributions for each component produced in the batch ball milling of a multisized feed ore (for the case of having two classes of composite particles).

Cumulative Size Fraction Passing Stated Size*

Size (mesh)	Free Sphalerite	Free Gangue	Binary (<50% ZnS)	Binary (>50% ZnS)
10	0.132	0.808	0.039	0.021
14	0.129	0.741	0.033	0.019
20	0.123	0.644	0.023	0.015
28	0.099	0.504	0.013	0.008
35	0.084	0.432	0.009	0.005
48	0.067	0.344	0.004	0.003
65	0.050	0.272	0.002	0.001
100	0.037	0.217	0.000	0.000

*This data is plotted in Figure 4.27.

TABLE IV-15. Computer-simulated size distributions for each component produced in the batch ball milling of a 10x14 mesh monosized feed (Grind time, 1 minute).

Cumulative Size Fraction Passing Stated Size*

Size (mesh)	Total	Free Sphalerite	Free Gangue	Binary
10	1.000	0.165	0.685	0.150
14	0.450	0.093	0.305	0.052
20	0.282	0.069	0.186	0.027
28	0.180	0.043	0.121	0.016
35	0.117	0.028	0.084	0.005
48	0.082	0.020	0.060	0.002
65	0.057	0.010	0.047	0.000
100	0.048	0.006	0.041	0.000

*This data is plotted in Figure 4.19.

TABLE IV-16. Computer-simulated size distributions for each component produced in the batch ball milling of a 10x14 mesh monosized feed (Grind time, 6 minutes).

Cumulative Size Fraction Passing Stated Size*

Size (mesh)	Total	Free Sphalerite	Free Gangue	Binary
10	1.000	0.208	0.736	0.056
14	0.938	0.200	0.688	0.050
20	0.874	0.192	0.639	0.043
28	0.737	0.168	0.541	0.028
35	0.635	0.151	0.470	0.014
48	0.509	0.122	0.380	0.007
65	0.390	0.091	0.299	0.000
100	0.319	0.058	0.261	0.000

*This data is plotted in Figure 4.20.

TABLE IV-17. Computer-simulated size distributions using corrected sphalerite assay (Grind time, 1 minute).

Cumulative Size Fraction Passing Stated Size*

Size (mesh)	Total	Free Sphalerite	Free Gangue	Binary
10	1.000	0.162	0.698	0.140
14	0.440	0.090	0.300	0.050
20	0.248	0.056	0.167	0.025
28	0.160	0.030	0.112	0.011
35	0.109	0.022	0.084	0.003
48	0.078	0.015	0.062	0.001
65	0.058	0.010	0.048	0.000
100	0.043	0.008	0.035	0.000

*This data is plotted in Figure 4.21.

TABLE IV-18. Computer-simulated size distributions using corrected sphalerite assay (Grind time, 6 minutes).

Cumulative Size Fraction Passing Stated Size*

Size (mesh)	Total	Free Sphalerite	Free Gangue	Binary
10	1.000	0.160	0.782	0.058
14	0.945	0.153	0.740	0.052
20	0.844	0.150	0.653	0.041
28	0.717	0.132	0.555	0.028
35	0.606	0.110	0.480	0.016
48	0.486	0.088	0.392	0.006
65	0.378	0.067	0.308	0.003
100	0.305	0.040	0.265	0.000

*This data is plotted in Figure 4.22.

TABLE IV-19. Computer-simulated size distributions for each component produced in the batch ball milling of a multisized feed (Grind time, 4 minutes).

Cumulative Size Fraction Passing Stated Size*

Size (mesh)	Total	Free Sphalerite	Free Gangue	Binary
10	1.000	0.142	0.802	0.056
14	0.926	0.138	0.740	0.048
20	0.819	0.127	0.656	0.036
28	0.680	0.109	0.545	0.026
35	0.542	0.086	0.440	0.016
48	0.421	0.068	0.348	0.005
65	0.325	0.052	0.272	0.001
100	0.260	0.040	0.220	0.000

*This data is plotted in Figure 4.23.

TABLE IV-20. Computer-simulated size distributions for each component produced in the batch ball milling of a multisized feed ore (for the case of having two classes of composite particles).

Cumulative Size Fraction Passing Stated Size*

Size (mesh)	Free Sphalerite	Free Gangue	Binary (<50% ZnS)	Binary (>50% ZnS)
10	0.145	0.800	0.037	0.018
14	0.140	0.750	0.033	0.016
20	0.128	0.661	0.027	0.013
28	0.107	0.565	0.018	0.009
35	0.088	0.450	0.011	0.005
48	0.069	0.356	0.006	0.002
65	0.052	0.270	0.002	0.001
100	0.034	0.200	0.000	0.000

*This data is plotted in Figure 4.27.

TABLE IV-21. Computer-simulated size distributions for each component produced in the batch ball milling of a multisized feed ore (for the case of having two classes of composite particles).

Cumulative Size Fraction Passing Stated Size*

Size (mesh)	Free Sphalerite	Free Gangue	Binary (<50% ZnS)	Binary (>50% ZnS)
10	0.144	0.806	0.032	0.018
14	0.134	0.740	0.028	0.016
20	0.128	0.674	0.016	0.013
28	0.110	0.560	0.010	0.005
35	0.092	0.462	0.006	0.003
48	0.076	0.365	0.002	0.001
65	0.053	0.282	0.002	0.001
100	0.034	0.210	0.000	0.000

*This data is plotted in Figure 5.7.

TABLE IV-22. Experimentally-determined breakage rates for free sphalerite, free gangue and composite particles.

Size (mesh)	S_a	S_b	S_{ab}	$S_{ab,1}$	$S_{ab,2}$
10x14	0.656	0.434	0.622	0.553	0.710
14x20	0.541	0.413	0.564	0.509	0.628
20x28	0.368	0.293	0.384	0.360	0.420
28x35	0.305	0.244	0.300	0.250	0.300
35x48	0.231	0.180	0.230	0.180	0.210
48x65	0.182	0.139	0.176	0.120	0.150
65x100	0.148	0.106	0.135	0.090	0.105
-100	0.000	0.000	0.000	0.000	0.000

TABLE IV-23. Normalizable B functions for gangue material.*

Size (mesh)	10x14 mesh	14x20 mash	20x28 mesh
14x20	0.950	--	--
20x28	0.484	0.950	--
28x35	0.275	0.484	0.922
35x48	0.227	0.290	0.530
48x65	0.173	0.230	0.313
65x100	0.137	0.169	0.239
-100	0.106	0.133	0.178

*This data is plotted in Figure 4.16.

TABLE IV-24. Normalizable B functions for sphalerite.*

Size (mesh)	10x14 mesh	14x20 mash	20x28 mesh
14x20	0.690	--	--
20x28	0.320	0.720	--
28x35	0.203	0.310	0.730
35x48	0.152	0.210	0.390
48x65	0.114	0.170	0.230
65x100	0.084	0.120	0.180
-100	0.070	0.100	0.135

*This data is plotted in Figure 4.17.

TABLE IV-25. Experimentally-determined breakage distribution functions for free sphalerite, free gangue and composite material.

Size (mesh)	B_a (Sphalerite)	B_b (Gangue)	B_{ab} (Binary)
10x14	0.000	0.000	0.000
14x20	0.384	0.080	0.278
20x28	0.293	0.436	0.161
28x35	0.140	0.210	0.063
35x48	0.030	0.050	0.010
48x65	0.040	0.055	0.031
65x100	0.030	0.046	0.005
-100	0.083	0.123	0.067

TABLE IV-26. Estimated breakage distribution functions for the composite particles.

Size (mesh)	$B_{ab,1}$	$B_{ab,2}$
10x14	0.000	0.000
14x20	0.161	0.196
20x28	0.138	0.168
28x35	0.065	0.079
35x48	0.014	0.018
48x65	0.018	0.023
65x100	0.011	0.013
-100	0.043	0.053

TABLE IV-27. Estimated and model-predicted breakage distribution functions for the composite particles.

Size (mesh)	Calculated	Model-predicted
10x14	0.000	0.000
14x20	0.230	0.330
20x28	0.365	0.330
28x35	0.175	0.140
35x48	0.040	0.040
48x65	0.047	0.035
65x100	0.038	0.025
-100	0.105	0.100

*This data is plotted in Figure 4.26.

TABLE IV-28. Computer-simulated liberation functions for sphalerite and gangue material.*

Size (mesh)	La (sphalerite)	Lb (gangue)
10x14	0.000	0.000
14x20	0.043	0.036
20x28	0.069	0.056
28x35	0.045	0.036
35x48	0.028	0.014
48x65	0.018	0.008
65x100	0.013	0.006
-100	0.016	0.013

*This data is plotted in Figure 4.18.

TABLE IV-29. Volumetric percent for free sphalerite and composite particles with number of particles examined.

No. of particles examined	Free sphalerite	Composite particles
600	5.1	15.6
1000	5.0	14.8
1600	5.6	16.0
2100	5.2	15.5
2700	5.3	15.2
3300	5.3	15.1
3800	5.3	15.1

*This data is plotted in Figure 5.2.

TABLE IV-30. Experimentally-determined and computer-simulated degree of liberation of sphalerite as a function of particle size.

Size (mesh)	Experimental	Computer-predicted
10x14	44.5	43.0
14x20	64.2	60.1
20x28	74.2	70.9
28x35	83.1	78.5
35x48	85.4	85.8
48x65	88.4	90.3
65x100	92.1	94.0

*This data is plotted in Figure 5.4.

APPENDIX V

COMPUTER PROGRAM FOR MASS BALANCE CALCULATION

```
C
C=============================================================
C
C ***  THIS COMPUTER PROGRAM SOLVES THE MASS BALANCE
C      EQUATIONS FOR THE SIZE REDUCTION/LIBERATION MODEL
C      OF GRINDING.  ***
C
C=============================================================
C
C
C      THE MATRIX FORM OF THE MASS BALANCE MODEL
C      DESCRIBING THE SIZE REDUCTION/LIBERATION PROCESS
C      IS GIVEN BY:
C
C
C         DMA/DT  = (BA-I)*SA*MA + LA*SAB*MAB  ..... (1)
C         DMB/DT  = (BB-I)*SB*MB + LB*SAB*MAB  ..... (2)
C         DMAB/DT = (BAB-I)*SAB*MAB  ............... (3)
C
C
C      WHERE THE VARIABLES ARE DEFINED AS:
C
C         MA,MB,MAB = MASS FRACTION OF PARTICLE TYPE A,
C                     B, OR AB CONTAINED IN EACH SIZE
C                     CLASS (VECTOR).
C
C         BA,BB,BAB = BREAKAGE DISTRIBUTION MATRIX FOR
C                       A, B, OR AB TYPE PARTICLES.
C
C         SA,SB,SAB = SELECTION MATRIX (BREAKAGE RATE)
C                     MATRIX FOR A,B, OR AB TYPE
C                     PARTICLES.
C
C         LA,LB     = LIBERATION DISTRIBUTION MATRIX
C                     FOR A OR B TYPE PARTICLES.
C
C
C      THE ABOVE 3N EQUATIONS (N=NUMBER OF SIZE
```

```
C       INTERVALS) HAVE BEEN SOLVED SIMULTANEOUSLY USING
C       IMSL SUBROUTINE.
C
C
C=============================================================
C
C       *** TO SIMULATE THE EQUATION ***
C
C=============================================================
C
C
      IMPLICIT REAL*8(A-H,O-Z)
C
      CALL  INPUT
      CALL  SETUP
      CALL  SIMUL
C
      STOP
      END
C
C
C=============================================================
      SUBROUTINE   INPUT
C=============================================================
C
C
      IMPLICIT REAL*8(A-H,O-Z)
      COMMON/PARA2/ A1(8,8), B1(8,8), C1(8,8), D1(8,8)
     &             ,E1(8,8), EMA(8), EMB(8), EMAB(8)
      DIMENSION     BA(8,8), SA(8,8), ELA(8,8), SAB(8,8),
     &              BB(8,8), SB(8,8), ELB(8,8), BAB(8,8)
C
      READ(5,*) (( BA(I,J),J=1,8),I=1,8)
      READ(5,*) (( BB(I,J),J=1,8),I=1,8)
      READ(5,*) ((BAB(I,J),J=1,8),I=1,8)
      READ(5,*) (( SA(I,J),J=1,8),I=1,8)
      READ(5,*) (( SB(I,J),J=1,8),I=1,8)
      READ(5,*) ((SAB(I,J),J=1,8),I=1,8)
```

```
      READ(5,*) ((ELA(I,J),J=1,8),I=1,8)
      READ(5,*) ((ELB(I,J),J=1,8),I=1,8)
      READ(5,*) ( EMA(I),I=1,8)
      READ(5,*) ( EMB(I),I=1,8)
      READ(5,*) (EMAB(I),I=1,8)
C
      WRITE(6,905)
  905 FORMAT(//,'  I N P U T     D A T A',//)
      WRITE(6,900)
  900 FORMAT(//)
      CALL USWFM('  BA   MATRIX', 13,  BA, 8,8,8, 3)
      WRITE(6,900)
      CALL USWFM('  BB   MATRIX', 13,  BB, 8,8,8, 3)
      WRITE(6,900)
      CALL USWFM(' BAB   MATRIX', 13, BAB, 8,8,8, 3)
      WRITE(6,900)
      CALL USWFM('  SA   MATRIX', 13,  SA, 8,8,8, 3)
      WRITE(6,900)
      CALL USWFM('  SB   MATRIX', 13,  SB, 8,8,8, 3)
      WRITE(6,900)
      CALL USWFM(' SAB   MATRIX', 13, SAB, 8,8,8, 3)
      WRITE(6,900)
      CALL USWFM(' ELA   MATRIX', 13, ELA, 8,8,8, 3)
      WRITE(6,900)
      CALL USWFM(' ELB   MATRIX', 13, ELB, 8,8,8, 3)
      WRITE(6,900)
      CALL USWFV(' EMA   MATRIX', 13, EMA, 8, 1, 3)
      WRITE(6,900)
      CALL USWFV(' EMB   MATRIX', 13, EMB, 8, 1, 3)
      WRITE(6,900)
      CALL USWFV(' EMAB  MATRIX', 13,EMAB, 8, 1, 3)
C
C     *** A1 MATRIX CALCULATION (A1 = (BA-I)*SA) ***
C
      DO 100 I=1, 8
  100 BA(I,I) = BA(I,I) - 1.0
C
```

```
      CALL VMULFF(  BA,  SA, 8,8,8, 8,8,  A1,8,  IER)
C
C     *** B1 MATRIX CALCULATION (B1 = LA*SAB) ***
C
      CALL VMULFF( ELA, SAB, 8,8,8, 8,8,  B1,8,  IER)
C
C     *** E1 MARIX CALCULATION (E1 = (BB-I)*SB) ***
C
      DO 110 I=1, 8
  110 BB(I,I) = BB(I,I) - 1.0
C
      CALL VMULFF(  BB,  SB, 8,8,8, 8,8,  E1,8,  IER)
C
C     *** D1 MATRIX CALCULATION (D1 = LB*SAB) ***
C
      CALL VMULFF( ELB, SAB, 8,8,8, 8,8,  D1,8,  IER)
C
C     *** C1 MATRIX CALCULATION (C1 = (BAB-I)*SAB) ***
C
      DO 120 I=1, 8
  120 BAB(I,I) = BAB(I,I) - 1.0
C
      CALL VMULFF( BAB, SAB, 8,8,8, 8,8,  C1,8,  IER)
C
       RETURN
       END
C
C
C=============================================================
      SUBROUTINE   SETUP
C=============================================================
C
C
C ***   SET UP  A  MATRIX   ***
C
C
      IMPLICIT REAL*8(A-H,O-Z)
C
```

```
      COMMON/PARA2/ A1(8,8), B1(8,8), C1(8,8), D1(8,8)
     &             ,E1(8,8), EMA(8), EMB(8), EMAB(8)
      COMMON/GLOBL/ A(24,24)
C
      DO 100 I=1, 24
      DO 100 J=1, 24
  100 A(I,J) = 0.0
C
      DO 200 I=1, 8
      DO 200 J=1, 8
            A(I   ,J   )  = A1(I,J)
            A(I   ,J+ 8)  = B1(I,J)
            A(I+8 ,J+ 8)  = C1(I,J)
            A(I+16,J+ 8)  = D1(I,J)
            A(I+16,J+16)  = E1(I,J)
  200 CONTINUE

      RETURN
      END
C
C
C=============================================================
      SUBROUTINE       SIMUL
C=============================================================
C
C
      IMPLICIT REAL*8(A-H,O-Z)
C
      COMMON/PARA2/ A1(8,8), B1(8,8), C1(8,8), D1(8,8)
     &             ,E1(8,8), EMA(8), EMB(8), EMAB(8)
      DIMENSION Z(24),  WK(500), C(24), W(24,24), IWK(24)
C
      EXTERNAL  FCN, FCNJ
C
C***  SET UP THE INITIAL CONDITIONS   ***
C
      DO 100 I=1, 8
      Z(I   ) = EMA(I)
```

```
      Z(I+8 ) = EMAB(I)
      Z(I+16) = EMB(I)
  100 CONTINUE
C
C***  THESE PARAMETERS ARE FOR IMSL ROUTINE
C     "DGEAR OR DVERK"  ***
C
      N     =  24
      T     =  0.0
      TOL   =  0.0001
      H     =  0.0001
      METH  =  1
      MITER =  0
      INDEX =  1
C
      WRITE(6,9901)
C
C
C*********************************************
C*  S I M U L A T I O N      S T A R T S  *
C*********************************************
C
C
      DO 2000  ITER = 1, 11
C
C
C   PRINT THE Z  MATRIX
C
      WRITE(6,901)  T
  901 FORMAT(///,' TIME (MIN.).............',F10.0,/)
      WRITE(6,911)  ( Z(I),I=1,24)
  911 FORMAT(/,8E15.6)
C
      TEND =  ITER
C
C.............................................................
C   CALL  IMSL   "DGEAR"    AND    CALCULATE
C
```

```
      CALL  DGEAR(N,FCN,FCNJ,T,H,Z,TEND,TOL,METH,MITER,
     &            INDEX,IWK,WK,IER)
      IF(IER .GT. 128)  GO TO 999
C.....................................................
C
C.....................................................
C   CALL  IMSL   "DVERK"    AND    CALCULATE
C
C     CALL  DVERK(N,FCN,T,Z,TEND,TOL,INDEX,C,20,W,IER)
C     IF(IER .GT. 128)  GO TO 999
C.....................................................
C
 2000 CONTINUE
C
  999 CONTINUE
C
C*****   F O R M A T    *******
C
 9901 FORMAT(///,132('-'),/,'  S I M U L A T I O N',
     &          '      S T A R T S',/, 132('-'),/   )
C
      RETURN
      END
C
C
C============================================================
      SUBROUTINE    FCN (N, T, Z, ZDOT)
C============================================================
C
C
      IMPLICIT REAL*8(A-H,O-Z)
C
      COMMON/GLOBL/ A(24,24)
      DIMENSION  Z(24), ZDOT(24)
C
      CALL  VMULFF(A, Z,  24, 24,1 ,24,24, ZDOT, 24, IER)
C
      RETURN
```

```
      END
C
C
C=======================================================
      SUBROUTINE   FCNJ(N,X,Y,PD)
C=======================================================
C
C
      IMPLICIT REAL*8(A-H,O-Z)
      DIMENSION  Y(N), PD(N,N)
      RETURN
      END
```

The vita has been removed from the scanned document